Towards advanced immunocompetent skin wound models for *in vitro* drug evaluation

Dissertation zur Erlangung des

naturwissenschaftlichen Doktorgrades

der Julius-Maximilians-Universität Würzburg

vorgelegt von

Chiara Griffoni

Parma, Italy

Würzburg, 2019

Eingereicht am: …………………………………..……..

<u>Mitglieder der Promotionskommission:</u>

Vorsitzender: Prof. Roy Gross

Gutachter: Prof. Thomas Dandekar

Gutachter: Prof. Katharina Maniura-Weber

Tag des Promotionskolloquiums: …………………..……

Doktorurkunde ausgehändigt am: …………………….

Summary

Current preclinical models used to evaluate novel therapies for improved healing include both *in vitro* and *in vivo* methods. However, ethical concerns related to the use of animals as well as the poor physiological translation between animal and human skin wound healing designate *in vitro* models as a highly relevant and promising platforms for healing investigation. While current *in vitro* 3D skin models recapitulate a mature tissue with healing properties, they still represent a simplification of the *in vivo* conditions, where for example the inflammatory response originating after wound formation involves the contribution of immune cells. Macrophages are among the main contributors to the inflammatory response and regulate its course thanks to their plasticity. Therefore, their implementation into *in vitro* skin could greatly increase the physiological relevance of the models. As no full-thickness immunocompetent skin model containing macrophages has been reported so far, the parameters necessary for a successful triple co-culture of fibroblasts, keratinocytes and macrophages were here investigated. At first, cell source and culture timed but also an implementation strategy for macrophages were determined. The implementation of macrophages into the skin model focused on the minimization of the culture time to preserve immune cell viability and phenotype, as the environment has a major influence on cell polarization and cytokine production. To this end, incorporation of macrophages in 3D gels prior to the combination with skin models was selected to better mimic the *in vivo* environment. Embedded in collagen hydrogels, macrophages displayed a homogeneous cell distribution within the gel, preserving cell viability, their ability to respond to stimuli and their capability to migrate through the matrix, which are all needed during the involvement of macrophages in the inflammatory response. Once established how to introduce macrophages into skin models, different culture media were evaluated for their effects on primary fibroblasts, keratinocytes and macrophages, to identify a suitable medium composition for the culture of immunocompetent skin. The present work confirmed that each cell type requires a different supplement combination for maintaining functional features and showed for the first time that media that promote and maintain a mature skin structure have negative effects on primary macrophages. Skin differentiation media negatively affected macrophages in terms of viability, morphology, ability to respond to pro- and anti-inflammatory stimuli and to migrate through a collagen gel. The combination of wounded skin equivalents and macrophage-containing gels confirmed that culture medium inhibits macrophage participation in the inflammatory response that occurs after wounding. The described macrophage inclusion method for immunocompetent skin creation is a promising approach for generating more relevant skin models. Further optimization of the co-culture medium will potentially allow mimicking a physiological inflammatory response, enabling to evaluate the effects novel drugs designed for improved healing on improved *in vitro* models.

Zusammenfassung

Aktuelle präklinische Modelle zur Bewertung neuartiger Therapien für eine verbesserte Heilung umfassen sowohl *in vitro* als auch *in vivo* Methoden. Ethische Bedenken im Zusammenhang mit der Verwendung von Tieren sowie die schlechte physiologische Übersetzung zwischen tierischer und menschlicher Hautwundheilung bezeichnen In-vitro-Modelle jedoch als hochrelevante und vielversprechende Plattformen für die Heilungsforschung. Während die aktuellen *in vitro* 3D-Hautmodelle ein reifes Gewebe mit heilenden Eigenschaften rekapitulieren, stellen sie dennoch eine Vereinfachung der *in vivo*-Bedingungen dar, bei denen beispielsweise die nach der Wundbildung entstehende Entzündungsreaktion den Beitrag von Immunzellen beinhaltet. Makrophagen gehören zu den Hauptverursachern der Entzündungsreaktion und regulieren ihren Verlauf durch ihre Plastizität. Daher könnte ihre Implementierung in die *in vitro* Haut die physiologische Relevanz der Modelle deutlich erhöhen. Da bisher kein volldickes, immunkompetentes Hautmodell mit Makrophagen berichtet wurde, wurden hier die für eine erfolgreiche Dreifach-Cokultur von Fibroblasten, Keratinozyten und Makrophagen notwendigen Parameter untersucht. Zuerst wurden die Zellquelle und die Kultur zeitlich festgelegt, aber auch eine Implementierungsstrategie für Makrophagen festgelegt. Die Implementierung von Makrophagen in das Hautmodell konzentrierte sich auf die Minimierung der Kultivierungszeit, um die Lebensfähigkeit und den Phänotyp der Immunzellen zu erhalten, da die Umgebung einen großen Einfluss auf die Zellpolarisation und Zytokinproduktion hat. Zu diesem Zweck wurde die Integration von Makrophagen in 3D-Gelen vor der Kombination mit Hautmodellen ausgewählt, um die *in vivo*-Umgebung besser nachahmen zu können. Eingebettet in Kollagenhydrogele zeigten Makrophagen eine homogene Zellverteilung im Gel, die die Zelllebensfähigkeit bewahrt, auf Reize reagiert und durch die Matrix wandert, die alle bei der Beteiligung von Makrophagen an der Entzündungsreaktion benötigt werden. Nachdem festgestellt worden war, wie Makrophagen in Hautmodelle eingeführt werden können, wurden verschiedene Kulturmedien hinsichtlich ihrer Auswirkungen auf Primärfibroblasten, Keratinozyten und Makrophagen untersucht, um eine geeignete Medienzusammensetzung für die Kultur immunkompetenter Haut zu identifizieren. Die vorliegende Arbeit bestätigte, dass jeder Zelltyp eine andere Supplementkombination zur Aufrechterhaltung der Funktionsmerkmale benötigt und zeigte erstmals, dass Medien, die eine reife Hautstruktur fördern und aufrechterhalten, negative Auswirkungen auf die primären Makrophagen haben. Hautdifferenzierungsmedien wirkten sich negativ auf die Makrophagen in Bezug auf Lebensfähigkeit, Morphologie, Fähigkeit, auf pro- und antiinflammatorische Reize zu reagieren und durch ein Kollagengel zu wandern aus. Die Kombination aus verwundeten Hautäquivalenten und makrophagenhaltigen Gelen bestätigte, dass das Kulturmedium die Teilnahme der Makrophage an der Entzündungsreaktion, die nach der Wunde auftritt, hemmt. Die beschriebene

Makrophagen-Einschlussmethode zur immunkompetenten Hautbildung ist ein vielversprechender Ansatz zur Generierung relevanterer Hautmodelle. Eine weitere Optimierung des Co-Kulturmediums wird es möglicherweise ermöglichen, eine physiologische Entzündungsreaktion nachzuahmen und die Auswirkungen neuartiger Medikamente zur verbesserten Heilung auf verbesserte In-vitro-Modelle zu bewerten.

Contents

List of figures

List of tables

List of abbreviations

2D: Two-dimensional

3D: Three-dimensional

BSA: bovine serum albumin

CCL22: C-C motif chemokine 22

CD197: C-C chemokine receptor type 7

CD206: mannose receptor C type 1

CD68: Cluster of Differentiation 68

CXCL10: C-X-C motif chemokine 10

CSF: colony-stimulating factor

DHT: dehydrothermal

DC: dendritic cell

DAB: 3,3'-Diaminobenzidine

DAPI: 4',6-diamidino-2-phenylindole

DMEM: Dulbecco`s modified eagle medium

DMSO: Dimethyl sulfoxide

ECM: extracellular matrix

EDC: 1-ethyl-3-(3-dimethylaminopropyl) carbodiimide

EDTA: ethylenediaminetetraacetic acid

EGF: epidermal growth factor

EU: European Union

FBS: fetal bovine serum

FGF: fibroblasts growth factor

FTAL: full thickness air-lift

FTSM: full thickness skin model

GAG: glycosaminoglycan

GAPDH: glyceraldehyde 3-phosphate dehydrogenase

GM-CSF: granulocyte-macrophage colony-stimulating factor

HDF: human primary dermal fibroblasts

HEK: human primary keratinocytes

IFN-γ: interferon-γ

IGF: insulin-like growth factor

IL: interleukin

KGF: keratinocyte growth factor

LCs: Langerhans cells

LPS: lipopolysaccharide

M-CSF: macrophage colony-stimulating factor

mDC: monocyte-derived dendritic cell

MMP: matrix metalloproteinase

NHS: N-hydroxysuccinimide

PBS: phosphate buffered saline

PDGF: platelet-derived growth factor

PFA: Paraformaldehyde

PSN: penicillin-streptomycin-neomycin

RPMI: Roswell Park Memorial Institute medium

RT-PCR: reverse transcription polymerase chain reaction

SEM: scanning electron microscope

TBS: Tris-buffered solution

TGF-β: transforming growth factor β

TNF-α: tumor necrosis factor α

TRIS: tris(hydroxymethyl)aminomethane

UV: ultraviolet

VEGF: vascular endothelial growth factor

Chapter 1:
Introduction

1.   Introduction

1.1.   Skin

1.1.1.   Skin structure

Skin is the largest organ of the human body, accounting for 12-15% of the total weight and providing the first line of defense from the external environment [1,2]. Structurally, skin is composed of three layers: epidermis, dermis and hypodermis (figure 1). Epidermis is the outer layer, where keratinocytes at different stages of differentiation organize themselves in a multi-layered architecture. The basal layer or stratum germinativum is the bottom part of epidermis, laying on a basement membrane that divides dermis from epidermis, where keratinocytes form a continuum of tight junctions to keep a stable structure [3]. The anchorage of basal cells to the basement membrane occurs through hemi-desmosomes, while the lateral connection within cells includes the formation of tight junctions, des-mosomes and adherens junctions to form a tight structure [1,4]. In the basal layer, keratinocyte pre-cursor cells are constantly dividing, with the process of differentiation encompassing a continuous migration of basal keratinocytes towards the skin surface [2–4]. The process involves a change of mor-phology from a cobblestone, rounded phenotype of dividing cells to a gradually flattened appearance of non-dividing and anucleated corneocytes [4]. The intermediate layers of epidermis include the spi-nous layer or stratum spinosum, overlying the basal layer, and the granular layer or stratum granu-losum, located more externally. Stratum spinosum consists of 4-8 layers of cells [1], which are inter-connected with disulfide bonds to form a tight structure, which is essential for providing mechanical strength to the tissue [4]. Cells of the spinous layer have a variety of shapes, structures and subcellular properties that depend on their location within the layer [2]. Suprabasal cells are smaller in size, poly-hedral in shape and have a rounded nucleus, while the upper layers present bigger cells that contain organelles in the cytoplasm called lamellar granules [2]. Those organelles contain a variety of mole-cules including glycoproteins, lipids and acid hydrolases needed for providing impermeability to the skin [2,4]. Likewise, stratum granulosum cells contain keratohyaline granules that produce the proteins loricrin, filaggrin, involucrin and envoplakin, as well as transglutaminases that are required to crosslink them. The association of all proteins provides structural support of the cell layer and also contributes to the formation of an impermeable and tight layer that confers to skin its barrier function [1,4]. Within the different layers, intermediate cytoskeleton filaments namely keratins provide mechanical stability and integrity to the epithelium [1]. Different keratin genes are expressed in the different layers, with keratins 5 and 14 specific for the basal layer and keratins 1 and 10 for the intermediate spinous layer

[4]. The cornified layer or stratum corneum encompasses terminally differentiated cells that are located on the outer side of the tissue, where 15-20 layers of flattened dead cells (corneocytes) release all the molecules present in their granules, thereby providing protection from water, pathogens and other molecules to the epidermis [1,4]. Desmosomes present to connect cells to each other through all the epidermal layers are lost in the stratum corneum, causing the outer part of the epidermis to shed and desquamate [5]. Notably, the processes of desquamation at the terminal layer and the cell proliferation in the basal layer are balanced, generating a complete renewal of the epidermis approximately every 28 days [6].
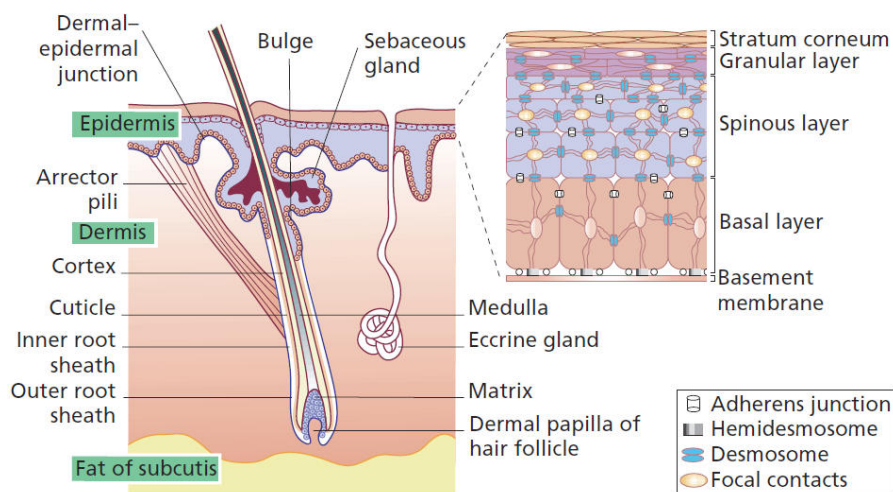
Figure 1. Schematic cross-section of skin with its appendages. Reprinted from [3] with permission from John Wiley and Sons.

Interposed in between the sub-layers of keratinocytes that represent 95% of the epidermal cell content, other resident cells are found in the epidermis [2,7]. Melanocytes are specialized cells residing in the basal layer, occurring approximately in a 1:10 ratio with keratinocytes, and represent 5-10% of the total number of epidermal cells in adults [1,8]. They are responsible for providing skin its characteristic pigmentation thanks to the secretion of melanin, which is produced in melanosomes [9]. Merkel cells are mechanoreceptors that belong to the sensory system, and are responsible for detection of different stimuli as pain, temperature and touch by forming a complex with neurites [10]. They are located in the basal layer of the epidermis, attached to basal keratinocytes with desmosomal junctions and connected to nerves that reside in the dermis [1,2]. Epidermis is also home to immune cells, which include dendritic cells (DCs), resident below the dermo-epidermal junction. Langerhans cells (LCs) are found in all layers of skin, with a higher abundance in the stratum spinosum and granulosum, representing a total of 2-6% of all epidermal cells [1,2].

Dermis is the middle layer of skin tissue, consisting of a cellular part and an abundant extracellular matrix (ECM) that is mainly secreted from the resident cells (fibroblasts). In adults, ECM is mostly com-

posed of collagen types I and III and elastic fibers, as well as other molecules such as the glycosamino-glycans hyaluronic acids and chondroitin sulfates [1–3]. The different orientation and composition of collagen fibers within the matrix allows to distinguish 2 dermal sublayers. The area closer to epidermis is called papillary dermis, consisting of small and organized collagen fibers [1,11]. Here, a complex network of capillaries is in charge of nourishing the above compartment. The name "papillary" refers to the shape of the characteristic finger-like projections named *papillae*, which extend toward the epidermis. In the reticular layer, located more deeply in the tissue, collagen and elastic fibers are denser and tightly packed to provide the tissue with strength, elasticity and resistance to stress [1]. The reticular layer is thicker than the papillary one, and contains sweat and sebaceous glands, hair follicles, and blood vessels. Dermis is also home to immune cells, which include tissue-resident macrophages and mast cells, the latest having the ability to also migrate in the epidermis through the basement membrane [1].

Hypodermis, the deeper layer of skin, connects the tissue to the underlying muscles and bones [11]. Adipocytes represent one third of the adipose tissue, the rest being composed of blood vessels, nerves, fibroblasts and adipocyte precursor cells [1]. The hypodermis provides thermal insulation to the body and also represents an energy reserve thanks to its fat-rich composition [5]. Adipocytes exist in two types, white and brown, with the first ones regulating energy balance and other physiological processes, whereas the second ones are involved in heat production and regulation of body weight [1].

1.1.2.   Skin functions

As the outermost organ of the body that is in constant contact with the external environment, skin represents a physical and mechanical barrier to potentially harmful factors such as infections, injuries and dehydration [11]. Skin functions are strictly associated with its structure and the most important ones are provided by the epidermal composition and architecture. Keratinocyte tight aggregation in each epidermal sublayer, together with the presence of a sealing matrix provided by lipids and proteins secreted in the upper layers, has been defined as a "bricks and mortar" structure [4,12]. The tight and impermeable epidermal organization provides skin with the protection against a series of external agents. Acting as a physical barrier, epidermis prevents excessive water loss from the body [13]. Indeed, loss of water from skin tissue is regulated by sweat glands, which are under the control of the central nervous system [14]. The epidermis also protects the body from UV radiation thanks to the presence of melanocytes, as the melanin they produce absorbs the majority of UV-B radiation that could cause cellular damage [15,16]. As first line of defense against pathogens, skin also provides defense to microbial invasion with different strategies. In addition to representing a physical barrier to

pathogens penetration, different skin-resident cells both in dermis and epidermis elicit other mechanisms of defense. Skin immunosurveillance is a process occurring constitutively, involving different cell types in the regulation of tissue homeostasis both in health and disease. In the epidermis, keratinocytes secrete short anti-microbial peptides to protect the tissue from pathogen invasion [17,18]. In case of infection, keratinocytes are also capable of secreting pro-inflammatory cytokines to attract immune cells [19], therefore participating in the skin immune response. LCs mainly participate in tissue homeostasis but can also take part in the adaptive immunity of the human body by processing foreign antigens [19] and activating T cells [20]. DCs have different functions during the immune response, which are correlated with the existence of different subtypes of DCs possessing diverse origins. Conventional DCs derive from bone marrow precursors and regulate T cell responses [21], while monocyte-derived DCs (mDCs) differentiate from extravasating blood Ly-6C^{hi} monocytes and perform immuno-surveillance and antigen-presenting functions [22]. A third type of DCs namely plasmacytoid DCs can be detected only in inflamed skin, contributing to viral infection responses [21] as well as wound repair [23] and systemic inflammatory responses [24]. In similarity with mDCs, another population of cells participating in skin immunity is represented by macrophages. The origin of skin-resident macrophages is not conventionally assessed, and has been reported to derive both from extravasating Ly-6C^{hi} monocytes, as for mDCs, and from precursors originated pre-natally [22,25,26]. Differently from mDCs, the main role of macrophages is not antigen-presentation during the adaptive response. Their function is strictly correlated to the different subtypes of macrophages that exist, all originating from a naïve phenotype that differentiates in the various subsets depending on the environmental cues [27]. Macrophages are involved both in the promotion and resolution of inflammation, existing both in a pro-inflammatory, classically activated or M1 phenotype and an anti-inflammatory, alternatively activated or M2, state [27–29]. The polarization to different subtypes depending on the stimuli is namely plasticity, and allows macrophages to change their phenotype depending on the environment as well as switching from one type to the other [27,29]. Mast cells are involved in allergic reactions [30] and also participate in infection responses, promoting the migration of other immune cells through the degradation of the ECM and the secretion of enzymes and cytokines that attract immune effectors [19,31]. T cells also participate in homeostasis by continuously migrating between skin lymph-nodes and peripheral tissue [19], however their number is highly increased during inflammation and infection, when they manage the recruitment of other immune cells [32]. Additionally, also sweat glands participate in the defense against pathogens, as the sweat they secrete also contains the antibiotic dermicidin [11].

1.2.   Skin wound healing

1.2.1.   Normal wound healing

When skin integrity is interrupted, the tissue has a remarkable ability to repair the injured area. Wound healing is a complex and multifactorial process that aims at restoring the structure and function of the tissue. It consists of 4 continuous and overlapping phases namely hemostasis, inflammation, proliferation and remodeling [7,33]. Hemostasis occurs within minutes after injury and involves the aggregation of platelets and plasma proteins to form a clot, which acts as a provisional matrix to prevent excessive blood loss from the tissue [7]. The signals that trigger the aggregation derive from both injured skin cells that release clotting factors and by the activation of thrombocytes occurring after contact with collagen [34]. Blood clots consist of fibrin, fibronectin, vitronectin and thrombospondins, which provide a temporary scaffold supporting cell migration and adhesion [33,35]. Hemostasis has a duration of hours and triggers the subsequent inflammatory phase [7,33,35]. Inflammation occurs 1 to 5 days after injury [7], and involves the participation of diverse cell types that trigger a complex signaling system. After aggregation, platelets that have been activated degranulate, releasing growth factors and chemokines that attract innate immune cells to the wound area [33,34]. Platelets together with the recruited leukocytes in turn secrete molecules that promote inflammation (interleukin (IL)-1, tumor necrosis factor α (TNF-α), IL-6), collagen synthesis (fibroblasts growth factor 2 (FGF-2), insulin-like growth factor 1 (IGF-1), transforming growth factor β (TGF-β)), fibroblast-to-myofibroblast differentiation (TGF-β), angiogenesis (vascular endothelial growth factor (VEGF), FGF-2, hypoxia-inducible factor 1 (HIF-1), TGF-β) and re-epithelialization (epidermal growth factor (EGF), FGF-2, IGF-1, TGF-β) [33,36]. Injured skin cells also participate in the recruitment of effector cells by releasing pro-inflammatory mediators after damage. For example, skin-resident immune cells, normally contributing to immunosurveillance, have the ability to recognize specific patterns present on dying cells or foreign invading organisms called danger-associated molecular patterns or pathogen-associated molecular patterns [34,37,38]. At the beginning of the inflammatory phase, also called early phase, neutrophils represent the most abundant cell type in the wound area, acting as first effectors of inflammation [33]. Following the clearance of foreign particles and organisms, neutrophils are removed from the wound area through incorporation into the eschar, which consists of dead tissue removed from the skin, or through phagocytosis by macrophages [28]. In the late inflammatory phase, monocytes represent the most abundant cell type in the wound area, guiding the inflammatory process from about 3 to 5 days after injury [28,33]. The recruitment of monocytes is triggered by the cytokines released in the wound area, that causes the extravasation of bone marrow-derived monocytes along the chemical gradient [39]. When in contact with the wound area milieu, monocytes undergo differentiation into macrophages,

which then participate and regulate the healing response [28]. As recruitment occurs during the inflammatory phase, the presence of pro-inflammatory cytokines in the environment induces the classical activation of monocytes, which leads to the generation of pro-inflammatory M1 macrophages approximately 2 days after wound formation [28]. Macrophages are responsible for removing microbes and foreign organisms from the area, both via phagocytosis and through secretion of molecules that activate defensive antimicrobial mechanisms, including TNF-α, nitric oxide and IL-1 [40]. The resolution of the inflammatory phase occurs when M1 macrophages undergo apoptosis or switch to the anti-inflammatory M2 phenotype, which are involved in the secretion of anti-inflammatory signals that promote tissue repair and regeneration [28,34,40]. The resolution of inflammation overlaps with the beginning of the proliferative phase, occurring between day 3 and day 10 after wound formation [33]. The proliferative phase, also called granulation phase, involves the replenishment of the wounded area via proliferation of the tissue-resident cells [28,33]. Different processes take place during granulation, including cellular proliferation and migration, wound contraction and angiogenesis [7,28]. Depending on the kind of injury, the completion of the proliferative process requires different time frames, as a partial thickness wound involving only the epidermis has a different impact on tissue integrity when compared to a full thickness wound involving also dermis and possibly hypodermis. From the wound edges, keratinocytes migrate to cover the wounded area and restore the stratified structure necessary for the skin barrier function, and at the same time fibroblasts are attracted to the wound bed to replenish the dermis [33]. The chemotactic stimuli for these migratory processes are growth factors and cytokines released from the injured cells located at the wound edge and from recruited platelets, neutrophils and macrophages [41], involving a myriad of different molecules such as bFGF, EGF, keratinocyte growth factor (KGF), IGF-1, nerve growth factor (NGF), platelet-derived growth factor (PDGF) and TGF-β [7,33,36,41]. In normal skin, each keratinocyte is tightly bound to the adjacent cells, triggering contact inhibition of signals involved in the regulation of membrane permeability. After wounding, the mechanical detachment of cells interrupts cell-to-cell contact inhibition, leading to the re-activation of the signals regulating membrane permeability [33]. The loosening of hemidesmosomes and desmosomes located between adjacent keratinocytes triggers membrane-associated kinases that increase the permeability of surrounding cells to ions such as calcium [33]. Activated keratinocytes competitively migrate along the fibrin matrix following a chemical gradient of cytokines [42,43] in a process called "keratinocyte shuffling" [44] and this migratory process is continued until the wound area is completely closed and migrating cells come into contact again. At the same time, also the surrounding fibroblasts migrate along the fibrin network following the chemokine gradient. Under the stimulation of cytokines as IFN-γ and TGF-β, fibroblasts increase the secretion of collagen and other molecules needed to restore the dermal matrix [33]. The process of replenishing the wound area is due to both proliferation of fibroblasts and increased secretion of collagen, and the balance between the two is

fundamental to promote a normal healing process [45]. Collagen secretion starts 3 days after injury and continues for approximately 3 weeks [41]. During the proliferative phase, it is fundamental for all cells involved to receive enough supplements for proliferation and migration. As full thickness wounds cause damage to blood vessels, the blood supply to the affected tissue area needs to be restored. Angiogenesis occurs at a high rate during proliferation, and begins with capillary sprouting following chemical gradients of growth factors such as VEGF present in the wound area, mainly released from keratinocytes and macrophages [36,46,47]. The binding of growth factors to surrounding endothelial cells activates a cascade of pathways that results in the ability of cells to secrete enzymes for dissolving the basal lamina and the surrounding tissue, resulting in their ability to migrate into the wound [33]. Through this process, the activated endothelial cells are able to sprout into the wound area and restore the blood supply to the injured tissue. The initial sprout formation in turn triggers the recruitment of pericytes and smooth muscle cells, which stabilize the structure and allow its differentiation into arteries and venules [33]. In the time frame between the proliferative phase and the last phase of wound healing, the transitional tissue present in the injured area acquires a characteristic composition and appearance. The high cell density including fibroblasts, macrophages and granulocytes, together with the presence of capillaries and newly synthetized collagen filaments is identified as granulation tissue [33]. Granulation tissue is detected until the number of fibroblasts is reduced, which occurs through the differentiation of cells to a myofibroblast phenotype through TGF-β stimulation, and consecutive apoptosis [48]. As myofibroblasts are highly contractile cells, their abundance in the wound area causes contraction of the wound to help the edges to get in proximity, which lasts until the tissue is repaired [48,49]. Remodeling is the last phase of wound healing, beginning around 21 days after injury and lasting up to 1-2 years, depending on the kind and extent of injury [7,33]. Since the dermal matrix secreted by fibroblasts during the proliferative phase is only provisional, remodeling is fundamental to provide a more organized and stable structure to the healed skin. As cellular components undergo apoptosis at the end of the proliferative phase, remodeling is characterized by the absence of cellular elements [7,50]. Because cellular components diminish, also the newly formed vasculature regresses due to the scarce nutrient demand, and the scar redness fades [28]. The main event during remodeling is the replacement of collagen III with collagen I, occurring through the production of matrix metalloproteinases (MMPs) by myofibroblasts and results in a more oriented structure that offers higher tensile strength [7].

1.2.2.   Nonhealing wounds

Healing is a complex process engaging many cell types having diverse functions, and involves the co-ordination of numerous processes to promote the restoration of tissue function. As all events that occur during the different healing phases require a precise sequence of actions, there are many ways for the healing process to go wrong. Impaired healing occurs at different degrees, and in the worst-case scenario results in the occurrence of chronic wounds. The incidence of nonhealing wound is poorly defined, as no standard definition of "chronic wound" exists [51], however lack of healing within 4-6 weeks is normally a sign of chronic wound occurrence [35,41]. As the majority of nonhealing wounds is correlated with conditions more common in older individuals [51–53], the current social state that outlines an increasingly aging society all over the world [54] suggests a progressive increase of the clinical occurrence of nonhealing wounds in the future [55]. Single events or a combination of factors might lead to the development of nonhealing wounds, including both systemic and local elements [7]. Systemic factors comprise age [52,53], nutrition state and concurrence of other conditions such as diabetes mellitus or vascular insufficiency, but also local elements such as pressure or friction of the wound area as well as the number of performed surgeries may affect healing progression [7,51,56]. Despite differences in etiology at the molecular level [35], some common features shared by chronic wounds include a constant inflammatory state, infection and biofilm formation, as well as the inability of the tissue to respond to the repair mechanisms, with wounds remaining stalled into the inflammatory phase (figure 2) [35]. In chronic wounds, fibroblasts are less responsive to PDGF and TGF-β [57,58], and resident cells proliferate less and have a morphology resembling senescent cells [51,57]. A constant influx of immune cells is encouraged by the continuous presence of pro-inflammatory cytokines, proteases and reactive oxygen species in the wound area, in turn leading to the continuous destruction of the newly synthetized ECM [35]. Simultaneously, pro-inflammatory cytokines affect the macrophages present in the area, maintaining their polarization state in a constant pro-inflammatory phenotype. As a result, neutrophils are not cleared from the area [59], and macrophages are unable to switch their phenotype to an anti-inflammatory state, which is essential for the promotion of tissue repair and for restoring tissue homeostasis [40,51]. Despite the high occurrence rates of chronic wounds in the clinics [35,51], many questions on the underlying mechanisms remain unsolved [33], which ultimately translates into a lack of effective therapies [56].
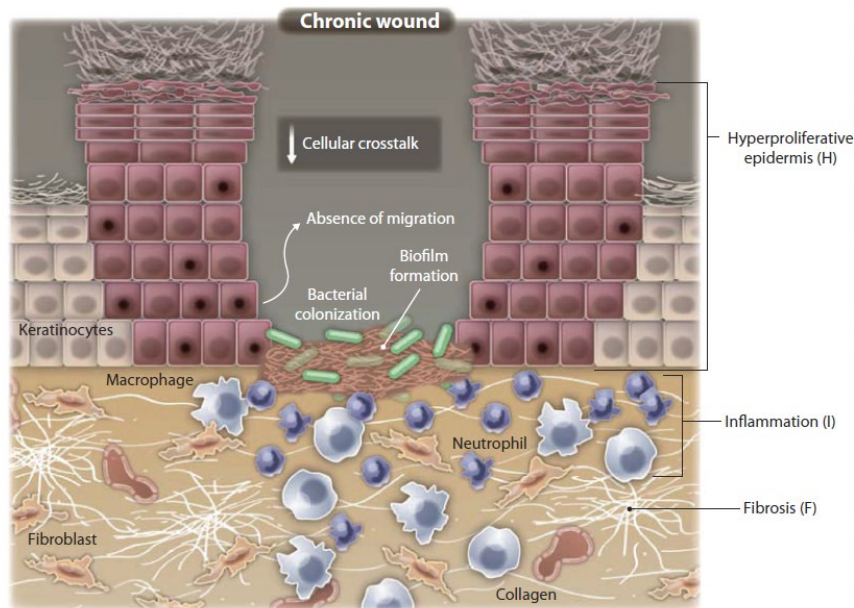
Figure 2. Schematic visualization of the cellular and molecular mechanisms occurring in nonhealing wounds. Adapted from [56] and reprinted with permission from The American Association for the Advancement of Science.

1.2.3.   Current treatments

The current methods employed in the clinics for the treatment of nonhealing wounds are various, as there is no standardized procedure for categorizing and treating the defects. Clinical classification and investigation of nonhealing wounds is highly dependent on clinicians, whose knowledge influences the choice of the treatment [51,56]. Therapies in use include the application of negative pressure, electrical stimulation, ultrasound, compression, hyperbaric oxygen, corticosteroids, cryotherapy, silicone gel sheeting, laser, cell-based therapies, application of wound dressings and local treatment with growth factors such as VEGF or PDGF [7,51,56]. However, in most of the cases, chronic wounds do not respond to the treatment, even when a combination of therapeutic approaches is employed [56]. The lack of tissue response reflects the scarcity of knowledge on the mechanisms involved in impaired healing, with therapies that do not take into account the coexistence of other pathologies and the possibility of a multifactorial failure in the healing process [56]. The exploration of novel, more functional therapies is therefore crucial for the effective treatment of chronic wounds, however the current preclinical platforms for assessing the efficacy of newly developed approaches are poorly mimicking the clinical settings [56].

1.3.   Current skin wound models

The first *in vitro* skin equivalent was reported in 1981 by Bell *et al.* [60], and since then several 3D skin models have been described in literature, serving different applications as reviewed by Groeber *et al.* [61]. While some skin models have been validated for the *in vitro* evaluation of corrosion and irritation [61], currently no standardized skin wound model has been established, resulting in the existence of different platforms where healing is preclinically evaluated.

1.3.1.   *In vivo* models

Wound healing research has for a long time relied on animal models, as a complex biologic environment is required to evaluate the factors participating in such an elaborated process. Tissue repair processes are highly conserved mechanisms common to all multicellular organisms, therefore the use of experimentally tractable models intends to favorably translate to human clinical applications [56]. The choice of animal models depends on diverse factors, including costs, ease of handling, availability and physiological similarities to humans [56]. Mice represent the main model for wound healing investigation, as they are economical, easy to handle and relatively simple to manipulate genetically [56]. The application of mice in wound healing research has allowed the investigation of incisional and excisional wounds, diabetic wounds, scar formation and burn wounds, however it presented a limited advancement in understanding human wound healing [62]. The poor translation of mice skin research to humans relates to the differences in anatomical and physiological characteristics between the two. Indeed, mice wounds close primarily by contraction [41], which led to the development of a standardized methodology that prevents this process by incorporating a splint around the wound [63]. Even though this method limits the contraction of the wound, it does not guarantee that healing occurs by re-epithelialization and then contraction, as it occurs in human skin. Therefore, a careful interpretation of such studies is required. In addition to the different healing mechanisms, also the structure of skin tissue itself presents differences, with mice skin having more hair and being thinner when compared to the human one [41,64]. Another difference between mice and human skin relates to the immune cell populations that reside in the tissue. Human epidermis is prevalently populated by LCs and T cells, while in mice a special population of T cells that is not present in humans is the predominant immune epidermal cell population [64], translating in the poor reflection of human disease in murine models [65].

Large animal models such as pigs have a closer similarity to humans with regard to skin anatomy and physiology [62]. Pigs have a relatively thick epidermis, a similar dermal composition and structure, a comparable distribution of immunohistochemical skin markers and hairs being more similar to humans than the rodent's fur [62]. Furthermore, the size of pigs is more comparable to humans and

thus allows for bigger wound implementation compared to rodents [41]. Porcine models have been employed for the investigation of chronic, diabetic and burn wounds as well as hypertrophic scar formation, also enabling the evaluation of various substances and procedures aiming at wound healing improvement [62]. The downside of the porcine model is however, besides ethical concerns, the bigger size and a longer lifespan that translates in high maintenance costs, more difficult surgical procedures and housing concerns [51].

1.3.2.   *In vitro* models

The ethical concerns related to the use of animals for research purposes has led to an increased interest in *in vitro* models for studying skin wound healing. A number of *in vitro* assays and methods to investigate the molecular mechanisms involved in healing and for assessing novel treatments for improved healing have been developed [66,67]. As the lack of cell migration is a limiting event in wound closure, healing assessment has been extensively analyzed through the evaluation of the migration ability of skin cells [66,67]. The most classical wound healing assays consist of removing parts of a confluent cell monolayer to mimic the injury that occurs during wounding, which is then followed by microscopic documentation of cell migration into the gap and quantification of wound closure [68]. Two-dimensional (2D) healing assays provide the analysis of cell migration after implementation of different etiologies of wounds [66]. Of these, mechanical wounding with sharp objects is the most common, known as scratch wound assay [69]. As an alternative, wounds can be created by stamping, causing the destruction of the cell monolayer by applying pressure [66]. To replicate the thermo-mechanical damage found in some kinds of wounds, electrical wounding and thermal wounding have been developed. Electrical wounding involves the culture of cells on top of an electrode, and following application of an elevated current pulse, cells undergo electroporation and death [70,71]. Thermal wounds are generated by applying high temperatures on the cell monolayer causing its disruption, and can be highly reproducible when optical wounding methods as lasers are used [66]. Using time lapse microscopy to monitor cell migration into the wounded area, those methods allow to monitor and quantify the wound closure rate over time in an easy and intuitive manner. Furthermore, supplementation of drugs to the culture medium allows to study the effects of different compounds on cell migration in a simple setting, identifying promising candidates for improved migration of cells during wound healing [67]. The use of *in vitro* three-dimensional (3D) skin models for wound healing research represents a higher level of complexity, and reflects an increasing research focus since the first skin model was established in 1981 by Bell *et al.* [60]. Up to the present, several 3D skin models have been described in literature, with a variety of applications and culture protocols [31]. The *in vitro* generation of skin models firstly consists of seeding fibroblasts in a scaffold, using special hanging inserts as Transwell®, Snapwell™ or CellCrown™ systems as culture vessels. The scaffolds used for culture include

components with different origins, from biologically derived materials like collagen or decellularized sections of organs, to synthetic materials such as electrospun polycaprolactone or polylactic-co-glycolic acid [72]. Despite a number of materials and fabrication methods have been described to serve as scaffolds for skin culture [72], the use of collagen still represents the most popular material for skin tissue engineering due to its abundance in *in vivo* ECM [73]. The main advantage of using a biological material as collagen is the presence of cell-binding specific motifs that enhance cell attachment and spreading in the matrix. However, biological materials are mainly of animal origin, introducing cross-species variables. Additionally, the mechanical stability of, for example, collagen hydrogels is rather low. Synthetic materials, on the other hand, can provide great mechanical stability with the drawback of lacking the natural signals that promote cell adhesion and survival [31,61]. Once fibroblasts have spread in the scaffold and started to secrete their own matrix, keratinocytes are seeded on top of the gel and cultured until a confluent layer has formed. Thereafter, skin equivalents are maintained with air-lift culture, a technique that mimics the *in vivo* situation, where nutrients are provided to the model from the bottom of the dermis, through the cell culture insert membrane, while the epidermis is left exposed to air (figure 3). Alternative terminologies for this specific culture technique are air-liquid interface or air-liquid interphase. Skin equivalents can be generated by employing either cell lines or primary cells, with the latter one normally being isolated from donor skin samples [31]. While both approaches have demonstrated the ability to form of a mature epidermal structure, only few cell lines have been shown to achieve a fully differentiated epidermis so far [61,74,75].
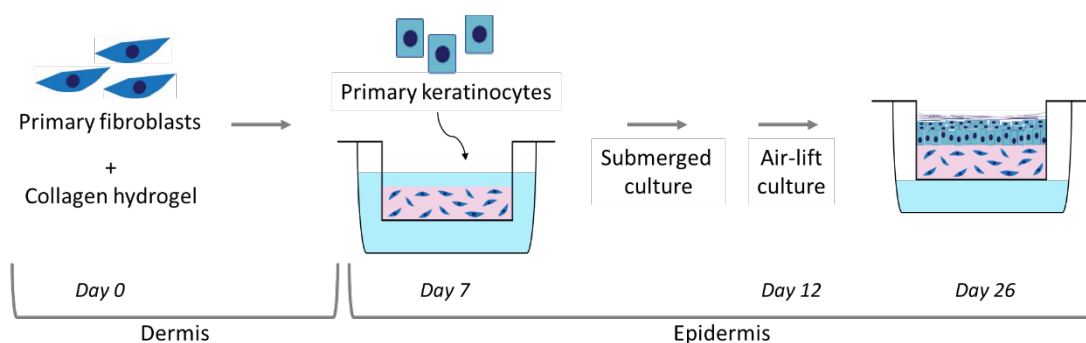
Figure 3. Schematic illustration of the different steps conventionally used to culture *in vitro* skin equivalents. Initially, fibroblasts are embedded in a collagen hydrogel and cultured for 7 days to generate a dermal compartment. Then, keratinocytes are seeded on top of the gel and cultured in submerged conditions for 5 days, to promote the formation of a confluent layer of cells on the surface. Afterwards, the cultures are exposed to air-lift culture for 14 days to promote the formation of a mature epidermis.

Regarding the application of such models to wound healing investigation, both epidermal and dermo-epidermal models, also referred to as full thickness skin models (FTSMs), have been employed for evaluating wound closure rates, with a prevalent use of FTSMs. Different kinds of wounds have been implemented in such *in vitro* models. Incisional wounds have been created by the use of scalpel blades [76–78] or skin meshers [76] and were reported to reproduce the dynamic healing response as

it occurs *in vivo* [76,77], providing evidence that fibroblasts participate and facilitate wound closure [78]. Excisional wounds have been implemented in skin models mainly employing biopsy punches of different diameters [79–82], obtaining full thickness wounds that affect both dermis and epidermis. To limit the introduction of human error and reducing sample manipulation during the wounding process, a fully automated wounding device has also been described, which aims at generating more reproducible wounds [83]. The implementation of excisional full thickness wound has been used for the evaluation of the re-epithelialization process [79,81], as well as for the investigation of novel wound healing therapies by injecting materials into the wound area [80] or by applying substances topically on top of the injured skin [82]. A different kind of wound etiology has been reproduced *in vitro* by creating cold or burn wounds. For this, a metal bar is placed in liquid nitrogen or in an oven for cooling or heating, and then is applied on the tissue for a specified amount of time [75,78,82,84]. The application of cold and burn wounds to skin equivalents also predominantly aims at studying re-epithelialization [78] or evaluating novel therapies for wound treatment [82,84]. A method used to implement thermal wounds under more reproducible settings is represented by the use of lasers. Different kinds of lasers have been exploited, allowing the creation of both full thickness [82,85] or partial-thickness wounds, with the latter one affecting only the epidermal layer [86].

To preserve the complex structure of skin and simulate a wound healing environment more similar to the *in vivo* one, human *ex vivo* models have also been used [87]. Explanted portions of skin tissue normally obtained from reduction surgeries can be maintained in culture for short periods of time, allowing the implementation of wounds on a more complex environment where paracrine signaling between different cell types is preserved [88].

1.3.3.   Limitations of current skin wound models and future directions

Gaining more insight into the mechanisms that regulate the process of wound healing and identifying novel treatments for improving care of nonhealing wounds have been pushing forward the development of *in vivo*, *in vitro* and *ex vivo* models. The use of animals for preclinical research has represented for decades the standard method, contributing to a major advancement in human biology understanding [89]. However, the emerging of alternative methods has initiated a debate on the use of animals for research purposes. The 3Rs principle was introduced for the first time in 1959, describing the need for a more responsible and ethical use of animals for research purposes [90]. The 3Rs stand for Replacement, Reduction and Refinement, inviting the scientific community to use alternative methods to animal experimentation, when possible, and if not, to employ fewer animals and minimize the stress and pain inflicted. A successful step towards the reduction of animal use was obtained in 2009 in the

European Union (EU), with the issue of a ban forbidding the use of animals for testing finished cosmetics products [91]. In 2010, the EU released another document to guarantee the protection of animals used for scientific purposes [92]. In parallel to the ethical concerns that have been increasingly underlining the need for more conscious methods to perform research, animal models also present other downsides, as previously described. While a specific model might mimic one desired aspect of the human condition and allow a comprehensive understanding, there is no animal model completely matching the human physiology [89]. The presence of concurrent clinical conditions normally detected in humans is another non-reproducible aspect in animal models [89]. This represents a big shortcoming for wound healing research, as defective healing is primarily observed in patients with a complicated clinical picture, with concurrent pathological conditions that might influence wound healing [41]. The data obtained from animal experiments also carries translational concerns, as the anatomical and physiological analogies may not be enough to draw valid conclusions at a preclinical level [89].

The use of *ex vivo* skin has enabled to evaluate wound healing in human-derived tissue, which possesses all the native structures of human skin, including an intact basement membrane [88]. However, limited availability of skin explants represents a shortcoming in the use of *ex vivo* skin, which together with the lack of immune cells and blood supply restrict their use to very limited applications [88].

Since the establishment of the 3Rs principles [93] and the ban on animal testing [91], the development and use of alternative *in vitro* platforms has greatly increased. Preclinical screening of novel substances for improved healing can be assessed with 2D assays as well as with more complex 3D skin wound models. Despite 2D assays represent fast and cost-efficient methods to evaluate the migration ability of skin cells, they do not take into account cell-cell crosstalk or the presence of a native 3D cellular environment. Indeed, it is well known that 2D cultures fail to represent the complex *in vivo* conditions [94], which is particularly relevant when investigating wound healing, as this is a result of several processes involving different cell types and phases [94]. The implementation of a more physiologically relevant environment is provided by the use of *in vitro* 3D models. Wound healing is a combination of different events that overlap, and 3D epidermal wound models aim at recapitulating the re-epithelialization occurring after injury, which is one of the key elements of wound closure. Epidermal models are intuitive, as they allow a simple evaluation of wound closure by imaging techniques. However, as re-epithelialization only represents one of the events occurring during healing, they only provide a partial picture of how healing is progressing. Furthermore, the crosstalk between fibroblasts and keratinocytes can affect re-epithelialization [95,96], as both cell types release cytokines that for example attract immune cells to regulate the inflammatory response [96]. FTSMs represent more closely what happens *in vivo*, as they encompass a dermal compartment with fibroblasts and a fully differentiated epidermis on top, preserving the paracrine signaling between cells. 3D *in vitro* skin models depict one of the most advanced and promising tool to evaluate novel wound healing therapies, as their similarity

with human skin have already granted the acceptance of FTSMs as validated platforms to evaluate irritation, corrosion and sensitization of chemicals, as well as for assessing UV exposure [97], bacterial adhesion [98] and penetration/permeability studies [99]. However, to date no *in vitro* wound healing system has been validated by the Organization for Economic Co-operation and Development. The application of FTSMs to wound healing investigation has succeeded in reproducing the healing process *in vitro*, demonstrating the contribution of both fibroblasts and keratinocytes to healing [78], allowing the detection of pro-inflammatory cytokines secreted after wounding [75,76,81,85] and tracking re-epithelialization with end-point analyses [75,77,79–81,86,87]. Furthermore, wounded FTSMs demonstrated to be suitable platforms to evaluate the effects of novel therapies aiming at enhancing wound healing [82,84]. However, a limitation to the advancement of skin models as validated preclinical platforms for wound healing investigation is the heterogeneity of culture conditions, representing a hurdle for skin models reproducibility and consequently for the creation of a standardized model. The *in vitro* 3D skin wound models described so far are characterized by variable implementation methods, choice of immune cell source, as well as heterogeneous culture parameters and wounding techniques. Primary cells or cell lines have been used, as well as biologically derived or synthetic scaffolds, different culture times and a wide range of media employed for generating *in vitro* skin [31]. Even though efforts have been made towards the standardization of the methods in use [83,100], the lack of common guidelines precludes the classification of 3D skin wound models as validated platforms for evaluating novel drugs and materials developed for improved healing. There is the need for more common procedures, allowing more reproducible models and more comparable results between groups, to achieve a broader use of *in vitro* skin models for wound healing assessment. *In vitro* FTSMs also represent a valuable tool to investigate skin pathophysiology. The *in vitro* mimicking of impaired conditions has been described by using biopsies of diseased patients as cell source, and skin models recapitulating certain aspects of chronic wounds [101] and hypertrophic scars [102] were generated. Engineered cell lines mimicking nonhealing wound conditions have been also reported [103], paving the way for *in vitro* investigation of diseased conditions without the need of patient-derived material. Similarly, the *in vitro* replication of skin cancer has been achieved by employing carcinoma cell lines, which have succeeded in recreating the altered conditions occurring *in vivo*, unraveling some of the mechanisms involved in tumor invasion [104–106]. However, in particular when evaluating wound healing disorders, the co-culture of fibroblasts and keratinocytes only reproduces a fraction of the conditions coexisting in chronic wounds. Even though two cell types have shown to support the formation of a fully mature tissue model and maintain the cross-talk occurring during healing, the preclinical evaluation of novel therapies would acquire higher impact and significance with an improved physiological setup.

The lack of the accessory structures such as vasculature or an immune system limits skin models use for investigating more complex processes [31]. Advanced physiologically relevant models should include more appendices to the *in vitro* structure. However, the more variables are introduced the less control over the parameters can be achieved. Depending on the application and on the process under investigation, diverse appendages have been implemented into skin models. The incorporation of melanocytes allowed to investigate skin response to UV radiation [100] and melanoma progression [107]. Successful implementation of LCs was also described [108], enabling to elucidate the mechanisms of LCs recruitment into the epidermis [109] and providing an advanced platform to evaluate skin sensitization into immunocompetent models [110]. Co-culture of both LCs and DCs within skin equivalents provided an insight into immune cells role in UV radiation [111], while DCs incorporation generated immunocompetent skin responsive to sensitizer application [112]. Co-culture of T cells in skin equivalents revealed a protective role of fibroblasts upon fungal infection [113], while incorporation of endothelial cells resulted in the generation of a vascularized skin equivalent [114]. When wound healing is under investigation, of all cellular components involved in the process macrophages represent the one cell type persisting in the wound area during all phases. Either skin-resident or recruited from blood circulating precursors, their contribution to healing is crucial and a dysregulation of their function results in unsuccessful resolution of inflammation. Therefore, the incorporation of macrophages is the most influential and relevant for investigation of novel healing therapies. During wound healing, macrophages acquire a diverse set of phenotypes, each contributing to the process with different functions. The dualistic roles and functions of macrophages represent a challenge when aiming at implementing them into 3D skin models. An effort to include macrophages into *in vitro* skin cultures has been described by Linde *et al.* [106] and Bechetoille *et al.* [115]. In both reports, the immune cells were included in the dermis as a co-culture with fibroblasts and then stimulated with lipopolysaccharide (LPS) [115] or first seeded with a tumoral epidermis and then stimulated with IL-4 [106]. Although the models demonstrated the survival of cells until 1 week [115] and 3 weeks [106] after seeding, the lack of epidermis [115] or the presence of a diseased epidermis [106] limits the relevance of the models. Indeed, skin response to injury is the result of synergistic signaling between dermis and epidermis [116–118], thus the lack of one of the components [115] or the presence of a tumor [106] affect the signals triggered by skin tissue. RAW.264.7 macrophages were also co-cultured with skin by seeding immune cells on the bottom of a well and placing mature skin equivalents in Transwell® inserts on top [119]. While this system allowed to investigate the cross-talk between immune cells and tissue, the composite 2D-3D environment does not reflect the signaling that occurs *in vivo*, and in addition a combination of primary cells and a cell line was employed. Indeed, it is well known that primary cells are physiologically more relevant compared to cell lines, exhibiting a faster and more intense response to infection [120]. The high sensitivity that macrophages have towards the surrounding environment

translates in the challenge of creating and maintaining *in vitro* culture conditions that allow the physiological cross-talk between cells and the preservation of the desired differentiated phenotype [31]. It is fundamental to precisely regulate the microenvironment where immune cells are introduced, as even small variations may affect cell fate and behavior. The identification of suitable conditions for immunocompetent skin culture is at the base of the successful incorporation of functional cells into skin wound models, having as final goal the evaluation of healing in a physiologically relevant preclinical setting. This extends to the identification of a suitable inclusion strategy preserving immune cell viability and to the selection of the appropriate culture conditions to grant both skin tissue maturation and the support of the physiological immune response of macrophages. The incorporation of macrophages into immunocompetent skin models would greatly enhance the relevance of wound healing investigation. The successful generation of a triple co-culture could potentially provide improved skin equivalents required to assess novel therapies for impaired healing, increasing the impact that preclinical models have in the transition from the bench to the bedside.

Chapter 2:
Aim of the thesis

2.   Aim of the thesis

The need for more relevant preclinical models to investigate the effects of novel wound healing therapies is prompting the development of advanced 3D *in vitro* models. To date, no *in vitro* skin model combines the incorporation of immune cells with wound implementation. The aim of this study was to identify the suitable conditions for the implementation of macrophages into 3D skin wound models.

To achieve this, first a suitable cell source, scaffold, medium and culture time to generate *in vitro* skin models with a structure comparable to human skin were identified. The development of fully differentiated skin equivalents focused on limiting the contraction of the model for improved reproducibility.

Preserving the main focus on generating a reproducible process, the implementation of full thickness wounds in the 3D skin models was then investigated. While evaluating different wounding techniques, diverse healing assessment methods were explored, to determine the most relevant for *in vitro* drug evaluation. The healing process analysis was applied to the identification of a suitable drug carrier system for *in situ* drug delivery. Fibrin was selected and evaluated for its effects on wound closure and the inflammatory response.

To achieve the culture of functional immunocompetent models, first a strategy to implement macrophages into skin equivalents was identified. Cell isolation and culture parameters were then set, with the aim of obtaining primary human macrophages capable to polarize to pro- and anti-inflammatory phenotypes *in vitro*. Cell functionality was assessed both in 2D and 3D cultures, as the identified implementation method included macrophage embedding in 3D collagen hydrogels. As immunocompetent skin models consist of a complex, triple co-culture, a special focus on the identification of a suitable culture medium promoting both skin maturation and immune cell functionality was set. Combination of macrophages and wounded skin equivalents was ultimately investigated, assessing the immune response occurring after wound formation in presence of the immune cells.

Chapter 3:
Materials

3. Materials

3.1. Chemical and reagents

Chemical/solution	Supplier	Catalog no
Accutase®	Sigma-Aldrich	A6964
Acetic acid	Sigma-Aldrich	695092
L-ascorbic acid-2-phosphate sesquimagnesium salt hydrate	Sigma-Aldrich	A8960
Bovine serum albumin (BSA)	Sigma-Aldrich	9048-46-8
Calcein AM	Sigma-Aldrich	17783
Calcium chloride dihydrate (CaCl$_2$•2 H$_2$O)	Merck	10035-04-8
Calcium pantethonate	European Pharmacopoeia Reference Standard	C0400000
L-Carnitine	Sigma-Aldrich	C0283
Casyton	OLS OMNI Life Science	5651808
CellTiter 96® AQueous One Solution Cell Proliferation Assay (MTS)	Promega	G3582
Chondroitin sulphate A sodium salt	Sigma-Aldrich	9082-07-9
Citric acid monohydrate	Sigma-Aldrich	C7129
Collagen solution from bovine skin	Sigma-Aldrich	C4243
Collagen solution from rat tail	Sigma-Aldrich Würzburg University	C3867
3,3'-Diaminobenzidine (DAB) + substrate chromogen system	Dako	K3468
Digitonin	Sigma-Aldrich	D5628
Dimethyl sulfoxide (DMSO)	Sigma-Aldrich	67-68-5
ELISA stop solution for TMB	Abcam	Ab171529
Eosin in alcoholic solution	Sigma-Aldrich	HT1101132
Ethanol (EtOH)	Sigma-Aldrich Fluka	64-17-5
Ethidium homodimer	Sigma-Aldrich	46043
1-ethyl-3-(3-dimethylaminopropyl) carbodiimide (EDC)	Sigma-Aldrich	25952-53-8

Ethylenediaminetetraacetic acid (EDTA)	Sigma-Aldrich	E7889
Fetal bovine serum (FBS)	Sigma-Aldrich	F9665
FibriCol® purified bovine collagen solution 10 mg/mL	Advanced Biomatrix	5133
Fibrinogen from human plasma	Sigma-Aldrich	F3879
Fibronectin	Sigma-Aldrich	F2006
Formalin, buffered solution 10%	Sigma-Aldrich	HT501128
Keratinocyte growth factor (KGF)	Sigma-Aldrich	K1757
L-Glutamine solution	Sigma-Aldrich	G7513
Glutaraldehyde solution 25%	Sigma-Aldrich	111-30-8
Granulocyte-macrophage colony-stimulating factor (GM-CSF)	Sigma-Aldrich	G5035
Goat serum	Sigma-Aldrich	017k8414
Harris HTX hematoxylin	Histolab	01800
Heparin	Roth	
Hydrochloric acid (HCl)	Sigma-Aldrich	7647-01-0
Hydrocortisone	Sigma-Aldrich	H0888
N-hydroxysuccinimide (NHS)	Sigma-Aldrich	6066-82-6
Insulin from porcine pancreas	Sigma-Aldrich	I5523
Interferon-γ (IFN-γ)	Miltenyi Biotec	130-096-484
Interleukin 4 (IL-4)	Miltenyi Biotec	130-093-922
DL-Isoproterenol hydrochloride	Sigma-Aldrich	I5627
Lipopolysaccharide (LPS)	Sigma-Aldrich	L7770
Lymphoprep™	Stemcell Technologies	07811
Macrophage colony-stimulating factor (M-CSF), recombinant human	Gibco	PHC9501
2-Mercaptoethanol	Sigma-Aldrich	63689
Paraformaldehyde (PFA)	Sigma-Aldrich	30525-89-4
Penicillin-Streptomycin-Neomycin solution stabilized	Sigma-Aldrich	P4083
Pepsin stabilized solution	Biosystems	pss060
Phosphate buffered saline (PBS)	Sigma-Aldrich	D8537
	Biochrom GmbH	L182-50
2-Propanol	Fisher Chemical	67-30-0
PureCol® type I bovine collagen solution 3 mg/mL	Advanced Biomatrix	5005
Rose Bengal	Sigma-Aldrich	198250

Roti®-Histokitt II	Roth	T160.2
L-Serine	Sigma-Aldrich	S4311
Sodium hydroxide (NaOH)	Sigma-Aldrich	1310-73-2
Thrombin from human plasma	Sigma-Aldrich	T4393
Tris(hydroxymethyl)aminomethane (TRIS)	Sigma-Aldrich	77-86-1
Trisodium citrate dihydrate	Sigma-Aldrich	S1804
Triton™ X-100	Sigma-Aldrich	9002-93-1
TrypLE™ Express	Gibco	12605-028
Trypsin/EDTA, 2.5%	Gibco	1509-046
Tween-20	Sigma-Aldrich	9005-64-5

3.2.   Buffers and solutions

Description	Composition
10x DMEM	D5648 medium from Sigma-Aldrich dissolved in 100 mL ddH$_2$O, filter sterile
Antibody dilution solution for IHC	5% goat serum in 0.3% Triton-X-100-in-PBS
L-Ascorbic acid-2-phosphate stock solution	50 mg/mL in ddH$_2$O, stored as single use aliquots at -20°C
Blocking solution for IHC	10% goat serum in 0.3% Triton-X-100-in-PBS
Blood stabilizing solution	2% FBS + 1mM EDTA in PBS
Calcium chloride solution	50 mM of calcium chloride dihydrate in ddH$_2$O, filter sterile, stored at 4°C
Calcium pantethonate stock solution	20 mg/mL in ddH$_2$O, stored at 4°C
L-Carnitine stock solution	0.1 M solution in ddH$_2$O, stored as single use aliquots at -20°C
L-Carnitine working solution	100 µM solution in ddH$_2$O, stored as single use aliquots at -20°C
Citrate buffer	For 150 mL: 3 mL of citric acid solution and 13.7 mL of trisodium citrate dihydrate solution in 133 mL ddH$_2$O. pH adjusted to 6.
Citric acid stock solution	21 g of citric acid monohydrate in 100 mL ddH$_2$O, stored at 4°C
Collagen-chondroitin-4-sulphate solution	5 w/v% collagen I and 0.05 w/v% chondroitin sulphate in 0.05 M acetic acid
DAB working solution	1 drop of DAB in each mL of buffer
Digitonin working solution	0.1% digitonin in PBS

DMEM 10x solution	Dissolve D5648 in 100 mL ddH$_2$O, filter sterile
EDC crosslinking solution	5 mM of EDC and 5 mM of NHS in ddH$_2$O
ELISA capture antibody solution	Capture antibody diluted 1:250 in ELISA coating buffer
ELISA coating buffer	Coating buffer diluted 1:10 in ddH$_2$O
ELISA diluent	ELISASPOT concentrated diluted 1:5 in ddH$_2$O
ELISA wash buffer	0.05% Tween-20 in PBS
Fibrinogen working solution	Dissolved in TBS by incubation at 37°C for 1 hour. Concentration measured with NanoDrop and adjusted to 10 mg/mL with TBS
Fibronectin stock solution	1 mg/mL in ddH$_2$O, stored as single use aliquots at -80°C
Fibronectin working solution	50 µg/mL in ddH$_2$O, stored as single use aliquots at -20°C
Formalin, buffered, working solution	Dilute to a concentration of 4% in ddH$_2$O
GM-CSF stock solution	10 µg/mL in ddH$_2$O, stored as single use aliquots at -80°C
Heparin	100 IU/mL in PBS
Hydrocortisone stock solution	1 mM solution in ddH$_2$O, stored as single use aliquots at -20°C
IFN-γ stock solution	0.1 mg/mL PBS, stored as single use aliquots at -80°C
IL-4 stock solution	0.1 mg/mL PBS, stored as single use aliquots at -80°C
Insulin stock solution	5 mg/mL in 5 mM HCl in ddH$_2$O, stored as single use aliquots at -20°C
DL-Isoproterenol hydrochloride stock solution	1 mM solution in ddH$_2$O, stored as single use aliquots at -20°C
KGF stock solution	10 µg/mL in PBS, stored as single use aliquots at -80°C
Live/dead staining solution	1 µM Calcein AM and 1 µM Ethidium homodimer in RPMI phenol-free medium
LPS stock solution	1 mg/mL in PBS, stored as single use aliquots at -80°C
Lysis buffer for RNA isolation	1 µL of 2-Mercaptoethanol each mL of RLT Buffer solution
MACS buffer	0.5% FBS + 2mM EDTA in PBS
M-CSF stock solution	100 µg/mL in ddH$_2$O, stored as single use aliquots at -80°C
MTS staining solution	1:10 solution in phenol-free RPMI medium
PFA working solution	4% PFA in PBS
Rose Bengal stock solution	1% in PBS
Rose Bengal working solution	1:10 dilution of the stock in PBS
L-Serine stock solution	2.5 M solution in ddH$_2$O, stored as single use aliquots at -20°C
Thrombin stock solution	20 IU/mL in 0.1% BSA-in- ddH$_2$O, stored at -20°C

Thrombin working solution	10 IU/mL, obtained by diluting the stock solution 1:1 in calcium chloride solution right before use
Tris-buffered solution (TBS)	50 mM Tris-Cl and 150 mM NaCl in ddH$_2$O, pH adjusted to 7.6
Trisodium citrate dihydrate stock solution	Dissolve 29.4g of trisodium citrate dihydrate in 100 mL ddH$_2$O, store at 4°C

3.3.   Cells

Cell type	Source and description
Primary dermal fibroblasts (HDF)	Human juvenile Caucasian single donor, isolated from foreskin CELLnTEC Advanced Cell Systems AG
Primary keratinocytes (HEK)	Human juvenile Caucasian single donor, isolated from foreskin CELLnTEC Advanced Cell Systems AG

3.4.   Cell culture media

Description	Basal medium	Supplements	Supplier
Cryo medium	CRYO Defined, Animal Component Free Freezing Medium CnT-CRYO-50	No supplements	CELLnTEC
3:1 keratinocyte seeding	3 parts DMEM D5546, 1 part F-12 Ham's N4888	5% FCS 1% PSN 2 ng/mL KGF 1 µM hydrocortisone 1 µM isoproterenol 0.1 µM insulin	
Skin differentiation medium 2	3 parts DMEM D5546, 1 part F-12 Ham's N4888	1.25% FCS 1% PSN 2 ng/mL KGF 1 µM hydrocortisone 1 µM isoproterenol 0.1 µM insulin 0.1 µM L-carnitine 0.01 M L-serine 50 µg/mL ascorbic acid-2-phosphate	

DMEM low glucose	D5546	1% L-Glutamine 1% PSN	Sigma-Aldrich
F-12 Ham's	N4888	1% L-Glutamine 1% PSN	Sigma-Aldrich
Skin differentiation medium 1	CnT-Prime Airlift, Full Thickness Airlift Medium CnT-PR-FTAL	No supplements	CELLnTEC
HDF medium	DMEM D5796	1% L-Glutamine 1% PSN 10% FBS	Sigma-Aldrich
HEK medium	Epithelial cell culture medium CnT-PR	No supplements	CELLnTEC
RPMI control medium	RPMI-1640 R0883	1% L-Glutamine 1% PSN 10% FBS	Sigma-Aldrich
Phenol free medium	RPMI-1640 R7509	No supplements	Sigma-Aldrich

3.5.   Antibodies

Antibody	Supplier	Catalog no	Concentration used
CD68, mouse IgG	Abcam	Ab955	1:100
Collagen IV, mouse IgM	Monosan	MON 4006	1:20
Cytokeratin 10, rabbit IgG	Abcam	ab76318	1:2500
4',6-diamidino-2-phenylindole (DAPI)	Sigma-Aldrich	28718-90-3	1:1000
Loricrin, rabbit IgG	Abcam	ab176322	1:250
Phalloidin Alexa Fluor® 546	Invitrogen	A22283	1:500
Vimentin, rabbit IgG	Abcam	ab92547	1:250

3.6. Primers

Gene	Primer name	Sequence 5' → 3'
Glyceraldehyde-3-phosphate dehydrogenase	GAPDH-forward	AGTCAGCCGCATCTTCTTTT
	GAPDH-reverse	CCAATACGACCAAATCCGTTG
C-C chemokine receptor type 7	CD197-forward	GTGGTTTTACCGCCCAGAGA
	CD197-reverse	CACTGTGGTGTTGTCTCCGA
C-X-C motif chemokine 10	CXCL10-forward	CAGTCTCAGCACCATGAATCAA
	CXCL10-reverse	CAGTTCTAGAGAGAGGTACTCCTTG
C-C motif chemokine 22	CCL22-forward	GCGTGGTGTTGCTAACCTTC
	CCL22-reverse	CCACGGTCATCAGAGTAGGC
Mannose receptor C type 1	CD206-forward	GCTACCCCTGCTCCTGGTTT
	CD206-reverse	CGCAGCGCTTGTGATCTTCA

3.7. Kits

Description	Supplier	Catalog number
Cell Proliferation ELISA, BrdU for quantification of proliferation	Roche	11647229001
Human IL-6 ELISA for quantification of IL-6 in cell culture supernatant	Invitrogen	88-8086-86
Human IL-8 ELISA for quantification of IL-8 in cell culture supernatant	Invitrogen	88-7066-76
ImmPRESS™ HRP Anti-Mouse IgG (Peroxidase) Polymer Detection Kit, made in Goat	Vector	MP-7452
iQ™ SYBR® Green for gene expression quantification	Bio-Rad	170-8882
iScript™ cDNA Synthesis kit for synthesis of cDNA from RNA	Bio-Rad	170-8891
MACS Pan Monocyte Isolation Kit, human	Miltenyi Biotec	130-096-537
RNeasy® Micro Kit for isolation of RNA from cell lysates	Qiagen	74004

3.8.   Laboratory equipment

Device/Material	Model	Supplier
Aluminium foil		Carl Roth
Automated wounding device	ARTcut® ICP3020	Fraunhofer-Institut für Silicatforschung ISC
Balance	AE200 MT5	Mettler Toledo
Biopsy punch	2 mm ø – BPP20F 8 mm ø – BP80F	Kai medical
Brushes	Various dimensions	KreatiVPinsel
CASY cell counting device	Model TT	Innovatis
Cell culture flasks	25 cm^2 - 90026 75 cm^2 - 90076 150 cm^2 - 90151	TPP Techno Plastic Products AG
Cell scraper	TPP 99003 and 99010	TPP Techno Plastic Products AG
Cell strainers	30 µm – 130-110-315	Miltenyi Biotec
Centrifuges	Sigma 2-16k 5804 R 5810 R 5424 5417 R	Kühner Eppendorf Eppendorf Eppendorf Eppendorf
Conical centrifugation tubes	15 ml – 91115 50 ml - 430829	Corning
Counting chamber	Neubauer	Marienfeld
Coverslips, glass	24x50 mm - 631-0146 24x40 mm - 631-0145 24x32 mm - 631-0143	VWR
Cryovials	Cryo tube 20, 89020	TPP Techno Plastic Products AG
Combitips advanced®	1 mL - 0030089430 5 mL - 0030089456 10 mL - 0030089464	Eppendorf
Compression stamps and rings in Teflon	Custom-made	Empa
Confocal laser scanning microscope	LSM 780	Carl Zeiss Microscopy

Dako pen	S2002	Dako
Disposable bags, autoclavable	759705	Brand
Embedding cassettes	81-0025-00 81-0022-00 81-0026-00	Biosystems Switzerland AG
Embedding station	Shandon Histocentre 3	Thermo Scientific
Freeze drier	Beta 1-16	Christ
Gloves	Sempercare nitrile 0121	Sempermed
Ice machine	Micro-cube ice	Kibernetik AG
Incubator	Hera cell 240	Thermo electron corporation
Laminar flow clean bench	Scanlaf Safe 1800	Vitatek
MACS MS separation columns	130-042-201	Miltenyi Biotec
Magnetic stirrer	MR 3000 INAMAG® RET-GS Rotamix SHP-10	Heidolph Janke & Kunkel GmbH Tehtnica
Metal weights for compression	Custom-made	Empa
Microscopes	Microvert Axiocam 105 color Keyence with objective VH-Z100R DM4000 B LED	Zeiss Keyence Leica
Microscopy slides	Superfrost Plus	Thermo Scientific
MilliQ water dispenser	Chorus 1 Analytics	ELGA Labwater
Mini section dryer	JAX-0300-00A	CellPath
Multi-channel pipettes	Various	Eppendorf
Multi-well plate reader	Mithras^2 LB943	Berthold Technologies
Multi-well plates	12 wells – 92012 12 wells – 665180 12 deep well - 665110 24 wells – 92024 96 wells – 92096 96 wells, clear high bind bottom Multiplate®for PCR – MLL9601	TPP Techno Plastic Products AG Greiner bio-one Greiner bio-one TPP Techno Plastic Products AG TPP Techno Plastic Products AG Corning® Costar® Bio-Rad
Multi-channel reservoir	21012	SPL Lifesciences
NanoDrop Spectrophotometer	ND-1000	Thermo Fischer
OctoMACS™ Separator	130-042-109	Miltenyi Biotec
Paraffin dispenser	47311	Medax
Paraffin tissue floating bath	24900	Medax

Parafilm®	Different formats	Parafilm
Pen, ethanol resistant	52877-310	VWR
Petri dishes	Different formats	Greiner bio-one
pH meter	744	Metrohm
Pipette aids	CellMate II	Matrix
	Pipetus	Hirschmann
	Pipetgirl	Vitaris
Pipettes	Various models (0.1 µL -5 mL)	Eppendorf
	Multipette® M4 - 4982000012	
Power supply	Power Pac 200	Bio-Rad
Reaction tubes	0.2 mL – 0030124.332	Eppendorf
	0.5 mL – 0030121.023	
	1.5 mL – 0030120.086	
	5 mL – 0030119.401	
Reservoir	Different Formats	VWR
Scanning electron microscope (SEM)	Hitachi S-4800	Hitachi High-Technologies
Scratch wound mask	Custom-made, in Teflon	Empa
Serological pipettes	2 mL - 710183	Greiner bio-one
	5 mL - Stripette® 4487	Corning® Costar®
	10 mL - Stripette® 4488	Corning® Costar®
	25 mL - Stripette® 4489	Corning® Costar®
	50 mL - Stripette® 4490	Corning® Costar®
Shaker	MS 3 digital	IKA® works, Inc.
Spatulae	Teflon-coated	Vomm
Sponges for embedding cassettes	47-1061-00	Medite Service AG
Syringe, monouse	5 mL – 62.4717	Codan
	20 mL – 4200-000V0	Henke-Sass Wolf GmbH
	50 mL – 62.8426	Codan
Syringe filter, sterile	SFM33PE0022S	Cobetter Lab
Thermal cycler	C1000™ with CFX96™ Real-time system	Bio-Rad
ThinCert™ cell culture Inserts	24 well – 662630	Greiner bio-one
	12 well - 665630	
Timer	Various models	Hanhart
Tips	Various volumes (0.1 µL -5 mL)	Eppendorf
	Filter tips maximum recovery™	Axygen

Tissue processor	STP 120	Thermo Fischer
Transfer pipets	Various formats	Falcon, Corning®
Transwell® permeable supports	12 Well - 3462	Corning® Costar®
Tweezers	Various models, Teflon-coated	Vomm
Vacuum pump	Mini-Vac E1	Ch.horni
Vortex mixer	VWR Mixer Mini Vortex 12620-848	VWR
Water bath	Typ P73 - 1019116871	Julabo Labortechnik GmbH

3.9.   Software

Software	Source
Adobe Illustrator CS6	Adobe Systems Incorporated, San Jose, USA
Adobe Photoshop CC 2014	Adobe Systems Incorporated, San Jose, USA
Endnote 7	Clarivate Analytics, Philadelphia, USA
GraphPad Prism 7	GraphPad Software, San Diego, USA
Kaluza Analysis Software	Beckman Coulter, Indianapolis, USA
Microsoft Office Standard Edition 2010	Microsoft, Redmond, USA
Pal PC	Isel, Eichenzell, Germany
ZEN 2012 (blue and black edition)	Carl Zeiss AG, Oberkochen, Germany
MikroWin Version 5.19	Berthold Technologies GmbH, Bad Wildbad, Germany
CFX Manager Software Version 2.1	Bio-Rad, Hercules, USA

Chapter 4:
Methods

4.   Methods

4.1.   Cell culture

4.1.1.   Cell thawing

Frozen cell vials were briefly warmed with gentle swirling in a water bath set at 37°C until just melted, and the content was quickly transferred in 10 mL of pre-warmed medium. To remove the excess of dimethyl sulfoxide (DMSO), the tube was centrifuged at 200xg for 5 minutes, the supernatant discarded and pellet resuspended in fresh pre-warmed medium. Primary human dermal fibroblasts (HDF) were seeded at a density of 1'000 cells/cm^2, while primary human juvenile keratinocytes (HEK) were used at a density of 4'000 cells/cm^2, as recommended by the supplier.

4.1.2.   Cell isolation

Primary monocytes were isolated from peripheral blood of healthy blood donors with obtained informed consent and approval from the local ethical committee (BASEC Nr PB_2016_00816). To prevent coagulation, freshly drawn blood was mixed with heparin to a final concentration of 25 IU/mL. Heparinized blood was first diluted 1:1 in blood stabilizing solution, and then carefully layered on top of Lymphoprep™ in 15 mL conical tubes. 9 mL of diluted blood were placed on top of 5 mL Lymphoprep™. The tubes were carefully transferred to a centrifuge and centrifuged at 800xg for 30 minutes, to separate the various blood components within the Lymphoprep™. After centrifugation, the white blood cell fraction was visible as a white ring between the plasma components and the Lymphoprep™. The white ring was carefully collected, transferred to new tubes and washed twice with PBS to avoid carryover of solvents into the following steps. To purify and enrich the monocytic population, specific negative selection was performed using the MACS Pan Monocyte Isolation Kit, according to the manufacturer's instructions. In brief, the cell suspension was divided in 1.5 mL tubes, resuspended in MACS buffer, then Fc blocking solution and a biotin-antibody cocktail were added and the suspension was incubated for 5 minutes at 4°C. The biotin-antibody cocktail is composed of monoclonal antibodies against antigens that are not expressed on human monocytes, to label all the non-monocytic populations. After dilution of the antibody in MACS buffer, anti-biotin MicroBeads were added to the samples, mixed thoroughly and incubated at 4°C for 10 minutes. Anti-biotin MicroBeads are conjugated to monoclonal anti-biotin antibodies that bind to the labeled cells of the previous step. After a washing step in MACS buffer, the cell suspension was transferred in MACS columns placed in an OctoMACS™ Separator, to perform magnetic separation. By flowing through a magnetic field, the labeled non-monocytes are

retained in the column, while the unlabeled cells flow through the column and can be collected. After magnetic separation, purified monocytes were counted with a Neubauer chamber and seeded at a density of 62'000 cells/cm^2 in RPMI control medium supplemented with 20 ng/mL of M-CSF (macrophage colony-stimulating factor) to promote cell survival. For investigating the effects of CSFs on macrophage polarization, the monocyte-to-macrophage differentiation was alternatively performed in RPMI control medium supplemented with 20 ng/mL of granulocyte-macrophage colony-stimulating factor (GM-CSF), 20 ng/mL M-CSF + 20 ng/mL GM-CSF or 20 ng/mL M-CSF + 2 ng/mL GM-CSF. Medium was changed after 3 days, placing the non-adherent cells back in culture after centrifugation, and differentiated cells were used at days 6.

4.1.3.   Cell cultivation

HDF were cultured in HDF medium and used up to passage 8. Confluent cells were detached by incubation with trypsin/EDTA for 5 minutes. HEK were cultured in HEK medium and used up to passage 6. Sub-confluent cells were detached by incubation with Accutase® for 8 minutes.

4.1.4.   Cell counting

After detachment, cells were collected in a falcon tube and 100 µL of the suspension was added to 10 mL of Casyton solution for counting. 400 µL of the suspension were counted with Casy, and a measurement was considered valid when the counts/mL value was between 3000 and 8000. Each cell type had a specially designed counting protocol in respect of the different cell dimensions. For macrophages, counting was performed with a Neubauer chamber. 10 µL of the cell suspension were mixed with 10 µL of Trypan blue and loaded into the chamber. The calculation of viable cells was performed as follows:

$$\frac{\text{total viable cells counted}}{\text{n° squares counted}} * \text{dilution factor} * 10^4 * \text{V of the cell suspension}$$

4.1.5.   Cell freezing

For freezing, harvested cells were counted with Casy. After centrifugation at 200x*g* for 5 minutes, the supernatant was discarded and the pellet resuspended in cold Cryo medium with a concentration of 2 million cells/mL. According to the manufacturer's instructions, 1 mL of the suspension was quickly transferred in each cryotube to store vials with 1 million cells each, and the tubes were placed at -80°C in a controlled rate freezing box. After 24 hours, the vials were transferred in liquid nitrogen for long-term storage.

4.1.6.   Macrophage polarization

6 days after monocytes isolation, differentiated macrophages were detached by incubation in TrypLE™ Express for 20 minutes, followed by gentle scraping with a cell scraper. The enzyme was neutralized with warm PBS, and the collected cells were counted with a Neubauer chamber. After a centrifugation step for 5 minutes at 200xg, macrophages were seeded at a density of 95'000 cells/cm^2 in 24-wells plates. For M1 polarization, RPMI control medium was added with 100 ng/mL lipopolysaccharide (LPS) and 20 ng/mL interferon-γ (IFN-γ), while for M2 polarization medium was supplemented with 20 ng/mL IL-4. Cells were incubated for 24 hours prior to RNA isolation.

For the conditioned media experiments, macrophages were seeded at a density of 95'000 cells/cm^2 in 12-wells plates, and a Transwell® insert containing a skin equivalent was placed in each well to allow paracrine signaling between skin tissue and immune cells. Polarization medium was prepared as previously explained in this paragraph, and 2 mL were added to each well and incubated for 24 hours prior to RNA isolation.

4.2.   Scratch wound assay

For scratch wound assay, cells were seeded in 24-wells plates according to the densities indicated in "4.1.1 Cell thawing" and cultured until confluency was reached. Before scratch formation, each well was marked with a pen on the outer part, to have a reference position for image capture. On the day of scratching, the lid of the plate was removed and a sterile custom-made scratch wound mask was positioned on the plate. Scratches were performed using a sterile pipette tip for 20-200 µL pipets. The tips were placed in the upper end of the guided apertures of the mask until the bottom was reached, then with application of constant pressure the tip was guided until the lower end of the mask. The tip was replaced every third well to avoid carryover of cell debris in the following wells. After scratching, wells were washed 3 times with warm sterile PBS, and then supplemented with pre-warmed medium containing the substance under investigation. Different drugs were added to the medium for evaluation, namely calcium pantothenate (20-120 µg/mL), hyaluronic acid with different molecular weights (low, high and a mixture of low and high, 0.1-0.5%), ascorbic acid-2-phosphate (10-20 µg/mL), betulin (4-8 µM), epigallocatechin-3-gallate (20-50 µM) and hepatocyte growth factor (20-50 ng/mL), all known to influence cell migration. Control samples were only supplemented with medium. Pictures were taken right after wound implementation and then 5 hours after scratching, using the pen marks as references to monitor cell migration in the same position over time. Cell migration was measured by analyzing the images with ImageJ, by manually selecting the wound area and measuring scratch

area. Wound area closure was calculated as percentage closure at the analyzed time point (t1) from the initial time point (t0):

$$\frac{A_{t0} - A_{t1}}{A_{t1}} \%$$

4.3.   Immunohistochemistry

CD68 (Cluster of Differentiation 68) marker was selected to specifically stain macrophages. CD68 is expressed by all cells in the monocytic lineage including macrophages, and is located in the cell membrane as it is a transmembrane glycoprotein. Macrophages were fixed for 10 minutes in 4% paraformaldehyde, permeabilized in 0.2% Triton-X 100 in PBS for 15 minutes, and blocked for 60 minutes in 1% bovine serum albumin (BSA). CD68 antibody was diluted 1:100 in 0.1% BSA, and samples were incubated in the solution overnight at 4°C. On the following day, the secondary antibody Alexa Fluor® 488 conjugate was incubated for 1 hour as a 1:500 dilution in 0.1% BSA. 4',6-diamidino-2-phenylindole (DAPI) was used to counterstain cell nuclei, supplemented as a 1:1000 solution in 0.1% BSA. Pictures were taken with LSM-780 confocal laser scanning microscope.

4.4.   Cell activity characterization

4.4.1.   MTS assay

HDF and HEK were seeded according to the densities indicated in "4.1.1 Cell thawing", and macrophages according to "4.1.6 Macrophage polarization" prior to viability evaluation, which was performed using CellTiter 96® AQueous One Solution Cell Proliferation (MTS) assay. After medium removal from the wells, 110 µL of MTS solution were added to each well and incubated for 2 hours at 37°C. Before measurement, the content of each well was mixed by thorough pipetting and 100 µL of the solution were transformed to a new multi-well plate. Absorbance was read at 490 nm with Mithras LB943 plate reader, and the blank values of the MTS solution were subtracted from each value. Data were normalized to cells cultured for 1 day in the respective cell type proliferation medium: RPMI control medium for macrophages, HDF medium for fibroblasts and in HEK medium for keratinocytes.

4.4.2.   Quantification of cell proliferation

Proliferation was measured with Cell Proliferation ELISA, BrdU according to the manufacturer's instructions. In brief, cells were incubated in presence of BrdU for 2 hours and fixed. DNA denaturation followed, then anti-BrdU POD conjugated antibody was supplemented to the wells to bind to the labeled cells. Detection of the immune complexes was performed by adding the substrate solution, and the

reaction product was quantified by reading absorbance with Mithras LB943 plate reader. Data were normalized to cells cultured for 1 day in the respective cell type proliferation medium: RPMI control medium for macrophages, HDF medium for fibroblasts and in HEK medium for keratinocytes.

4.5.   Gene expression analysis

4.5.1.   RNA isolation

RNA isolation was performed using the RNeasy Micro Kit according to the manufacturer's instructions. In brief, cells were lysed with a guanidine-isothiocyanate buffer supplemented with β-mercaptoethanol, and then homogenized by high-speed centrifugation through a biopolymer-shredding column. RNA was purified by specific binding to the silica-membrane of RNeasy MinElute spin columns and consecutive washings steps in increasing ethanol-containing buffers. A purification step with RNase-free DNase was performed to digest unwanted genomic DNA contamination, then total RNA was eluted in RNase-free water. RNA concentration and purity were measured with NanoDrop spectrophotometer, and RNA was stored at -80°C until use.

4.5.2.   cDNA synthesis

Total RNA isolated from macrophage cultures was reverse-transcribed using iScript™ cDNA synthesis Kit, with a starting concentration of 150 ng of RNA per sample and a volume of 15 μL per reaction mix. The thermal cycler was set to the following transcription protocol: 5 minutes at 25°C followed by 30 minutes at 42°C and 5 minutes at 85°C. The obtained cDNA was then diluted 5 times in water and used as a template for gene quantification, or alternatively it was stored at -20°C for later use.

4.5.3.   Reverse transcriptase-polymerase chain reaction

Gene expression quantification was performed with the iQ™ SYBR® Green Supermix. Primers were added at a concentration of 10 μM and the final reaction volume was adjusted to 15 μL with RNase-free water. The thermal cycler was set to 95°C for 3 minutes, followed by 39 cycles of 10 seconds at 95°C and 30 seconds at 57°C. The final steps were performed at 95°C for 10 seconds, at 65°C for 5 seconds, and then at 95°C. Glyceraldehyde 3-phosphate dehydrogenase (GAPDH) was used as a reference gene, and the analyzed markers were C-C chemokine receptor type 7 (CD197), C-X-C motif chemokine 10 (CXCL10), mannose receptor C type 1 (CD206) and C-C motif chemokine 22 (CCL22). Calculations for

the quantification were performed using the $2^{-\Delta\Delta CT}$ method, and always normalized to unstimulated cells cultured in RPMI control medium.

4.6.   Skin model generation

4.6.1.   Scaffold preparation and evaluation

To generate the freeze-dried scaffolds, at first the collagen or collagen-chondroitin-4-sulphate solutions were frozen at -20°C or -80°C overnight. The material was then placed in a Beta 1-16 freeze dryer overnight, setting the temperature value to 12°C and pressure to 0.85 mbar. The obtained sponges were imaged with scanning electron microscopy (SEM). To this end, a biopsy punch of 2 mm diameter was used to cut samples, which were then fixed on adhesive sample holders and sputtered with 7 nm gold/palladium. SEM imaging was performed with a Hitachi S-4800 SEM with an accelerating voltage of 2 Kv. For crosslinking, the freeze-dried scaffolds were cut with a biopsy punch of 10 mm diameter. Chemical crosslinking was performed by placing the samples in 24 wells plates and submerging them with the 1-ethyl-3-(3-dimethylaminopropyl) carbodiimide (EDC) crosslinking solution. The scaffolds were incubated for 4 or 12 hours at room temperature and then washed with ddH$_2$O for 3 times, each step leaving in immersion for 1 hour. For dehydrothermal (DHT) crosslinking, the samples were placed for 24 hours at 50 mTorr and 105°C.

For the evaluation of different dilutions of FibriCol®, the collagen solution was either used at the supplied 10 mg/mL concentration or diluted in 0.01 M HCl to final concentrations of 7.5, 5 and 3 mg/mL prior to seeding. Compressed collagen scaffolds were prepared by first neutralizing PureCol® collagen into ThinCert™ inserts, which was then incubated at 37°C for 1 hour to allow polymerization. Lateral compression was performed by positioning a Teflon ring with a diameter of 1 mm on top of each gel, then adding culture medium and incubating overnight. On the following day, the Teflon ring was carefully removed with the use of a sterile tweezer and medium was changed. Confined compression was performed with a custom-made setup manufactured in Empa. First, a Teflon compression stamp, designed to precisely fit in a ThinCert™ insert, was positioned on top of the gel. The stamp was then progressively loaded with metal weights of 50 g each, one added after 1 minute, another after 2 minutes and the last after 3 minutes, for a total compression weight of 150 g and 5 minutes of compression time. The Teflon compression stamp was designed to obtain a fixed final gel height of 1 mm, and the water removed during compression was absorbed by filter paper positioned below the ThinCert™ insert.

4.6.2. Dermis preparation

Prior to seeding, the freeze-dried scaffolds were sterilized with a UV lamp for 30 minutes on each side. The collagen sponges were then pre-incubated with HDF medium for 1 hour, following removal of the solution for seeding. HDF were detached and counted, and then resuspended in HDF medium at a concentration of 3 million cells/mL. Freeze dried scaffolds were seeded with 25 μL of the cell suspension and incubated for 30 minutes at 37°C. Then, 2 mL of HDF medium were added below the insert and 1 mL inside the insert and the construct was cultured for 7 days, with a medium change every 2-3 days. For samples prepared using pure collagen, the solution was first neutralized and added with cells as shown in table 1. The proportions of the components to be mixed enclosed 8 parts of collagen, 1 part of 10x DMEM and 1 part with all other components, which included the cell suspension, NaOH for pH neutralization and water. Everything was kept on ice to prevent premature gel formation. After mixing, pH was measured with filter paper indicators and eventually adjusted with NaOH to obtain a value between 7 and 7.5. For the final skin model culture protocol, 400 μL of the solution were seeded in each insert, while for the initial experiments different volumes were tested (300-750 μL) and calculations were adjusted respecting the 8:1:1 component ratio. After seeding, plates were incubated for 60 minutes at 37°C to allow gel formation. After collagen polymerization, 2 mL of HDF medium were added in the well and 500 μL inside the insert, then the gels were cultured in submerged conditions for 7 days, with a medium change every 2-3 days.

Table 1. Dermal compartments seeding mixture.

Component	Parts	Volume for 1 sample of 400 μL
Collagen I gel	8	320 μL
10x DMEM	1	40 μL
0.5 M NaOH	1	7.5 μL
Cell suspension		25 μL
ddH$_2$O		7.5 μL
Final volume		400 μL

4.6.3. Epidermis preparation

Prior to HEK seeding, medium was removed from the dermal compartments and 50 μL of the fibronectin working solution were added on top of each gel. After incubation for 30 minutes at 37°C, the dermal compartments were washed 3 times with sterile PBS. Sub-confluent HEK were detached and

counted, centrifuged and resuspended at a concentration of 2.5 million cells/mL in HEK medium. 100 µL of the suspension was seeded on top of each dermal compartment, and the plate was transferred at 37°C for 30 minutes to enhance cell adhesion. 2 mL of 3:1 keratinocyte seeding or skin differentiation medium 1 were then added in the well and 400 µL inside the insert, and the construct was cultured for 5 days, with a medium change every 2-3 days. After 5 days in submerged culture conditions, where medium is added both in the wells and in the inserts, samples were raised to air-liquid interface. For this, medium was removed and the inserts containing the skin models were transferred to deep 12-well plates. 4 mL of skin differentiation medium 1 or skin differentiation medium 2 was added below each insert and culture was performed for further 14 to 21 days, with a medium change every 4 days.

4.7.   Skin wound formation

4.7.1.   Samples preparation

Before biopsy punch wounding, an acellular collagen hydrogel was prepared to be placed below the wounded skin equivalents right after wound formation. The acellular gel served as a scaffold for keratinocyte and fibroblast migration into the wound area, as full-thickness wounds result in the exposure of the cells to the Transwell® polyester membrane. Acellular collagen gels were prepared respecting the 8:1:1 ratio of the components as in "4.6.2 Dermis preparation", with the cell suspension volume being replaced with cell culture medium. 300 µL of the suspension were transferred to each insert, and incubated at 37°C for 1 hour to allow polymerization. After biopsy punch wound formation, the samples were removed from the insert and transferred on top of new Transwell® containing the acellular collagen gel and placed back in culture.

4.7.2.   Biopsy punch wounding

For creation of full-thickness wounds, a biopsy punch of 2 mm diameter was employed. First, the skin equivalents were removed from the inserts by cutting the Transwell® polyester membrane and placing the tissue on a sterile petri dish. The biopsy punch was then pressed through the skin sample until the bottom of the petri dish was reached. With the application of pressure and a small rotational movement, the circular portion of tissue enclosed in the biopsy punch was removed from the skin model, creating a full thickness wound. With the use of a sterile spatula and tweezers, all Teflon-coated to prevent tissue adhesion to the instruments, the wounded skin was placed on top of the acellular collagen gel or a macrophage-containing gel. Unwounded skin control samples were also transferred on top of gels and placed back in culture.

4.7.3.   ARTcut® automated wounding

The ARTcut® wounding machine, developed by Fraunhofer-Institut für Silicatforschung ISC, has been designed to generate wounds in an automated setting, as it consists of a computer-driven drill which coordinates are set by the user. By placing a multi-well plate containing the skin equivalents into the sample holder and setting the wounding coordinates in the Pal PC software, the drill introduces a wound in the center of each insert. Additionally, ARTcut® is equipped with a laser and a camera in correspondence of the drill tip (figure 4). The camera records the generation of wounds into the samples, while the laser enables the detection of the sample surface. Prior to wounding, ARTcut® was switched on and the desired wounding parameters were inserted into the Pal PC software. This included depth of wounding and number of samples to be wounded. While medium was removed from the plates and samples were placed in a new 12 wells plate, the inner chamber of the machine was UV-treated for 30 seconds to sterilize the environment. The plate was then placed into the ARTcut® plate holder, the lid was removed and the door of the machine was closed (figure 4). Drill speed was set to 20'000 rpm per minute, and a drill tip of 2 mm in diameter was used. Wound depth was assessed independently for each experiment by first wounding one single sample, in order to determine the required depth value for generating partial thickness wounds. After wound formation, samples were washed 3 times with PBS to remove tissue debris from the wound area. The wounded skin equivalents were then re-transferred into deep well plates and placed back in culture. Alternatively, wounded samples were transferred on top of macrophage-containing gels for immunocompetent skin wound model generation.
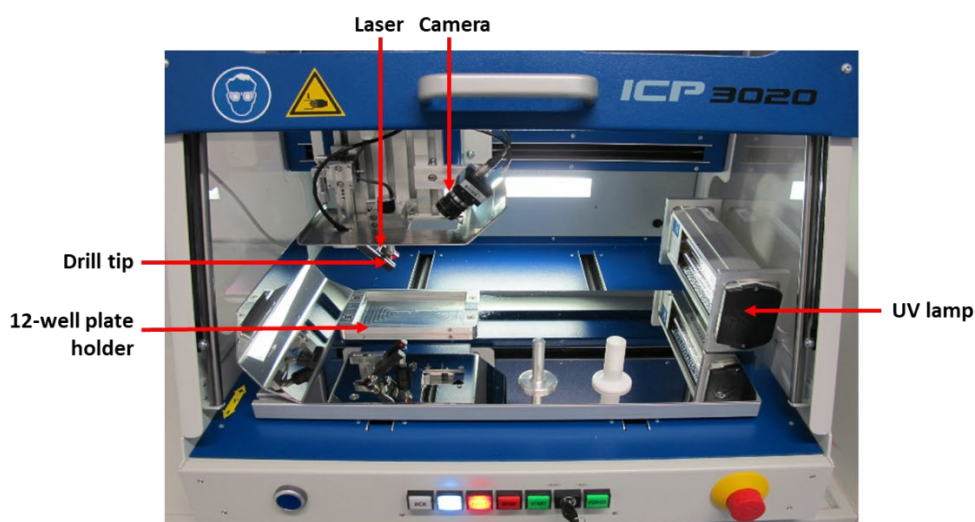
Figure 4. Overview of the mechanical components of the ARTcut® automated wounding machine, displayed with the main door opened.

4.7.4.   Fibrin hydrogel preparation

In vivo wound healing involves the migration of cells along a fibrin matrix to close the wound area and restore the injured tissue. To mimic the process and provide cells with a support for migration, a fibrin hydrogel was placed in the wound area. The components to generate fibrin hydrogels were mixed in a sterile Petri dish by first adding 50% of the volume with the fibrinogen working solution, then 30% of the volume with TBS or the desired drug concentration and the remaining 20% with the thrombin working solution. The solution was mixed by gentle pipetting up and down 4 times, then 2-5 µL were added to the wound area. The volume needed to fill the wound area depended on the wound size, as biopsy punch wounds had a bigger area than ARTcut®-implemented wounds.

4.8.   Immune compartment culture

4.8.1.   Macrophage 3D embedding

For embedding of macrophages in 3D gels, cells were first harvested and counted as indicated in "4.1.4 Cell counting". A cell suspension of 5 million cells/mL was then prepared in RPMI control medium. Cell encapsulation in collagen hydrogels followed the same procedure used for the dermal compartment preparation described in "4.6.2 Dermis preparation", with a difference in the final volume of each gel, which was here set to 300 µL. The neutralized collagen seeding suspension was transferred to each insert, and incubated at 37°C for 1 hour to allow polymerization. For viability assessment, gels were cultured in RPMI control medium, skin differentiation medium 1 or skin differentiation medium 2 for 7 days, with a medium change every 2-3 days. For polarization, media were supplemented with cytokines as described in "4.1.6 Macrophage polarization" and stimulated for 24 hours before analysis.

4.8.2.   Vertical invasion assay

To assess the migration ability of macrophages within collagen gels, vertical invasion assay was performed. Before cell seeding, acellular collagen hydrogels were prepared respecting the same procedure described in "4.6.2 Dermis preparation", with the cell suspension volume being replaced with cell culture medium. 150 µL of the seeding suspension was transferred to each 24-well insert, and incubated at 37°C for 1 hour to promote gel formation. Before cell seeding, the gels were supplemented with RPMI control medium, skin differentiation medium 1 or skin differentiation medium 2, adding 700 µL in the well and 100 µL inside the insert. Macrophages were harvested and counted, and a cell suspension of 4 million cells/mL was prepared in RPMI control medium. 25 µL of the cell suspension

were added to each insert on top of the gel and samples were incubated for 48 hours prior to migration assessment.

4.8.3.   Imaging of 3D-embedded macrophages

For 3D-embedded macrophages visualization, the collagen gels containing the immune cells were stained with live/dead assay, according the manufacturer's instructions. Medium was removed, the staining solution was added inside and below the inserts and the samples were incubated at 37°C for at least 1 hour. After 3 washes in PBS, pictures were taken immediately with LSM-780 confocal laser scanning microscope. For each sample, 3 images at different gel positions were taken. Viability quantification was performed using ImageJ software, manually counting living and dead cells.

4.9.   Wound healing assessment

4.9.1.   Wound imaging

Macroscopic imaging of the wounded skin equivalents was performed at days 1, 3 and 7 after wound formation with a Keyence stereomicroscope. To better visualize the wound area, some samples were stained with Rose Bengal prior to imaging. Rose Bengal is a dye that cannot penetrate into mature skin due to the impermeability of the stratified epithelium, enabling to clearly distinguish the wound area from the surrounding mature epithelium. For staining, Rose Bengal working solution was added on top of the wounded skin equivalents and incubated for 5 minutes. After 3 washes in PBS, each with a duration of 5 minutes, skin samples were imaged with a Keyence stereomicroscope. For confocal imaging, live/dead staining solution was added on top of the skin equivalents and samples were incubated at 37°C for 1 hour. Optical Coherent Tomography (OCT) was performed by Prof. Simon Pot at the department of veterinary ophthalmology, University of Zürich.

4.9.2.   Cytokine quantification

The evaluation of the inflammatory response after wound formation was assessed through pro-inflammatory cytokine secretion quantification. Skin cultures supernatants were collected 24 and 72 hours after wound formation, which included a medium change at 48 hours. For this, skin culture supernatants were first mixed thoroughly by pipetting up and down 10 times, then 1 mL was transferred into a 1.5 mL tube. To remove eventual cellular debris that could interfere with the quantification, medium was centrifuged for 5 minutes at 200xg, then supernatants were carefully transferred to new tubes and stored at -80°C for later measurements. The day before ELISA quantification, 96 multi-well plates

with clear, high bind bottom were coated with the capture antibody solution, sealed and placed over-night in a humid chamber at 4°C. On the following day, wells were blocked in ELISA diluent for 1 hour, washed with ELISA wash buffer and then duplicates of samples and standards were added to the wells. Skin samples supernatants were first diluted in culture medium to adjust the cytokine concentration to the detection range of the respective kits. For hIL-6 ELISA, samples were diluted 1:250, while for hIL-8 ELISA a dilution of 1:400 was performed. Samples were incubated for 2 hours, followed by 4 washes in ELISA wash buffer and addition of the detection antibody for 1 hour. After 4 washes, avidin-HRP was added, other 6 washes followed and the 1x TMB solution was supplemented for color development. The solution was incubated for 15 minutes, then ELISA stop solution was added and the values were read immediately at 450 nm with a Mithras LB943 plate reader, using as reference wavelength 570 nm. For calculations, 570 nm values were subtracted from the 450 nm ones, and the values of the medium blank controls were subtracted from each sample. Interleukin concentrations were obtained according to the values of the standard curves, multiplying the samples values for the dilution factor.

4.10.   Histology and immunohistochemistry

4.10.1.   Paraffin embedding

For visualization of skin structure, samples were first fixed in 4% formalin overnight. Paraffin embed-ding followed, or alternatively the samples were stored in a 50% EtOH for later processing. For paraffin embedding, at first dehydration was performed by incubation in increasing ethanol concentrations, followed by xylene and paraffin incubation steps, all performed under stirring conditions (table 2). Samples were cut in half and embedded in paraffin blocks using an embedding station.

Table 2. Steps for the embedding of fixed samples in paraffin, performed with a tissue processor.

Solvent	No of steps	Duration of each	Stirring
50% EtOH	1	1 hour	70 rpm
70% EtOH	1	1 hour	70 rpm
80% EtOH	1	1 hour	70 rpm
96% EtOH	1	1 hour	70 rpm
100% EtOH	3	1 hour	70 rpm
Xylene	3	90 min	70 rpm
Paraffin	2	90 min	60 rpm

4.10.2.   Hematoxylin and eosin staining

For H&E staining, 5 µm thick sections were cut from paraffin-embedded samples using a manual rotary microtome. Tissue sections were placed on glass slides, incubated at 60°C for 30 minutes and then at 37°C for at least 2 hours to remove eventual water drops interposed between the tissue and the glass slide. Prior to H&E staining, samples were deparaffinized and dehydrated through sequential immersion in xylene, decreasing concentrations of ethanol and water. Then, staining was performed and samples were dehydrated (table 3). Mounting was performed by using Roti-Histokitt II as mounting medium, and slides were let dry overnight.

Table 3. Steps for eosin and hematoxylin staining of paraffin-embedded tissue.

	Solvent	No of steps	Duration of each step
Deparaffinization	Xylene	2	10 min
Rehydration	100% EtOH	2	2 min
	96% EtOH	1	2 min
	90% EtOH	1	2 min
	80% EtOH	1	2 min
	70% EtOH	1	2 min
	ddH$_2$O	1	5 min
Staining	Hematoxylin	1	5 min
	Running tap water	1	8 min
	Eosin	1	30 sec
Dehydration	ddH$_2$O	1	2 min
	70% EtOH	1	2 min
	80% EtOH	1	2 min
	96% EtOH	1	2 min
	100% EtOH	1	2 min
	2-Propanol	1	2 min
	Xylene	2	2 min

4.10.3.   Immunohistochemistry

To detect the expression of specific markers in the *in vitro* skin equivalents, immunohistochemistry was performed. Prior to the staining, the slides were deparaffinized and rehydrated as in "4.10.2 Hematoxylin and eosin staining", then an antigen retrieval step was performed for some of the antibodies, as indicated from the manufacturer. Enzymatic antigen retrieval with pepsin was performed prior to CD68 and collagen IV staining, by incubating the slides with the stabilized pepsin solution for 5 minutes at 37°C. Heat-mediated antigen retrieval was performed prior to staining with cytokeratin 10, and also on human skin control samples before staining with loricrin. The process consisted in the immersion of samples in citrate buffer, which was then incubated at 70°C for 1 hour. Two washes in PBS, each of 10 minutes, followed, then the slides were placed in a humid chamber and incubated with blocking solution for 1 hour. The primary antibody diluted at the appropriate concentration in antibody diluent was added and the slides were incubated at 4°C overnight. On the following day, the slides were washed 3 times in PBS, each with a duration of 10 minutes. An anti-host peroxidase-conjugated secondary antibody diluted 1:100 in antibody diluent was added to the slides and incubated for 1 hour at room temperature. To develop CD68 staining, ImmPRESS™ HRP Anti-Mouse IgG kit was used. For the other samples, development was performed with the 3,3'-Diaminobenzidine (DAB) working solution. DAB was incubated from 30 seconds to 30 minutes until visible color development, then slides were washed for 3 times in PBS, each time for 10 minutes. Counterstaining was performed by incubation in hematoxylin for 1 minute, then dehydration and mounting were performed as in "4.10.2 Hematoxylin and eosin staining".

4.11. Statistics and data analysis

The GraphPad software was used to plot all obtained data. For evaluation of pro-inflammatory cytokines secretion in fibrin-filled wounds, an unpaired t test was used, while one-way ANOVA was employed for scratch wound assay analysis. Data obtained from 3D-embedded macrophages polarization and migration and the monocyte-to-macrophage differentiation data set were analyzed using a Kruskal-Wallis test, with a Dunn post-hoc test for multiple comparisons, assuming a non-parametric distribution. For all other data, a two-way ANOVA with a Sidak or Tukey post-hoc test for multiple comparisons was used. Statistical significance was assumed at $p < 0.05$.

Chapter 5:
Results

5. Results

5.1. *In vitro* skin generation

5.1.1.   Collagen scaffolds for *in vitro* skin culture

A key feature of *in vitro* skin wound equivalents is the standardization of the models, to allow the evaluation of wound closure in reproducible settings. As it is well known that collagen gels tend to shrink in culture [121,122], we evaluated different approaches to prevent excessive contraction of the samples for skin wound model generation. Different collagen sources and concentrations were evaluated either without modifications or treated with diverse methods to improve mechanical stability, including freeze-drying, crosslinking, blending with glycosaminoglycans and compression (table 4). The obtained scaffolds were evaluated macroscopically for contraction and with histological analyses for assessing the formation of a mature skin structure.

When collagen was neutralized, mixed with cells and directly seeded in Transwell® inserts ("no treatment" groups), low concentration gels (starting density: 3 mg/mL) resulted in strong and uneven contraction of the constructs over time, independently of the collagen source (figure 5A). At higher concentrations (starting density: 10 mg/mL), collagen isolated from rat tail did not form gels after incubation at 37°C, while FibriCol® generated samples with reduced contraction.

The application of lateral compression on collagen gels generated with neutralized low-density collagen solutions resulted in less pronounced and more uniform contraction (figure 5B), when compared to uncompressed samples generated with the same collagen material (figure 5A). A mature skin structure was also detected (figure 5C), however the appearance of the gels was heterogeneous, showing a non-uniform compression on the sides of the material and a variable final thickness of the scaffold (figure 5D). The application of confined compression on collagen gels generated with neutralized low-density collagen solutions showed the generation of more reproducible samples (figure 5E). Despite the application of a high weight load on fibroblasts embedded in the gel already before compression, the formation of a mature skin structure was observed (figure 5F), and macroscopically the gels showed a uniform final thickness and low variability between samples (figure 5G). However, this approach generated samples with a low thickness of ≈100 µm, which represents a limitation for the wounding process, as it involves gel manipulation and transfer.
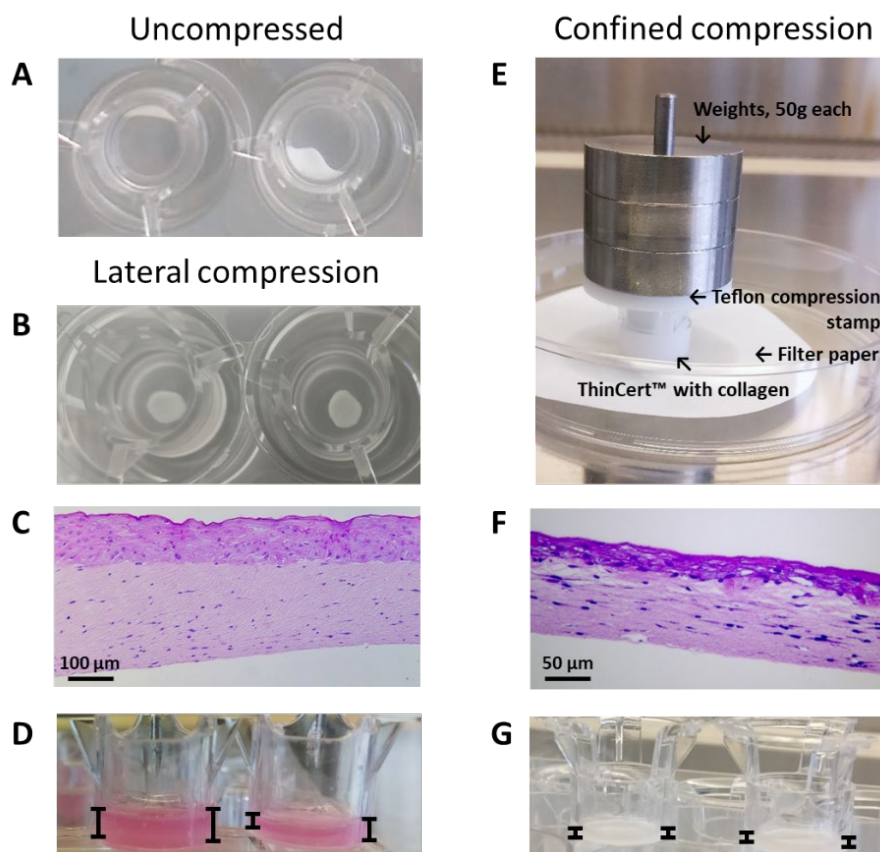
Figure 5. Evaluation of lateral and confined compression on collagen scaffolds for reduced contraction of skin equivalents. *In vitro* skin was generated by using a neutralized 3 mg/mL collagen solution as scaffold. Representative images of (A) uncompressed samples and (B) laterally compressed sample appearance after 2 weeks of air-lift culture. (C) H&E staining of skin equivalents cultured in a laterally compressed collagen scaffold after 2 weeks of air-lift culture. Scale bar: 100 µm. (D) Lateral view of laterally compressed collagen gels right after compression. Black lines indicate the heterogeneous final thickness of samples and the formation of an uneven surface within each gel. (E) Overview of the confined compression method setup with all its components. (F) H&E staining of skin equivalents cultured in a confined compressed collagen scaffold after 2 weeks of air-lift culture. Scale bar: 50 µm. (G) Lateral view of confined compressed collagen gels right after compression. Black lines indicate the homogeneous final thickness of samples. N=3.

The analysis of freeze-dried collagen gels showed the formation of porous structures for all evaluated materials, with pore sizes being dependent on the freezing temperature (figure 6). However, once sterilized and employed for dermal compartment seeding, the scaffolds contracted and eventually dissolved in the culture medium after 1 week of culture in all conditions tested. Thermal crosslinking or chemical crosslinking with EDC, as well as blending of collagen with chondroitin-4-sulfate did not enhance scaffold stability, as no difference between these samples and pure collagen freeze-dried samples was detected (data not shown).

Rat tail collagen, isolated	Rat tail collagen, commercial	Bovine collagen, commercial
Freezing T: -20°C	Freezing T: -80°C	Freezing T: -80°C
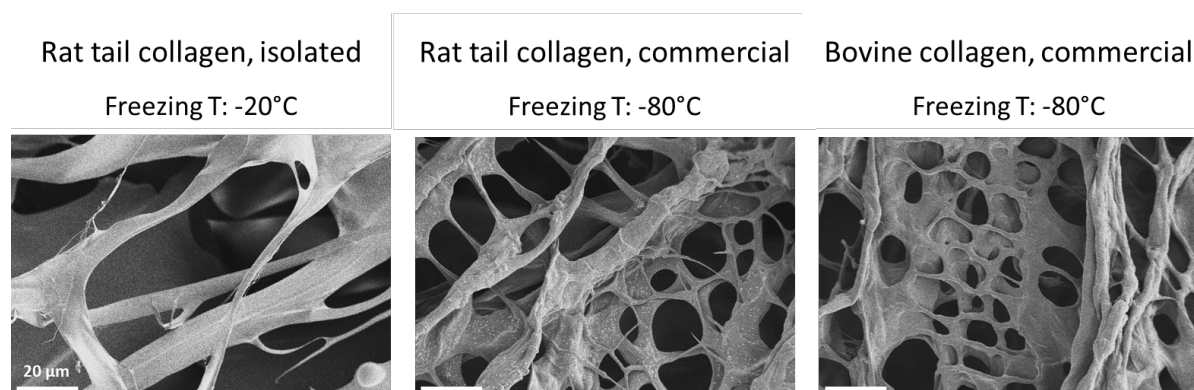
Figure 6. Evaluation of freeze-drying on collagen scaffolds with different origins for reduced contraction of skin equivalents. Representative SEM images of sponges obtained by freeze drying collagen solutions of different sources and at different temperatures. Scale bars: 20 μm. N=2.

Table 4. List of collagen materials and relative treatments employed as scaffolds for generation of skin models.

Material	Treatment	Observations
Bovine collagen, commercial (PureCol®) 3 mg/mL solution	No treatment	Contraction
	Freeze-drying (-20°C, -80°C) ± cross-linking (DHT, EDC) ± blending with chondroitin-4-sulfate	Contraction, dissolution
	Lateral compression	Heterogeneous, non-reproducible
	Confined compression	Reproducible, low thickness samples
Bovine collagen, commercial (FibriCol®) 10 mg/mL solution	No treatment	Limited contraction, higher reproducibility
	Freeze-drying (-20°C, -80°C) ± cross-linking (DHT, EDC) ± blending with chondroitin-4-sulfate	Contraction, dissolution
Bovine collagen, commercial 3 mg/mL solution	No treatment	Contraction
	Freeze-drying (-20°C, -80°C) ± cross-linking (DHT, EDC) ± blending with chondroitin-4-sulfate	Contraction, dissolution
Rat tail collagen, isolated 10 mg/mL solution	No treatment	No gel formation
	Freeze-drying (-20°C, -80°C) ± cross-linking (DHT, EDC) ± blending with chondroitin-4-sulfate	Contraction, dissolution
Rat tail collagen, commercial 3 mg/mL solution	Freeze-drying (-20°C, -80°C) ± cross-linking (DHT, EDC) ± blending with chondroitin-4-sulfate	Contraction, dissolution

Since the use of high concentrations of collagen resulted in less contracting samples and preserved scaffold thickness, different dilutions of FibriCol® ranging from 3-10 mg/mL were evaluated to identify the optimal collagen concentration for the *in vitro* skin culture. A concentration-dependent contraction of skin models was observed macroscopically, which was more pronounced in the samples with the lowest concentration of collagen (figure 7). The short culture time, which included 4 days in air-lift conditions, was not sufficient to allow for full epidermalization. However, all the evaluated collagen concentrations supported the formation of a multilayered epidermis (figure 7). Histological analysis also revealed that samples not only displayed horizontal contraction, which can be observed macroscopically, but also underwent vertical contraction, as a different tissue thickness was observed between samples (figure 7).
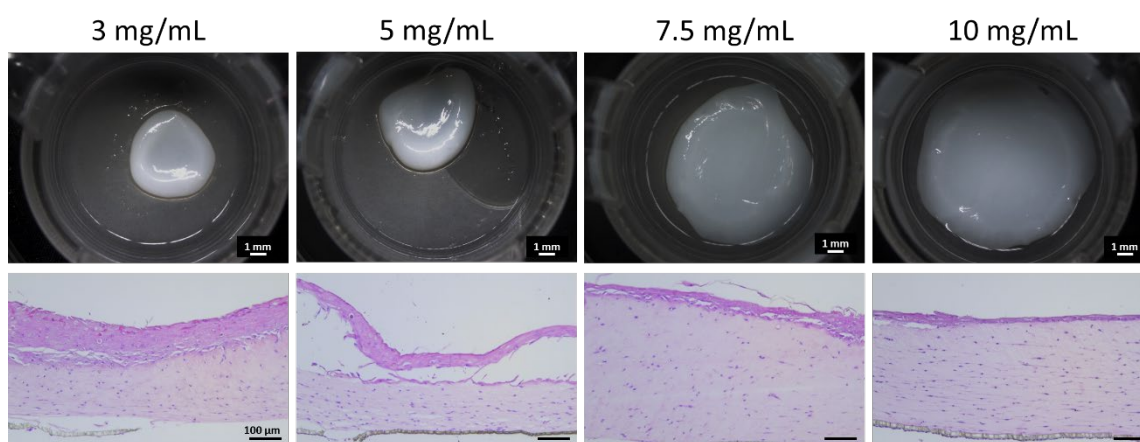
Figure 7. Evaluation of different collagen concentrations on the contraction and maturation of skin models. Different dilutions of the 10 mg/mL FibriCol® solution were neutralized and used as scaffolds for *in vitro* skin model culture. Samples were cultured for 4 days at air-lift culture, then stereoscopic images were taken and H&E staining was performed to evaluate tissue structure. Scale bars: upper row 1 mm, lower row 100 µm. N=2.

The culture of *in vitro* skin samples using FibriCol® as a scaffold indicated that an initial collagen concentration of 10 mg/mL generates the least contracting samples, however also resulted in a less stratified epidermis. To verify whether the dense collagen matrix allows nutrients to reach the epidermal layer promoting epidermalization, skin samples were generated by seeding different volumes of collagen in the Transwell® inserts and culturing the tissues at air-lift culture for 14 days. Histological analysis revealed that a mature stratified epithelium was formed independently of the initial collagen volume (figure 8). Therefore, the intermediate volume of 400 µL was selected to generate samples with suitable thickness and mechanical stability for wound healing application.
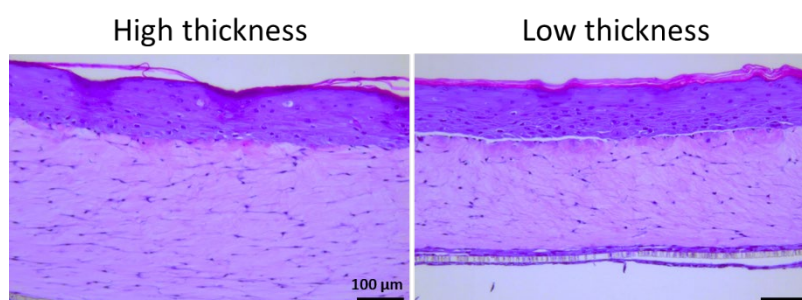
Figure 8. Evaluation of neutralized 10 mg/mL collagen scaffolds thickness on epidermal differentiation. Different volumes of the 10 mg/mL FibriCol® solution were used to culture skin models. High thickness: 500 μL/insert, low thickness: 300 μL/insert. After 14 days at air-lift culture, H&E staining of fixed samples followed. Scale bars: 100 μm. N=1.

5.1.2. Characterization of *in vitro* skin

To confirm the generation of fully mature *in vitro* skin models with the selected culture conditions, histology and immunohistochemistry (IHC) were performed on skin equivalents and compared to human skin samples. H&E staining revealed the presence of a stratified epithelium on top of a fibroblast-rich matrix, comparable to human skin structure (figure 9). IHC was also performed on these samples to check for skin-specific markers. The presence of a basement membrane between dermis and epidermis was confirmed by the positive collagen IV staining of *in vitro* skin equivalents (figure 9). Cytokeratin 10, an intermediate keratinocyte differentiation marker, and loricrin, a late keratinocyte differentiation marker, were also detected in *in vitro* skin (figure 9), confirming that the models possessed characteristics of a mature tissue that is comparable to human skin.
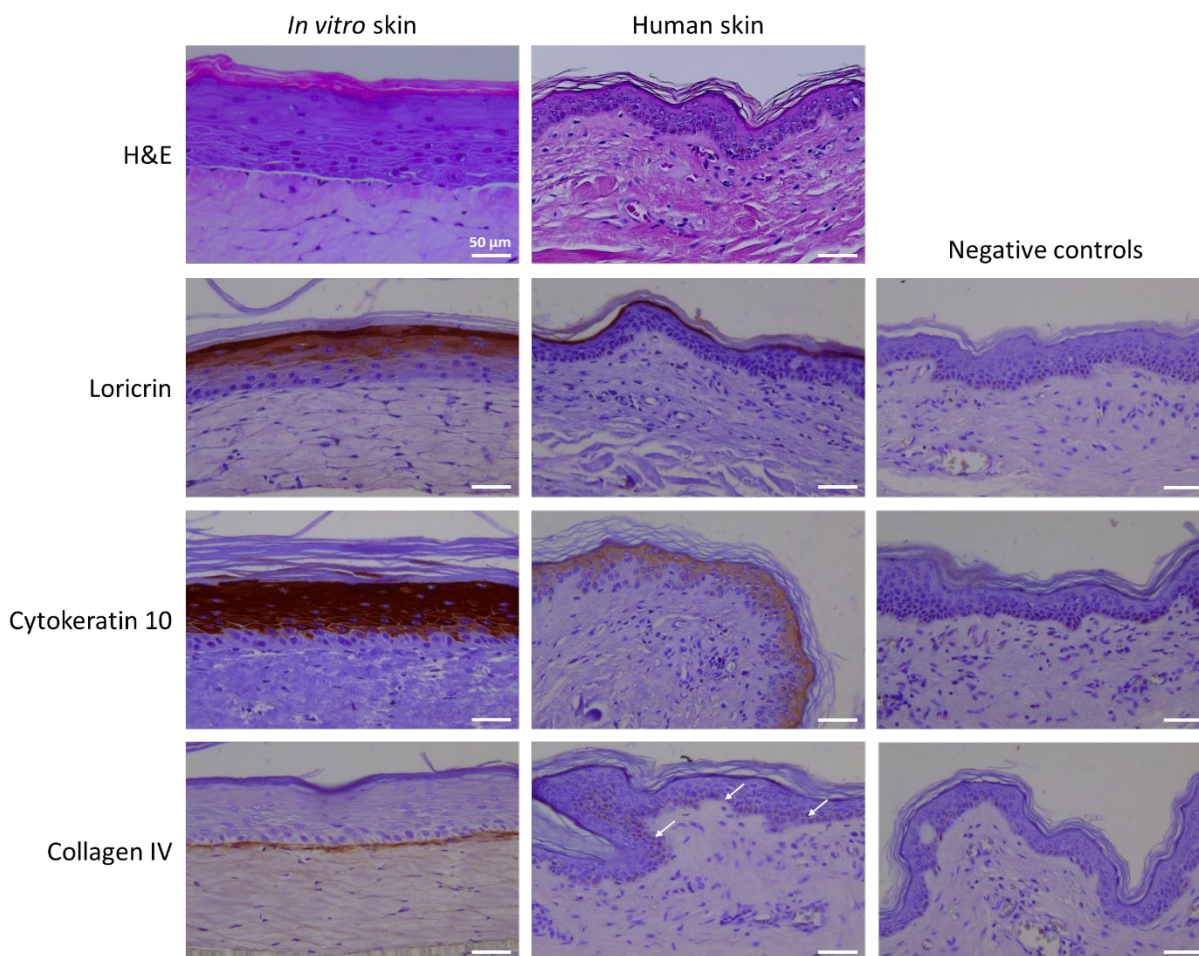
Figure 9. Evaluation of *in vitro* skin model structure in comparison with human skin. *In vitro* skin was generated by using a neutralized 10 mg/mL collagen solution as scaffold, and cultured at air-lift inter-phase for 14 days. Top row shows H&E staining, while other images display the expression of skin-specific markers upon IHC. Antibodies against loricrin, cytokeratin 10 and collagen IV were used, and the right-side images shows negative controls, only added with secondary antibody. White arrows indicate collagen IV positively stained cells in human skin samples. Scale bars: 50 µm.

The culture of *in vitro* skin showed the formation of a mature epidermis over time. However, differences were detected between experiments, as well as between samples generated within the same experiment (figure 10A). Although the terminal differentiation layer, the stratum corneum, was observed in all equivalents, in some cases the intermediate layers could not be detected after the histological processing (figure 10A). Additionally, different numbers of keratinocyte layers were detected in the epidermis (figure 10A). Skin thickness measurements also showed variations between samples, with an overall mean thickness of 350 µm and measures ranging from 200 µm to 450 µm (figure 10B).
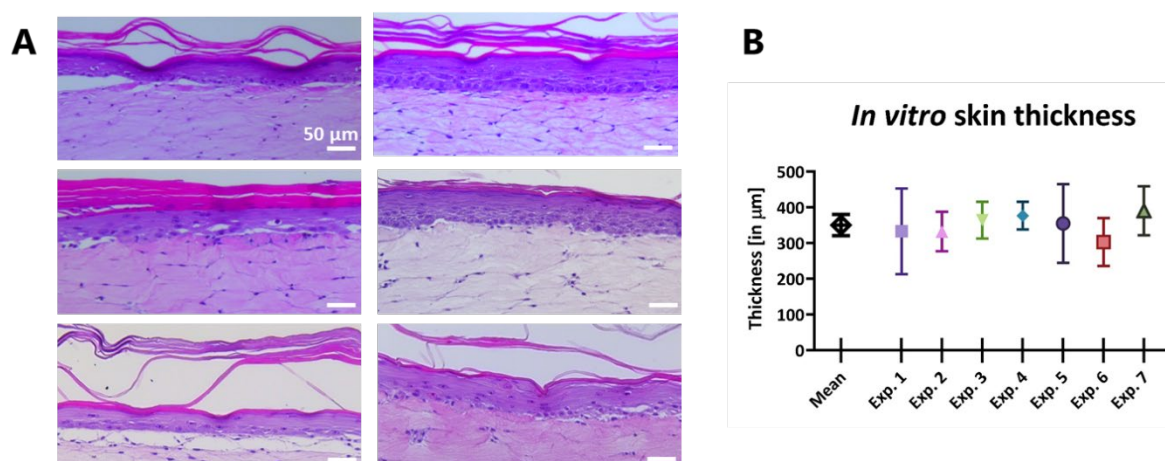
Figure 10. Evaluation of *in vitro* skin model reproducibility, in terms of structure and tissue thickness. *In vitro* skin was generated by using a neutralized 10 mg/mL collagen solution as scaffold, and cultured at air-lift interphase for 14 days. (A) Representative H&E staining of samples obtained from 6 independent experiments. Scale bars: 50 μm. (B) Skin sample thickness measurements performed on 7 independent experiments. The left value shows the mean thickness of all measurements performed, while other data points show the measures obtained for each experiment. Measurements were performed with ImageJ on 5 randomly chosen images per experiment, performing 3 measures each. Error bars represent standard deviation.

5.2.   *In vitro* wound healing assessment

5.2.1.   Wound implementation strategies

To generate reproducible wounds into skin models, two diverse wounding methods were evaluated, one being commonly used to implement full thickness wounds (biopsy punch) and one recently designed, involving the full automation of the process (ARTcut®). Macroscopically, wounds obtained with ARTcut® showed a reproducible circular shape, different from wounds implemented with biopsy punch that frequently acquired an elongated oval shape derived from the transfer of the sample in another Transwell® insert after wounding (figure 11A). However, the use of a biopsy punch to apply wounds involved extensive manipulation of the skin equivalents, often resulting in the detachment of the epidermis from the dermis (figure 11B). The implementation of wounds with the ARTcut® automated wounding device, conversely, involved less sample manipulation steps. The histological evaluation of samples wounded with ARTcut® revealed that, despite the wound shape was macroscopically more reproducible than biopsy punch-implemented wounds, the wounding process was heterogeneous with regard to wounding depth. Although the software settings instructed the generation of wounds with the same depth for all samples, some showed the implementation of full thickness wounds while others only presented a partially disrupted epidermis, thus implementing partial thickness wounds (fig-

ure 11C). Additionally, the removal of wounded tissue fragments was frequently incomplete, with detached tissue pieces being detectable in some of the samples in spite of the washing steps performed after wound formation (figure 11C).
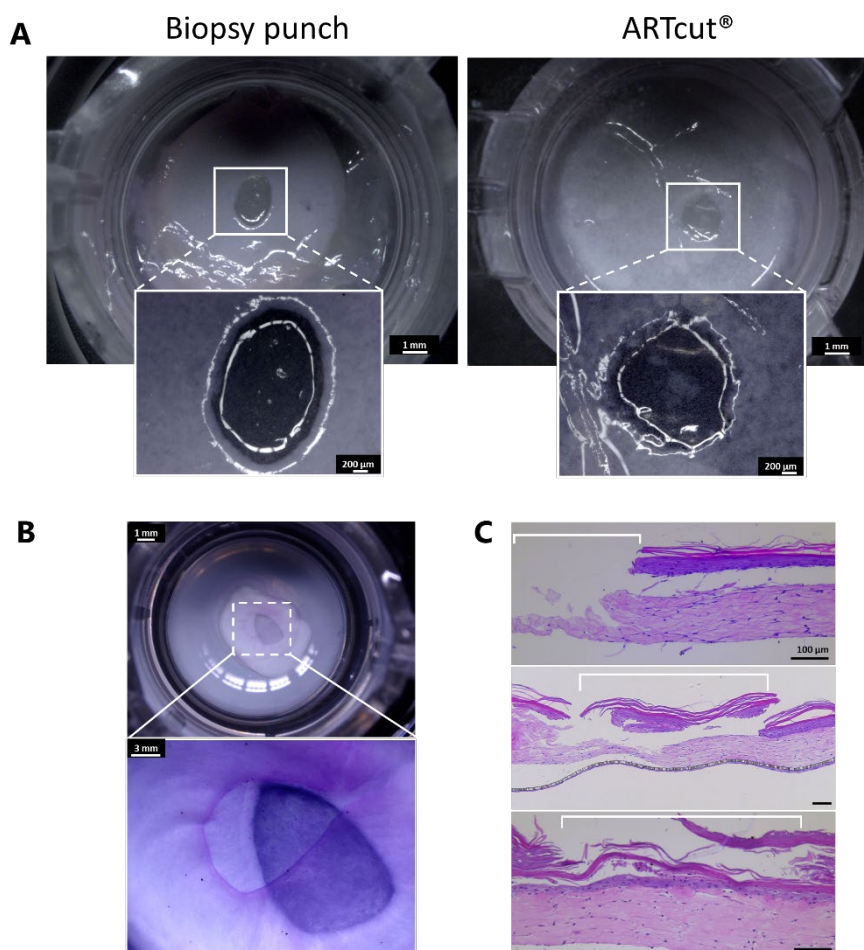
Figure 11. Evaluation of biopsy punch- or ARTcut®-implemented wounds. (A) Representative images showing the macroscopic appearance of wounds implemented with the two methods under investigation, 7 days after wound formation. Scale bars: upper images 1 mm, lower images 200 µm. (B) Rose Bengal staining of wounded skin after biopsy punch wound formation, showing disruption of the dermal-epidermal junctions and detachment of the epidermis. Scale bars: upper image 1 mm, lower image 3 mm. (C) Histological evaluation of ARTcut®-implemented wounds 1 day after wounding, upon H&E staining. Representative images of 3 independent experiments are displayed, all performed by setting the same wounding parameters in the ARTcut® software. White lines indicate the wound area. Scale bars: 100 µm. N=5 for biopsy punch wounding, N=10 for ARTcut® wounding.

5.2.2.   Drug carrier system for *in situ* wound delivery

The evaluation of drug effects on wound healing requires the use of a carrier system to precisely deliver the substance under investigation to the wound area, in order to assess its local effects instead of the systemic ones. A suitable drug carrier system should not interfere with the healing process, and as fibrin is a natural polymer contributing to wound healing during hemostasis, its effects on wound clo-

sure and response to inflammation were analyzed and compared to wounded samples where no material was added to the area. Fibrin polymerization occurred within seconds after mixing fibrinogen and thrombin but provided enough time to precisely place the hydrogel in the wound area. The hydrogel could be detected in the wound area by histological analyses up to 4 days after wounding (figure 12A) and then progressively degraded as a result of cellular activity. The evaluation of wound closure was initially assessed macroscopically, by analyzing wound images 1, 3 and 7 days after wound formation. Over time, the wound area turned from shimmering and transparent to opaque, demonstrating epithelial cell infiltration (figure 12B). The evaluation of wound closure in presence of fibrin was performed by manually measuring the diameter of the wound area from macroscopic images using ImageJ. In presence of fibrin, the wound area decreased to 58±11% after 4 days compared to the initial area measured at day 1, while wounds where no supplements were provided decreased to 64±11% (figure 12C). At day 7, the wound area was 37±12% in the fibrin-filled wound against 41±23% in wounds where no fibrin was added (figure 12C). No statistical significance was detected between groups.
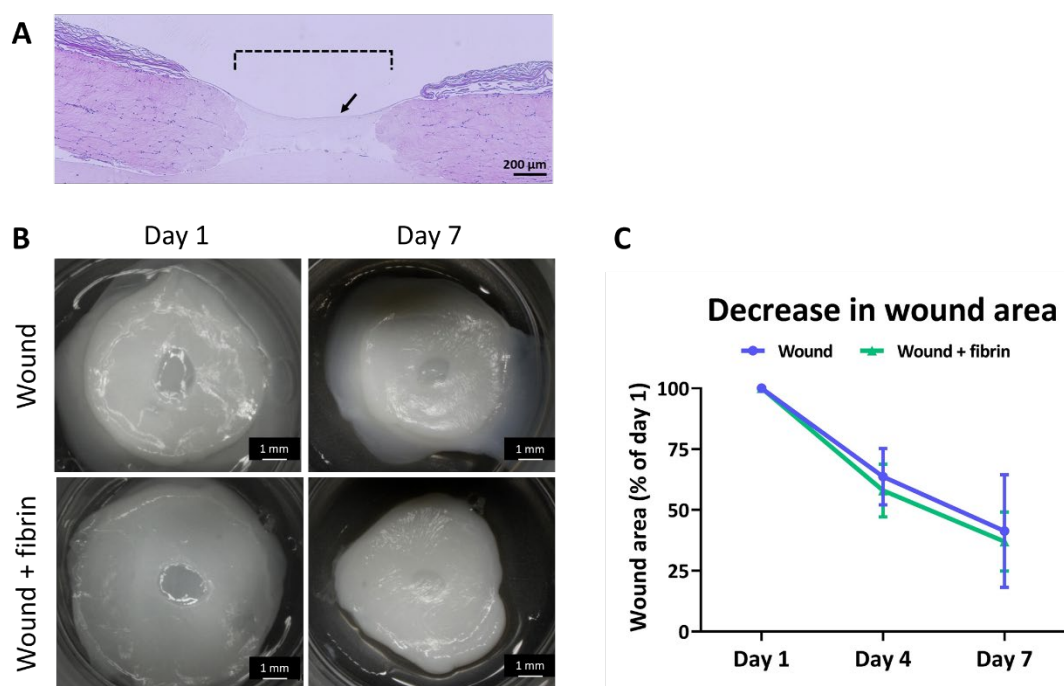
Figure 12. Evaluation of a fibrin hydrogel as carrier system to deliver drugs in the wound area. *In vitro* skin samples were wounded with a ⌀2 mm biopsy punch, and the wound area was either filled with a fibrin hydrogel ("Wound+fibrin") or left without supplements ("Wound"). (A) Representative image of a wounded skin model supplemented with fibrin, cultured for 4 days prior to H&E staining. The dashed line indicates the wound area, and the black arrow the fibrin hydrogel. Scale bar: 200 µm. (B) Macroscopic appearance of wounded skin samples 1 and 7 days after wound formation. Scale bars: 1 mm. (C) Quantification of wound closure, displayed as wound area decrease percentage 1, 4 and 7 days after wound formation. N=3, error bars represent standard deviation (two-way ANOVA, Sidak's multiple comparisons test).

Alternatively, cell migration into the wound area was assessed by means of confocal microscopy. Wounded skin samples displayed migration of epithelial cells into the wound area upon live/dead staining (figure 13A). The use of live/dead staining avoided fixation and embedding of samples, which could lead to disruption of the thin layer of migrating cells closing the wound during the initial phase of healing. Optical Coherent Tomography (OCT) represents another alternative for imaging wound closure in a real-time and non-destructive manner. Wounded skin samples imaged with OCT showed that detection of the dermal and epidermal layers was possible, despite the high thickness and non-transparency of the samples. Importantly, when monitoring the same samples over time, the migration of epithelial cells to close the wound area could be observed (figure 13B).
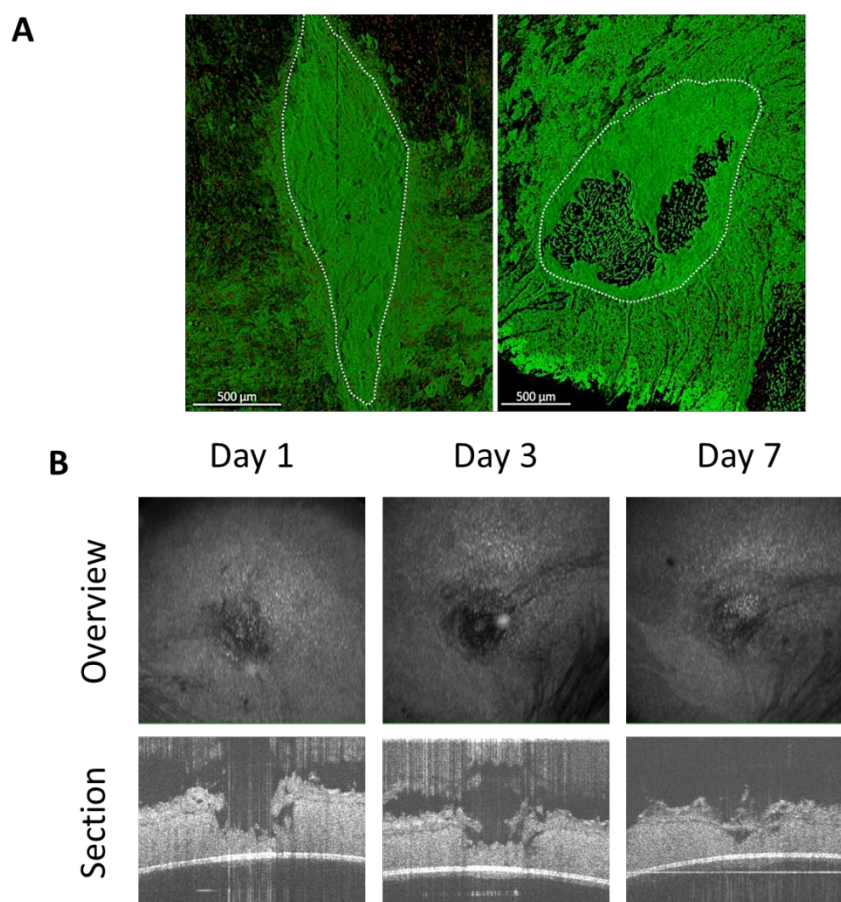
Figure 13. Assessment of wound healing with different imaging techniques. (A) Wounded skin samples were imaged with a confocal laser scanning microscope 7 days after wound formation and filling of the wound with a fibrin hydrogel, upon live/dead staining. Images are representative 3D reconstructions of 2x2 tile scans, and white sketched lines indicate the wound margins. Scale bars: 500 µm. (B) Wounded skin sample imaged with Optical Coherent Tomography (OCT) 1, 3 and 7 days after wound formation. The upper row shows an overview of the wounded skin sample, and the lower row displays sample cross-sections. Images were taken by Prof. Simon Pot at the department of veterinary ophthalmology, University of Zürich.

To assess whether fibrin triggered an inflammatory response in wounded skin equivalents, pro-inflammatory cytokines IL-6 and IL-8 were quantified in the supernatants. Wounded samples without fibrin in the wounds secreted 28±12 ng/mL of IL-6, against 29±12 ng/mL for fibrin-filled wounds (figure 14).

IL-8 concentrations were 95±16 ng/mL in wounds with no supplements, and 85±10 ng/mL in fibrin-filled wounds (figure 14). Notably, the secretion of IL-6 and IL-8 did not show any statistical significance between groups.
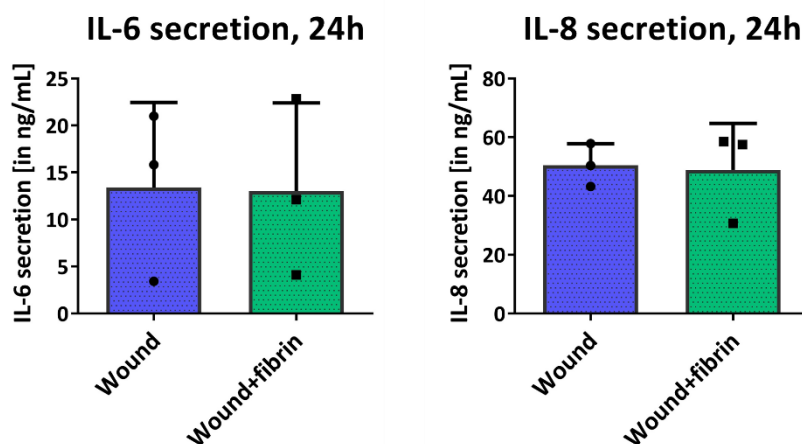
Figure 14. Evaluation of fibrin hydrogels effects on wounded skin inflammatory response. Wounded skin equivalents were wounded with a ⌀2 mm biopsy punch, and the wound area was either filled with a fibrin hydrogel ("Wound+fibrin") or left without supplements ("Wound"). 24 hours after wound formation, cell culture supernatants were collected and quantification of pro-inflammatory cytokines IL-6 and IL-8 was performed. N=3, error bars represent standard deviation (unpaired t test).

5.3. Parameters for immunocompetent skin generation

5.3.1. Primary macrophage implementation strategy

Primary blood monocytes were differentiated into macrophages prior to the incorporation in 3D collagen gels (figure 15A). Monocyte-to-macrophage differentiation was performed by supplementing the culture medium with M-CSF for 6 days. Compared to the day of isolation, when cells were only partially attached to the cell culture vessel surface, the majority of cells were adherent to the surface at day 6 and presented a spread and rounded morphology that is characteristic of macrophages (figure 15B). After monocyte-to-macrophage differentiation, cells were harvested and used for both 2D and 3D experiments. The evaluation of 3D embedded macrophages required the encapsulation of macrophages in collagen hydrogels, obtained with the same procedure employed for dermal compartment generation and also including the same number of cells per gel. Different volumes of neutralized collagen were employed for different experiments, however the number of macrophages seeded per gel remained constant. Cells were used for 3D gel generation only when viability after collection was above 80%. The encapsulation of macrophages in collagen hydrogels resulted in the homogeneous distribution of cells within the gel (figure 15C).
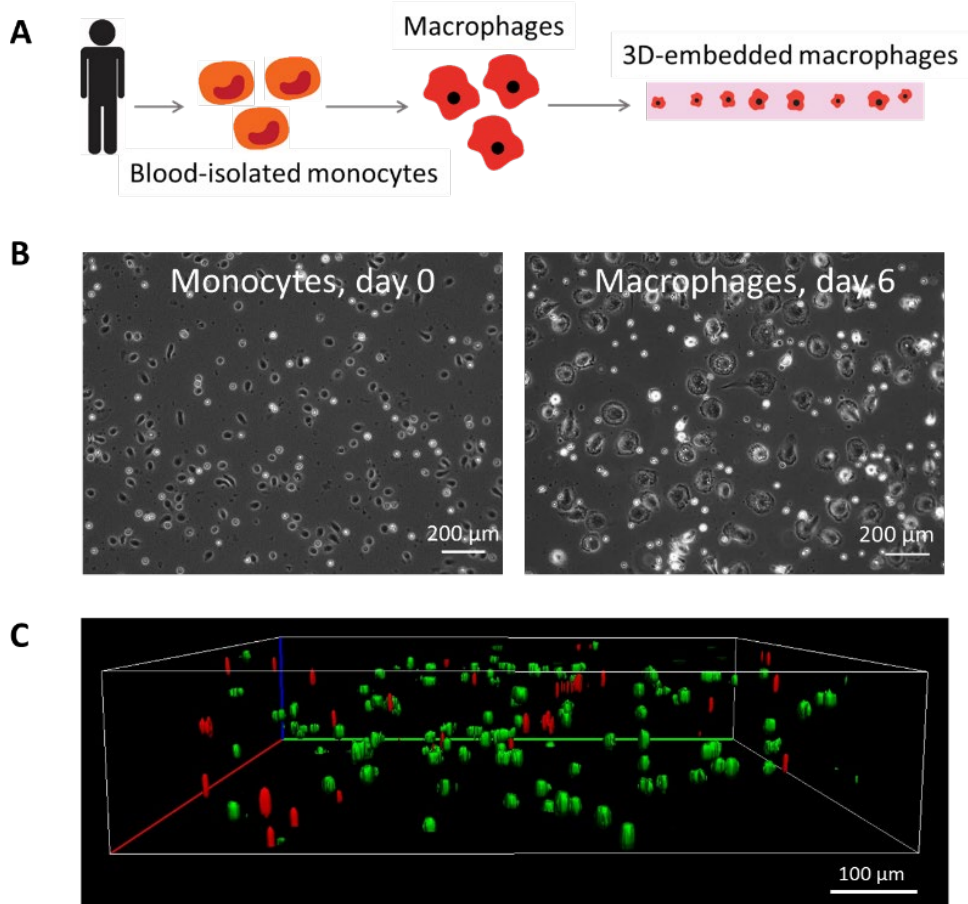
Figure 15. Embedding of primary macrophages in collagen hydrogels for immunocompetent skin models. (A) Visual schematic of the encapsulation procedure for blood monocytes-derived macrophages. (B) Morphology of primary blood-derived monocytes through the differentiation into macrophages. Monocytes were imaged right after isolation (day 0) and when differentiation into macrophages was completed (day 6). Scale bars: 200 µm. (C) Representative 3D reconstructed image of encapsulated macrophages imaged with confocal laser scanning microscope upon live/dead staining, 1 day after encapsulation. Scale bar: 100 µm.

5.3.2.   Culture medium for immunocompetent skin models

5.3.2.1.   The influence of medium on 2D cultures

The incorporation of immune cells in skin equivalents requires the use of a culture medium that is suitable for all cell types involved, namely fibroblasts, keratinocytes and macrophages. To identify a medium that supports immunocompetent skin culture, the effects of two skin differentiation media formulations ("Skin differentiation medium 1" and "Skin differentiation medium 2") and of macrophage medium ("RPMI control") were investigated in both 2D and 3D cultures.

To understand the influence of culture medium on the viability of single cell types, fibroblasts, keratinocytes and macrophages were cultured in RPMI control medium, skin differentiation media 1 and 2 for 7 days. Fibroblasts metabolic activity showed an increase over time for all conditions tested (figure 16). Culture in RPMI control medium presented higher metabolic activity values compared to skin differentiation media, in both combinations. Metabolic activity of primary keratinocytes showed increasing values over time in skin differentiation media, with the highest values detected in cells cultured in skin differentiation medium 1 at all time points. Conversely, RPMI control medium displayed decreasing values over time (figure 16). Macrophages viability showed a significant decrease in both skin differentiation media already after one day of culture, with values being similar for the two media. The values of both skin differentiation media were statistically significant at all time points analyzed compared to RPMI control medium (figure 16).
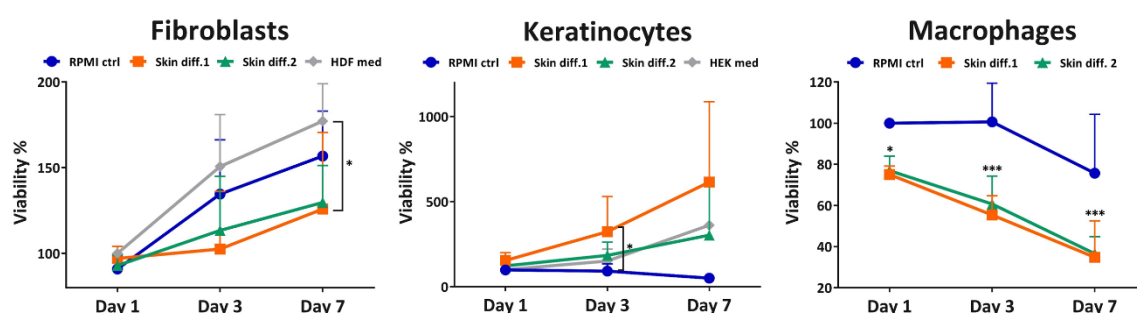
Figure 16. Metabolic activity of primary fibroblasts, keratinocytes and macrophages in the media under investigation. Cells were cultured in macrophage medium ("RPMI ctrl") and 2 formulations of skin differentiation media ("Skin diff. 1" and "Skin diff. 2") for 7 days, and metabolic activity was quantified at days 1, 3 and 7. Values were normalized to fibroblasts, keratinocytes or macrophages cultured for 1 day in HDF medium, HEK medium or RPMI ctrl, respectively. N=3 for fibroblasts and keratinocytes and N=5 for macrophages, error bars represent standard deviation (two-way ANOVA, Tukey's multiple comparisons test). Statistical significance is indicated with *p<0.05, ***p<0.001.

The proliferation of fibroblasts and keratinocytes in the media under investigation was also evaluated after 1, 2 and 3 days of culture. Fibroblast proliferation rates were higher in presence of skin differentiation medium 1, however no significant difference was detected between groups at any of the time points analyzed (figure 17). Similarly, keratinocytes showed increased proliferation in presence of skin differentiation medium 1, while culture in RPMI control medium resulted in lower values. Statistical significance was observed between skin differentiation medium 1 and RPMI control medium after 7 days of culture (figure 17).
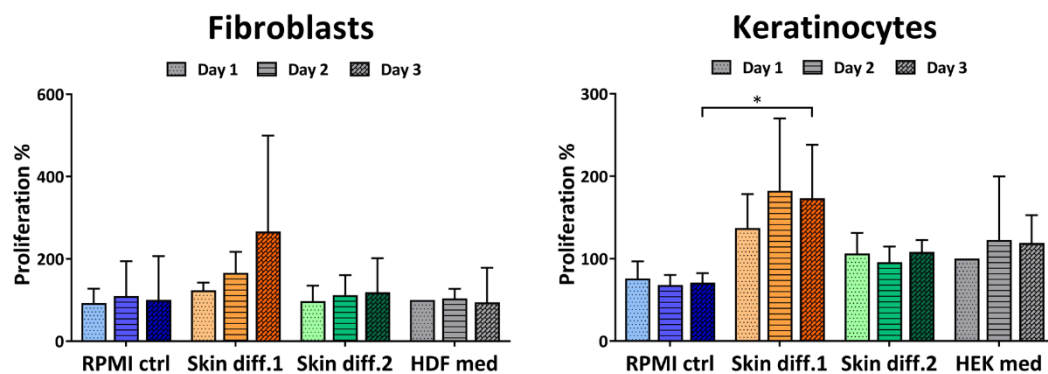
Figure 17. Proliferation rates of primary fibroblasts, keratinocytes and macrophages in the media under investigation. Cells were cultured in macrophage medium ("RPMI ctrl") and 2 formulations of skin differentiation media ("Skin diff. 1" and "Skin diff. 2") and proliferation was quantified after 1, 2 and 3 days of culture. Values were normalized to fibroblasts or keratinocytes cultured for 1 day in HDF medium or HEK medium, respectively. N=3, error bars represent standard deviation (two-way ANOVA, Tukey's multiple comparisons test). Statistical significance is indicated with *$p < 0.05$.

The culture of primary macrophages in the different media showed that cells acquired different morphologies over time. Staining with CD68, a monocyte and macrophage specific marker, revealed that macrophages in RPMI control medium had a spread and rounded morphology (figure 18). When culturing cells in either skin differentiation media, macrophages acquired a more elongated shape. The elongation to spindle-shaped macrophages was more evident in skin differentiation medium 1, with more elongated cells at day 7 comparing to day 3 (figure 18). In skin differentiation medium 2, macrophages were partially elongated, with an intermediate phenotype between RPMI control medium and skin differentiation medium 1. Staining with CD68 also revealed a different expression of the marker between the different conditions. The elongated cells detected in skin differentiation medium 1 also showed a brighter staining intensity comparing to the other conditions, effect more evident after 7 days of culture (figure 18).
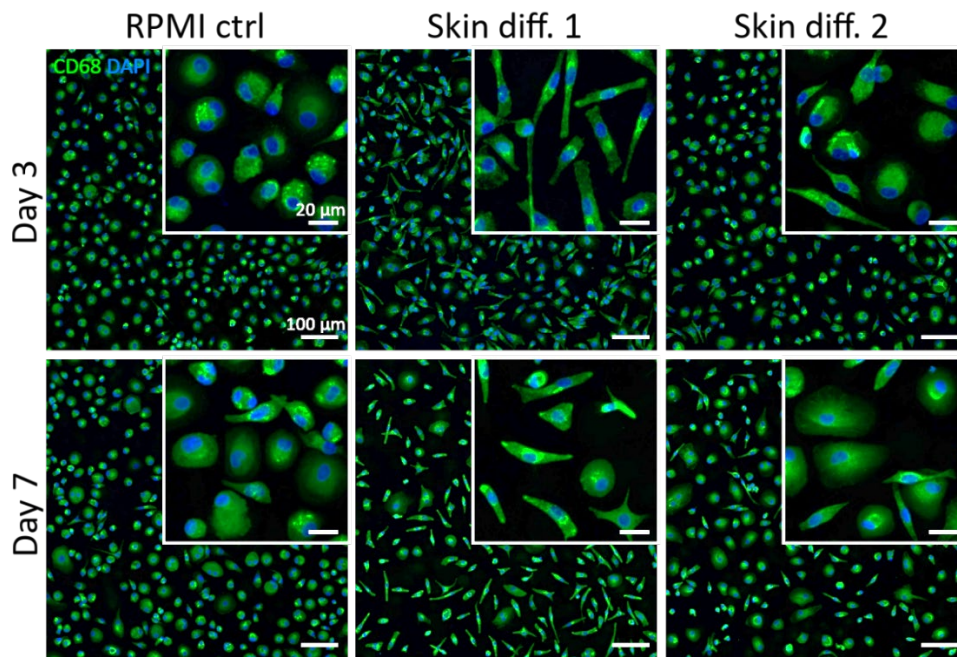
Figure 18. Expression of macrophage-specific marker CD68 in primary macrophages in the media under investigation. Cells were cultured in macrophage medium ("RPMI ctrl") and 2 formulations of skin differentiation media ("Skin diff. 1" and "Skin diff. 2"), and stained with CD68 and DAPI after 3 and 7 days of culture. Scale bars: 100 μm for the lower magnification, 20 μm for the higher magnification. N=3.

5.3.2.2. The influence of medium on macrophage polarization

An altered morphology of macrophages potentially indicates the polarization of cells to a pro- or anti- inflammatory subtype, which occurs depending on the stimuli present in the environment. To better understand the effects observed on macrophage morphology, gene expression of cells cultured in the different media was evaluated. Macrophages were either cultured alone or co-cultured with mature skin equivalents, to investigate the influence of skin paracrine signaling on macrophage polarization.

When macrophages were cultured in presence of the media under investigation, both skin differentiation media showed to affect gene expression. Single macrophage cultures displayed an upregulation of the pro-inflammatory markers CD197 and CXCL10 in presence of both skin differentiation media, compared to RPMI control medium (figure 19). In particular, macrophage culture in skin differentiation medium 2 significantly increased the expression of CD197. The quantification of M2 markers showed that skin differentiation media significantly decreased the expression of CCL22 compared to RPMI control medium, while a slight increase of CD206 was detected. The analysis of gene expression in presence of 3D skin equivalents showed the same effects detected in single cultures. Skin differentiation media caused a slight upregulation of the pro-inflammatory markers, with the exception of CD197 in presence of skin differentiation medium 2, which showed a decreased expression

(figure 19). Quantification of anti-inflammatory markers showed contradictory effect of skin differentiation media, as CD206 was upregulated while CCL22 was downregulated compared to RPMI control medium. The comparison of macrophage single cultures with macrophage-skin co-cultures showed that in presence of skin the immune cells were less responsive to pro-inflammatory stimuli. Conversely, the response to anti-inflammatory stimuli was contradictory. While CD206 fold expression rates significantly increased compared to single cultures, CCL22 showed a significant decrease (figure 19).
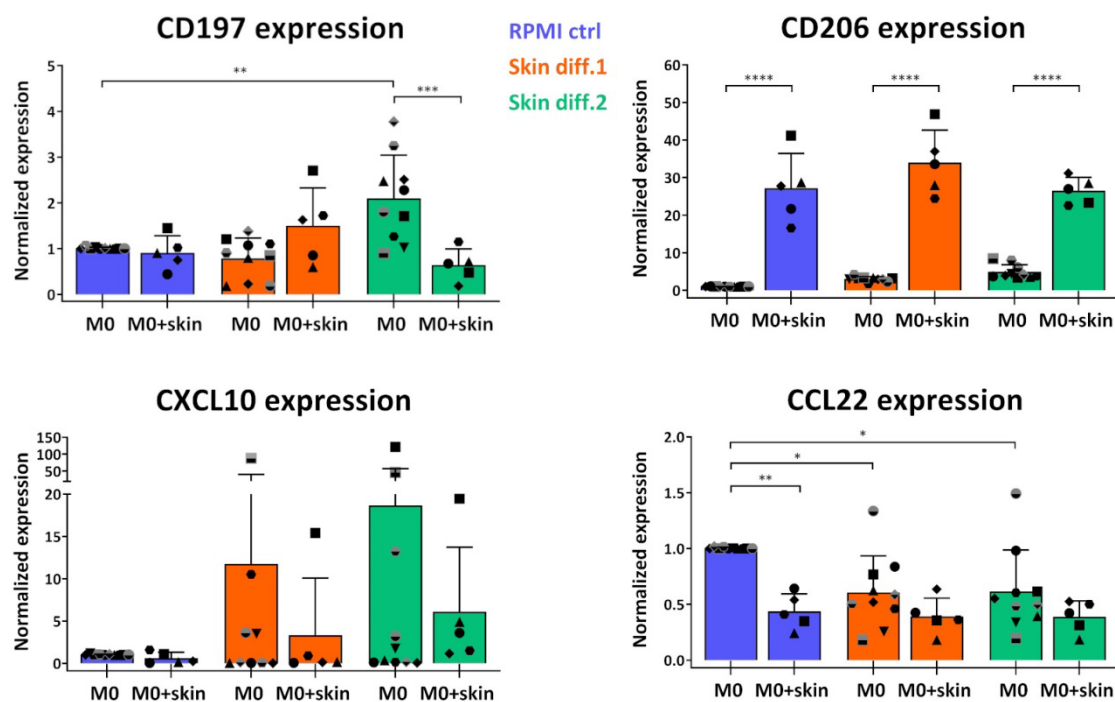
Figure 19. Gene expression of primary macrophages in the media under investigation. Cells were cultured in macrophage medium ("RPMI ctrl") and 2 formulations of skin differentiation media ("Skin diff. 1" and "Skin diff. 2"), in presence ("M1+skin"; "M2+skin") or absence ("M1"; "M2") of skin as a co-culture. The analyzed genes were the M1 markers CD197 and CXCL10 and the M2 markers CD206 and CCL22. All values were normalized to samples cultured in RPMI control medium, and GAPDH was used as reference gene. Each experiment was performed with macrophages derived from a different blood donor, indicated with different symbols. N=5 for macrophages cultured in presence of skin equivalents, N=10 for macrophages cultured alone, error bars represent standard deviation (two-way ANOVA, Tukey's multiple comparisons test). Statistical significance is indicated with *p<0.05, **p<0.01, ***p<0.001, ****p<0.0001.

Cultures were then further stimulated to M1 and M2 phenotypes by supplementing the media with either LPS and IFN-γ or IL-4, respectively. As expected, the detected gene expression variations reflected the same trends observed in unstimulated cells, with the exception of CCL22, which showed increased values in presence of skin co-cultures after M2 stimulation (figure 20). When macrophages were cultured alone, skin differentiation media downregulated the expression of CD197 and upregulated the expression of CXCL10. However, the combination of skin co-culture and skin differentiation media resulted in the downregulation of both M1 markers. Conversely, M2 markers were both upregulated in presence of skin co-cultures compared to macrophages alone (figure 20). Skin differentiation media slightly upregulated CD206 and downregulated CCL22 expression, however no statistical significance was observed for any of the markers evaluated.
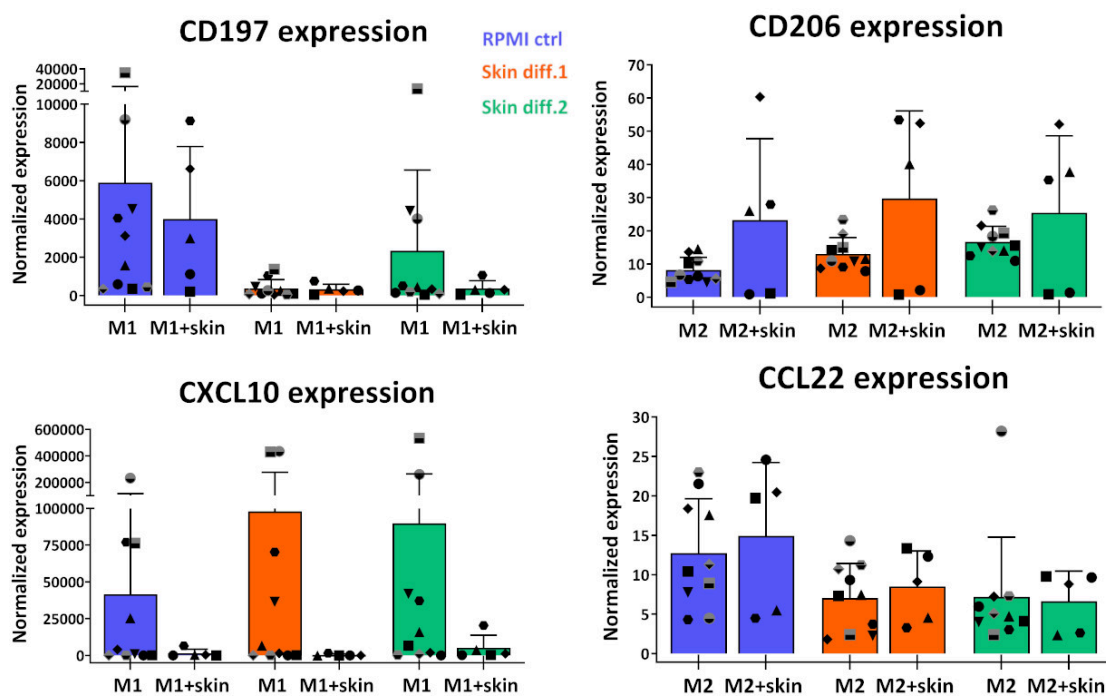
Figure 20. Gene expression of primary macrophages in the media under investigation upon stimulation to M1 or M2 phenotypes. Primary macrophages were polarized for 24 hours into M1- or M2-like cells in macrophage medium ("RPMI ctrl") and 2 formulations of skin differentiation media ("Skin diff. 1" and "Skin diff. 2"), in presence ("M1+skin"; "M2+skin") or absence ("M1"; "M2") of skin as a co-culture. M1-like stimulated cells were analyzed for the M1 markers CD197 and CXCL10, and M2-like stimulated cells were analyzed for the M2 markers CD206 and CCL22. All values were normalized to unstimulated samples cultured in RPMI control medium, and GAPDH was used as reference gene. Each experiment was performed with macrophages derived from a different blood donor, indicated with different symbols. N=5 for macrophages cultured in presence of skin equivalents, N=10 for macrophages cultured alone, error bars represent standard deviation (two-way ANOVA, Tukey's multiple comparisons test).

It has been reported that the monocyte-to-macrophage differentiation has an effect on cell polarization into M1 and M2 phenotypes [123]. Although CSFs are required for monocyte survival and differentiation into macrophages [124], GM-CSF has been shown to prime polarization towards a M1-like phenotype, while M-CSF steers the phenotype towards M2-like cells [123]. To exclude that the observed differences in gene expression resulted from the M-CSF supplementation during the monocyte-to-macrophage differentiation, gene expression of cells generated with GM-CSF supplementation was also evaluated. Compared to M-CSF-supplemented cultures, GM-CSF addition resulted in both an increased and decreased pro-inflammatory response, as CD197 was upregulated and CXCL10 downregulated (figure 21). The supplementation of a combination of M-CSF and GM-CSF resulted in lower expression of both M1 markers compared to M-CSF supplemented cultures, in both the analyzed ratios. On the contrary, M2 markers were upregulated in all conditions compared to M-CSF-supplemented cultures (figure 21). Despite the differences, no statistical significance was observed for any of the markers evaluated.
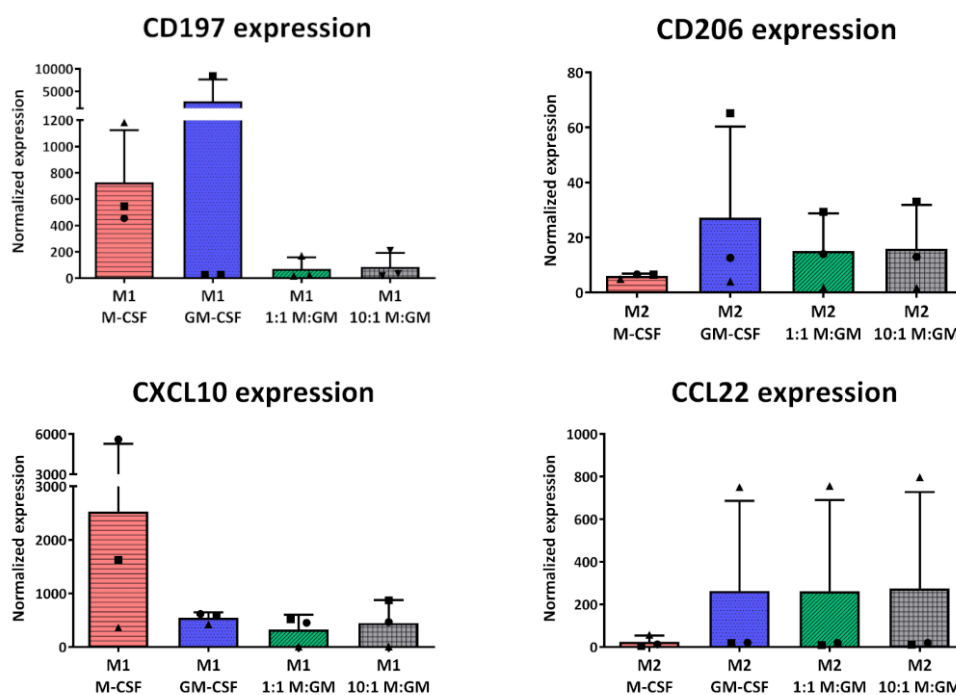
Figure 21. Gene expression of primary macrophages obtained with different monocyte-to-macrophage differentiation conditions, upon stimulation to M1 or M2 phenotypes. Blood-derived monocytes were supplemented with either 20 ng/mL M-CSF ("M-CSF"), 20 ng/mL GM-CSF ("GM-CSF") or a combination of the factors with a 1:1 or a 10:1 ratio of M-CSF:GM-CSF ("1:1 M:GM" and "10:1 M:GM", respectively). Upon differentiation, macrophages were polarized for 24 hours into M1- or M2-like cells, then gene expression of M1 stimulated cells was analyzed with the M1 markers CD197 and CXCL10, and the M2 stimulated cells were analyzed for M2 markers CD206 and CCL22. GAPDH was used as reference gene. N=3, error bars represent standard deviation (Kruskal-Wallis test, Dunn's multiple comparisons test).

5.3.2.3.   The influence of medium on skin differentiation

To investigate the influence of culture medium on tissue maturation, skin models were cultured in RPMI control medium, skin differentiation medium 1 or 2 and evaluated for epidermal stratification. Histological analyses revealed that both skin differentiation media supported the formation of a mature epidermal structure, as indicated by the presence of several layers of keratinocytes and of a stratum corneum on the apical part of the epidermis (figure 22). On the contrary, culture in RPMI control medium did not result in the formation of a mature epidermis, as no stratified keratinocyte layers were detected in the skin equivalents. Instead, only few cells adhered to the surface of the dermal compartment (figure 22).

| RPMI ctrl | Skin diff. 1 | Skin diff. 2 |
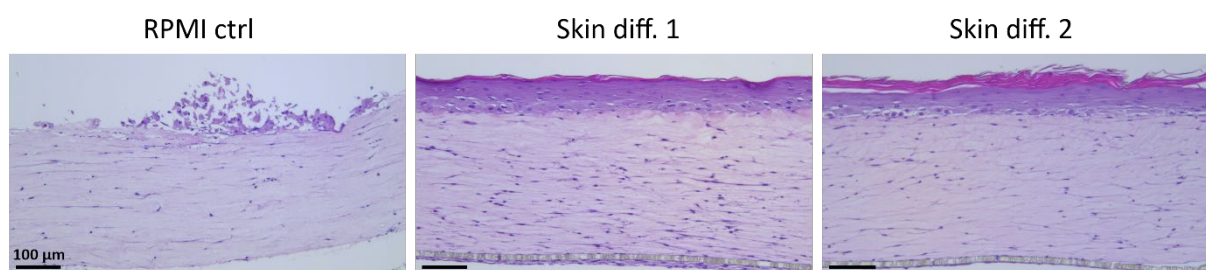
Figure 22. Evaluation of skin tissue maturation in the different media. *In vitro* skin equivalents were generated by culture in macrophage medium ("RPMI ctrl") and 2 formulations of skin differentiation media ("Skin diff. 1" and "Skin diff. 2") for 7 days at air-lift culture, then fixed and stained with H&E. Scale bars: 100 μm. N=3.

As RPMI control medium did not promote the formation of a stratified epidermis (figure 22), the feasibility of culturing immunocompetent skin in RPMI control medium for the theoretical duration of a potential inflammatory response was evaluated. For this, fully differentiated skin equivalents generated in skin differentiation medium 1 or 2 were transferred into RPMI control medium and cultured for further 7 days. Potential changes to the skin structure were evaluated with immunohistochemistry, by staining for the late differentiation marker loricrin. All samples were positive for loricrin when cultured in skin differentiation media 1 and 2 (figure 23), indicating full epidermal maturation in presence of both formulations. However, the replacement of skin differentiation media with RPMI control medium resulted in the loss of loricrin expression (figure 23).
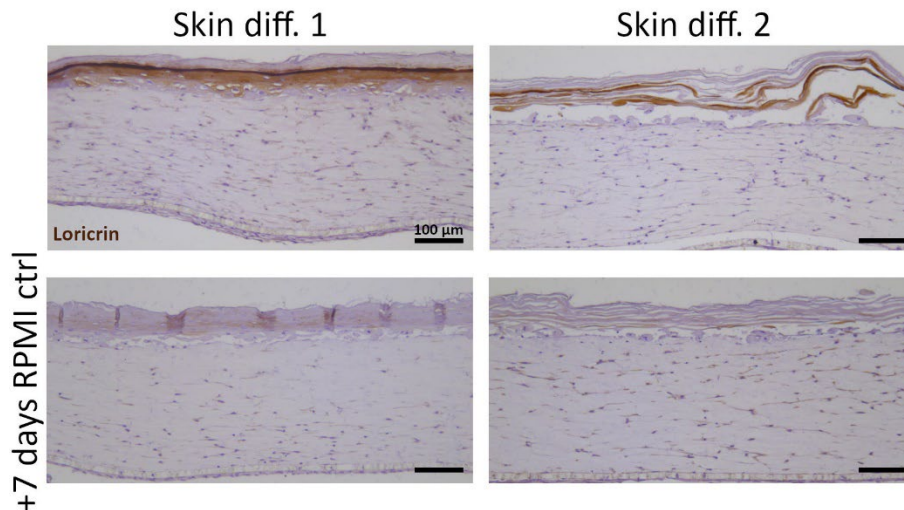
Figure 23. Evaluation of macrophage medium effects on epidermal structure. *In vitro* skin equivalents were generated by culture in skin differentiation medium 1 or 2 for 14 days at air-lift culture (upper row), and then further cultured for 7 days in RPMI control medium ("RPMI ctrl") (lower row). Immuno-histochemistry was performed on 5 µm thick slides, using a peroxidase conjugated secondary antibody and counterstaining with hematoxylin. Scale bars: 100 µm.

5.3.2.4.   The influence of medium 3D-embedded macrophages

In an immunocompetent 3D skin model, macrophages would be cultured within a 3D environment. Therefore, macrophages were embedded in collagen gels to study the effects of the media on 3D-embedded cells. Immune cell functionality was assessed in terms of viability, ability to polarize towards M1 and M2 phenotypes and migration ability.

After embedding in collagen hydrogels, cell viability showed decreasing values over time (figure 24A). Quantification of viability was performed by manually counting cells with ImageJ, with an average of 91 cells counted per image and 3 images per condition. Viability of macrophages in RPMI control medium was 75±2% at day 1, and decreased to 58±1% and 56±18% at day 3 and 7, respectively (figure 24B). Cells cultured in skin differentiation medium 1 had an initial viability of 76±8% at day 1, decreasing to 65±6% and 55±6% at day 3 and 7, respectively. Culture in skin differentiation medium 2 resulted in a higher decrease of cell viability, with 75±9% viable cells at day 1, 55±10% at day 3 and 17±10% at day 7, which resulted in differences that were statistically significant compared to the other groups (figure 24B).
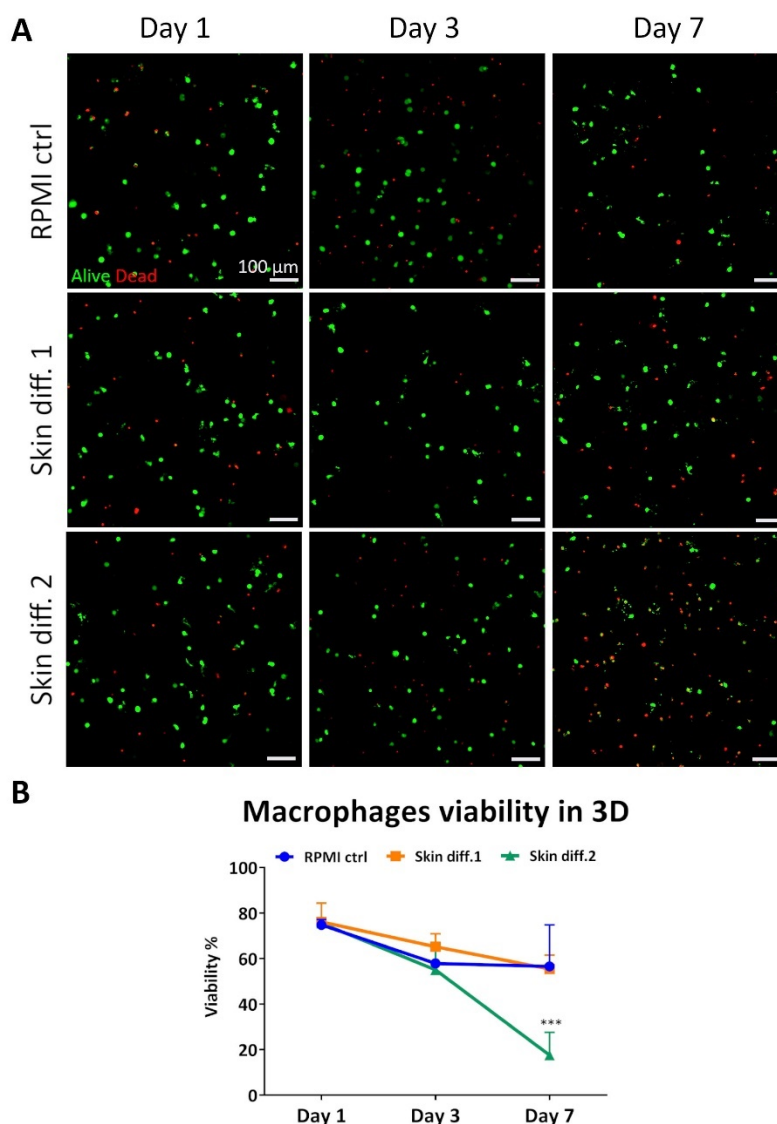
Figure 24. Viability of primary macrophages upon embedding in collagen hydrogels and culture in the different media. Primary macrophages were embedded in collagen hydrogels and cultured in macrophage medium ("RPMI ctrl") and 2 formulations of skin differentiation media ("Skin diff. 1" and "Skin diff. 2") for 7 days. (A) Representative maximum intensity projections obtained from 192 μm-thick Z-stacks, upon live/dead staining. Scale bars: 100 μm. N=3. (B) Quantification of primary macrophages viability performed on maximum intensity projections using ImageJ software. An average of 91 cells was counted per image. Viability is indicated as viable cells percentage on the total number of counted cells. N=3, error bars represent standard deviation (two-way ANOVA, Tukey's multiple comparisons test). Statistical significance is indicated with ***$p<0.001$.

As 3D embedding potentially affects the ability of macrophages to sense stimuli and consequently polarize to M1-like or M2-like phenotypes, macrophage-containing gels were stimulated with LPS and IFN-γ. After 24 hours of stimulation, the release of pro-inflammatory cytokines was quantified in culture supernatants. IL-6 secreted by macrophages cultured in RPMI control medium had a concentration of 15 ng/mL, whereas culture in skin differentiation medium 1 and 2 resulted in the detection of 4.5 ng/mL and 8 ng/mL, respectively (figure 25). Similarly, IL-8 secretion was lower in presence of skin differentiation media. IL-8 concentration of gels cultured in RPMI control medium was 201 ng/mL, against 60 ng/mL in skin differentiation medium 1 and 48 ng/mL in skin differentiation medium 2 (figure 25). Despite the differences, no statistical significance was detected between groups.
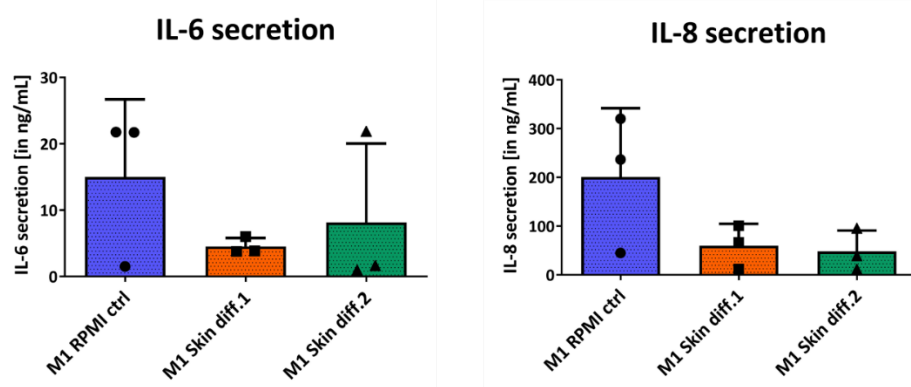
Figure 25. Cytokine secretion of primary macrophages upon embedding in collagen hydrogels and culture in the media under investigation. Primary macrophages were embedded in a collagen hydrogel and polarized to M1-like cells in macrophage medium ("RPMI ctrl") and 2 formulations of skin differentiation media ("Skin diff. 1" and "Skin diff. 2"). After 24 hours, culture supernatants were collected and the pro-inflammatory cytokines IL-6 and IL-8 were quantified. N=3, error bars represent standard deviation (Kruskal-Wallis test, Dunn's multiple comparisons test).

In vivo, macrophages are recruited to the wounded area through the extravasation of precursor cells that differentiate *in situ* under stimulation of the cytokines present in the environment. The ability of macrophages to migrate through the tissue is a crucial requirement for their recruitment during the inflammatory response, therefore a vertical invasion assay was performed. 48 hours after cell seeding, macrophages showed the ability to migrate through the dense collagen matrix in all conditions (figure 26A). The quantification of migration distance from the top of the gels showed that macrophages were able to penetrate into the gels with a depth of 168±21 μm in presence of RPMI control medium (figure 26B). Migration was increased in skin differentiation medium 1 cultured samples, as cells were detected up to a depth of 182±28 μm, while skin differentiation 2 decreased migration to a maximum of 157±22 μm. Differences were however not statistically significant, and could be related to a different number of cells that attached to the surface of the gel prior to migration. As a matter of fact, while the same number of cells was seeded per condition, overview images indicated that less cells were present on the surface of the gels cultured in skin differentiation medium 2 after 48 hours of culture (figure 26C).
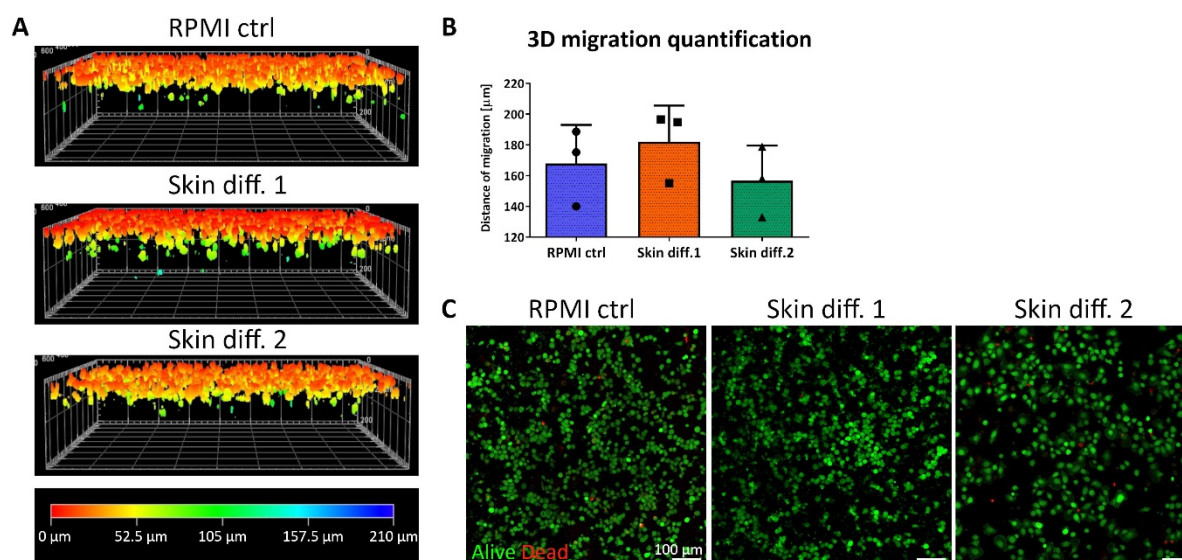
Figure 26. Vertical invasion assay of primary macrophages in the media under investigation. Primary macrophages were seeded on top of empty collagen I hydrogels and let migrate for 48 hours in macrophage medium ("RPMI ctrl") and 2 formulations of skin differentiation media ("Skin diff. 1" and "Skin diff. 2"). (A) Representative 3D reconstructed images of live/dead stained samples are shown, color coded for invasion depth. (B) Quantification of primary macrophages migration after vertical invasion assay in the media under investigation. 3D reconstructed images of live/dead stained samples were used to measure the migration distance from the top of the collagen hydrogel, using ImageJ software. N=3, error bars represent standard deviation (Kruskal-Wallis test, Dunn's multiple comparisons test). (C) Representative images of primary macrophages seeded on top of collagen hydrogels, after 48 hours in the three media under investigation, upon live/dead staining. Images show a top view of each condition 1 day after seeding the same number of cells per gel. Scale bars: 100 μm.

5.4.   Macrophage implementation in skin models

5.4.1.   Inflammatory response of immunocompetent skin

After embedding of macrophages in collagen gels, the immune compartment was placed below wounded skin equivalents and the immunocompetent skin was cultured for 7 days. To evaluate the contribution of macrophages to the inflammatory response, culture supernatants were collected and cytokine quantification was performed. The two pro-inflammatory cytokines IL-6 and IL-8 were quantified after 24 and 72 hours.

Overall, higher cytokine concentrations were detected after 24 hours, compared to 72 hours. The secretion of both cytokines increased after wound formation, compared to unwounded samples. When analyzing wounded skin samples cultured without macrophages, IL-6 and IL-8 secretion showed minor differences between wounds filled with fibrin and wounds where 80 µg/mL calcium pantothenate was supplemented to the fibrin hydrogel. This was observed in both the 24 hours (figure 27A) and the 72 hours (figure 27B) time points.

When macrophages were introduced into the skin equivalents, immunocompetent skin samples did not show increased IL-6 and IL-8 secretion. However, wounded samples secreted higher amounts of the cytokines compared to unwounded samples, with the exception of IL-8 after 72 hours. Differently than what was observed in skin samples without immune cells, the addition of calcium pantothenate in the wound area resulted in a decreased cytokine secretion. This was observed in both the 24 hours (figure 27A) and the 72 hours (figure 27B) time points.
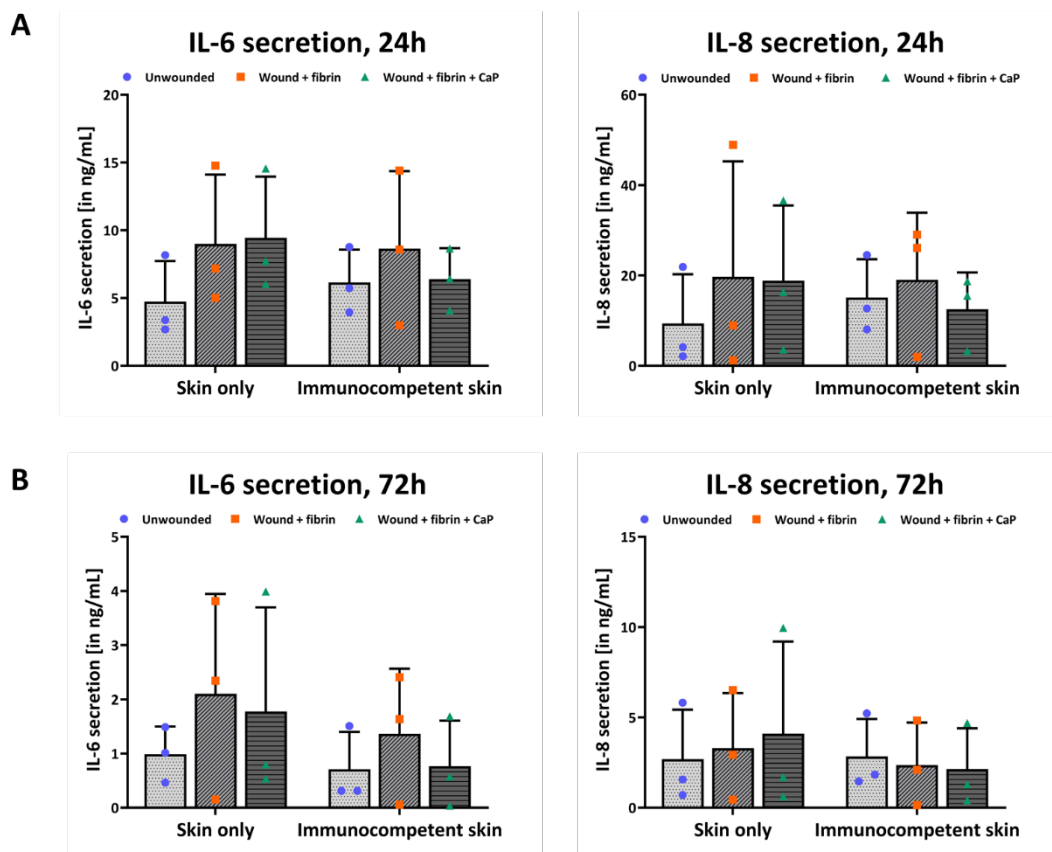
Figure 27. Cytokine secretion of skin equivalents 24 and 72 hours after wound formation. Supernatants were collected from samples where only skin was cultured ("Skin only") or from immunocompetent skin samples, where a macrophage-containing collagen gel was placed below the skin model after wound formation ("Immunocompetent skin"). The pro-inflammatory cytokines IL-6 and IL-8 were quantified after (A) 24 hours and (B) 72 hours for unwounded samples ("Unwounded") and for wounded samples which wounds were filled with a fibrin hydrogel ("Wound + fibrin") or with a fibrin hydrogel also containing 80 µg/mL calcium pantothenate ("Wound + fibrin + CaP"). N=3, error bars represent standard deviation (two-way ANOVA, Tukey's multiple comparisons test).

5.4.2.   Macrophage permanence in immunocompetent skin

The presence of macrophages in immunocompetent skin models over the 7-days healing process duration was assessed with IHC. Staining for CD68 marker confirmed the presence of immune cells in the skin equivalents until 7 days after combination of macrophage-containing gels with wounded skin samples (figure 28). However, staining for CD68 was not detectable in every sample, even in cells located within the macrophage-containing gel below the dermis. The cells detected in this compartment resulted CD68$^+$ in some samples (figure 28A) and CD68$^-$ in others (figure 28B).
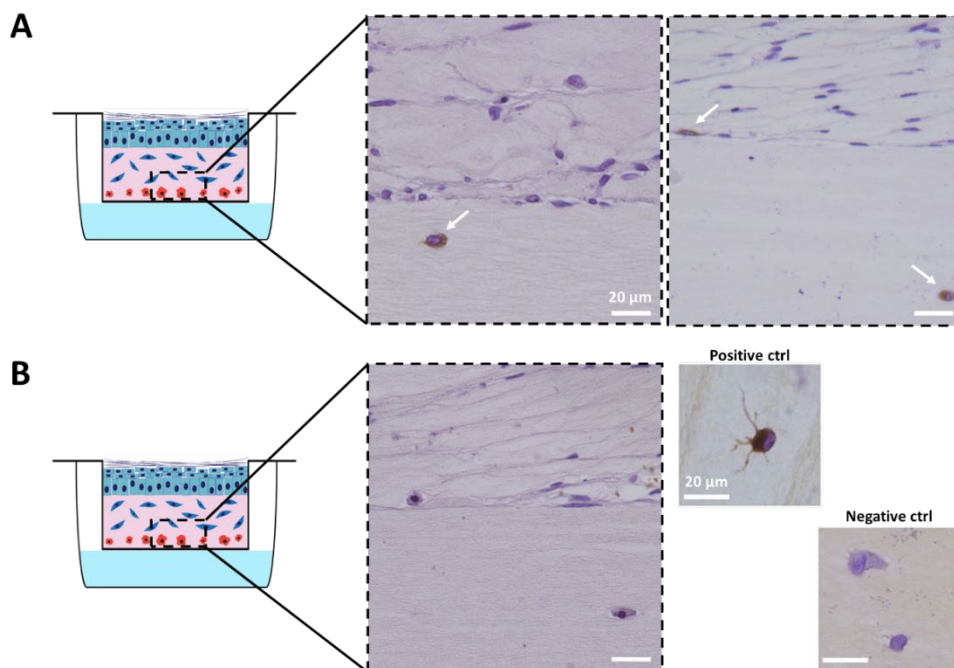
Figure 28. Expression of macrophage-specific marker CD68 in immunocompetent skin models. Macrophage-containing collagen gels were placed below wounded skin equivalents and cultured for 7 days. IHC showed both (A) positively CD68 stained and (B) negatively stained cells. White arrows indicate macrophages displaying positive CD68 staining. Small boxes on the right side show positive and negative controls, the latest only added with secondary antibody. Scale bars: 20 μm.

Chapter 6: Discussion

6.   Discussion

6.1.   Challenges of *in vitro* skin wound model generation

6.1.1.   Collagen scaffolds support mature skin culture but exhibit weak mechanical properties

Since the first skin equivalent was established in 1981 by seeding rat fibroblasts and keratinocytes in a collagen gel [60], collagen has become the primary material used as scaffold for the culture of 3D skin models and is now readily commercially available. One key advantage of using collagen rather than other materials is its availability, as it can be easily extracted from diverse animal sources. Furthermore, the inclusion of a biological material in culture ensures biocompatibility and the use of a well-established system [125]. Due to the large number of reports successfully employing collagen as a scaffold for dermal culture, the material was here employed for *in vitro* skin culture establishment. Collagen materials having different origins and concentrations were selected and evaluated. All materials were available in acidic solutions and obtained commercially, except one provided by a collaborator at the Translational Center for Regenerative Therapies (Würzburg University) that was isolated from rat tail. These selected collagen sources represented the most employed scaffolds for 3D tissue engineering purposes, as reviewed in Antoine *et al.* [73]. Low concentrations of collagen were initially used, as most of the models are generated with a starting material concentration between 1 and 5 mg/mL.

Commercial bovine collagen with an initial concentration of 3 mg/mL (PureCol®) showed to support cell proliferation and maturation, as the formation of a fully stratified epidermis with several cell layers was detected in the equivalents. While the *in vitro* development of a mature skin tissue was supported, collagen weak mechanical properties due to the high water content [72,126] resulted in contraction of the samples throughout culture in a significant and heterogeneous manner (figure 5A). As already demonstrated [122], contraction is the result of cellular activity within the material, as cells actively interact with the matrix. Once embedded in a scaffold, cells recognize and bind to specific motifs as RGD or FGOGER, which in case of collagen and skin cells involves the integrins $\alpha_1\beta_1$ and $\alpha_2\beta_1$ [127,128]. By forming those bonds, cells receive survival signals, proliferate and remodel the surrounding matrix [127]. Hence, the observation of contracting scaffolds indicated the successful interaction between cells and the material, showing desirable properties of the scaffold for cell culture. Nevertheless, for certain applications such as the investigation of drug effects on wound healing, scaffold contraction

does not represent a desirable feature. To perform a consistent and reliable healing evaluation and compare results between drug-supplemented wounds and control samples, a central requirement is the reproducibility of the skin models in terms of sample and wound size. On one side, the issue could be addressed by enlarging the initial size of each sample to obtain a final contracted gel area that is suitable for skin culture. This approach would enable the generation of samples with a larger surface size, but would not address the heterogeneous contraction of the gels. Scaling up the sample size would additionally involve a decrease in the experimental throughput, as well as an increase of the costs. As a matter of fact, more material as well as a higher number of cells would be employed. Furthermore, changing the format of the culture vessels would limit the use of standard cell culture materials, for instance deep-well plates, or devices such as ARTcut®, which are currently only available for a 12-well plate format. In the here presented work, the generation of more reproducible skin models for the 12-well plate format was therefore the focus of the scaffold investigations. To achieve that, the identification of a less- or even non-contractile scaffold was evaluated with diverse techniques aiming at limiting and controlling the contraction process. Reduced contraction of materials in culture generates more robust systems withstanding longer experimental duration and improving the material handling for the user [129].

Initially, a partial compression of the gels was performed by placing Teflon rings in the Transwell® insert after collagen polymerization. The rings, which have been designed to precisely fit 12-wells cell culture inserts, reached the bottom of the culture insert overnight, promoting a partial removal of the hydrogel water content. This method represented a fast and easy method to obtains denser gels, at the same time avoiding mechanical and shear stress on the encapsulated cells. Lateral compression did promote a more uniform appearance of the gels (figure 5B) and the formation of a stratified epidermis (figure 5C) after air-lift culture. However, the results were highly heterogeneous as the compressed gels presented an uneven, non-flat surface after compression (figure 5D), and the results were not comparable between different samples. Lateral compression relies on gravitational compression of gels after application of Teflon rings, which results are strictly dependent on neutralized collagen suspension homogeneity. However, self-assembly of collagen molecules during polymerization depends on almost all fabrication parameters, including temperature, pH and ionic strength [73], and might vary in samples in the millimeters size range, generating a random and heterogeneous fiber network distribution.

To increase reproducibility, a confined compression setup was designed similarly to the one developed from Braziulis *et al.* [130], creating custom-made Teflon components to compress gels directly in the culture inserts (figure 5E). Differently than lateral compression, confined compression applies a weight load to the hydrogels, promoting water removal independently of collagen suspension homogeneity. Additionally, the setup provided a tunable thickness of the hydrogels, which was obtained by modifying the height of the compression stamp to set a precise distance from the bottom of the insert. The

method showed to be more reproducible than lateral compression, as the gels had a uniform and flat surface after compression (figure 5G). Additionally, the compressed gels showed a more stable structure compared to uncompressed samples, in agreement with the materials described by Braziulis *et al.* [130]. Furthermore, the application of a weight load did not compromise the ability of cells to support the formation of a multilayered epidermis (figure 5F). However, the gels produced with the confined compression setup had a maximal thickness of ≈100 μm (figure 5F). ARTcut® has a technical wounding depth variation of ±100 μm, which represents an issue when employing samples having a low thickness. At the same time, the extensive manipulation of samples during the biopsy punch wounding process would benefit the use of thicker samples. Increasing the final gel compression height by modifying the Teflon stamp geometry would represent a solution to generate thicker gels. Anyhow, compressing the gels directly in ThinCert™ or Transwell® inserts displays the physical limit of collagen volume that can be added to a single culture insert. Therefore, in spite of the advantages represented by confined compression, the application of collagen-based skin models to wound healing requires thicker samples to enable an easier wounding process.

An alternative, well reported method to generate porous collagen scaffolds suitable for 3D cell culture is freeze-drying, commonly in use for both collagen alone [131–133] and collagen-GAG blends [134–137]. The generation of blends of collagen with other natural polymers has been reported to improve scaffold mechanical properties [134–138], by combining a material that provides stability with collagen, which is rich in cell-binding domains [126]. Additionally, the mechanical stability of collagen freeze-dried sponges can be easily improved by crosslinking [72]. Both thermal and chemical crosslinking have been extensively employed, all showing positive effects on scaffold mechanical strength [135,136,139–142]. The use of freeze-dried collagen and collagen-chondroitin sulfate materials was therefore investigated. Different freezing temperatures, namely -20°C and -80°C, and crosslinking methods were evaluated, including physical (DHT) and chemical (EDC) crosslinking. The generation of freeze-dried scaffolds showed the formation of porous structures for all collagen types evaluated, with a pore size dependent on the freezing temperature resulting in smaller pores for the lower freezing temperature (figure 6), in agreement with literature [134]. Despite the promising scaffold structure, neither freeze-drying, blending with chondroitin sulfate nor crosslinking resulted to be suitable for skin culture. The samples either displayed the same contraction observed in non-freeze-dried scaffolds or dissolved in culture over time. On one side, the procedures described here differ from the ones successfully reported in literature [133–136], as diverse starting materials, volumes and freezing conditions were employed, and such differences could have influenced the scaffold properties. For instance, acetic acid, the solubilization solvent for some of the analyzed collagen, influences the ice-crystal morphology and therefore pore formation during the freezing process [133]. An explanation for the dissolution of freeze-dried samples after culture might be related to the technical challenge to regulate the

temperature during the freeze-drying process. As the initial shelf temperature could not be controlled as in Schoof, *et al.* [133], this might have led to a partial melting of samples before sublimation at the beginning of the process. Also, while the investigation of the generated freeze-dried material was seldomly demonstrated suitable for skin culture [135], the majority of the findings report only the scaffold properties without evaluating its biological activity [133,134,136].

As none of the methods employing a low concentration of collagen provided suitable samples for the current application, a higher concentration of collagen as starting material was evaluated. The materials included isolated rat-tail collagen and commercial bovine collagen, both with an initial concentration of approximately 9.9 mg/mL. In opposition to low collagen concentrations (<4 mg/mL) that are readily available and easy-to-handle, high concentrations of collagen possess a high viscosity that requires the use of special equipment for handling, such as positive displacement pipets. Once neutralized, the isolated rat tail-derived material failed to form a gel. The lack of polymerization might be due to the presence of impurities not removed during the isolation procedure. Additionally, the shipment process may have affected the physical properties and thermal stability of the material. Conversely, the commercial bovine collagen, FibriCol®, showed the formation of samples with a homogeneous appearance after neutralization and polymerization. As already mentioned, a 10 mg/mL concentrated collagen solution is more difficult to handle as the incorporation of NaOH and the incorporation of cells requires a thorough mixing. Therefore, the process had to be modified and optimized, for instance including the performance of all steps on ice not to pre-maturely induce polymerization. After optimization of the neutralization and seeding procedures, the use of FibriCol® always resulted in a homogeneous sample appearance and in a uniform fibroblast distribution within the gel, indicating that all components had been properly mixed. The use of a higher concentration of collagen resulted in a lower contraction of samples during culture, when compared to lower concentrations (figure 7). Histological staining confirmed the presence of a viable fibroblast population in the dermis. On top, keratinocytes successfully formed multiple cell layers, indication that the presence of a dense matrix did not interfere with the delivery of medium supplements to the epidermal compartment (figure 7). A difference in the number of keratinocyte layers on top of the samples generated with different collagen concentrations was observed. This was probably due to an increasing cellular density in the lower collagen concentrations during gel contraction. As a matter of fact, all gels were seeded with an equal number of cells, but due to higher degrees of contraction, lower collagen concentrations underwent a reduction of the surface area, which resulted in the condensation of cells on a smaller area. When the highest collagen concentration, 10 mg/mL, was employed to generate scaffolds with different thicknesses, epithelialization was observed in all conditions (figure 8). This indicates that gel thickness does not influence the ability of *in vitro* skin to maturate, enabling the generation of thick samples able to withstand the extensive manipulation occurring during wound formation. Notably, there was a significant difference in

the number of keratinocyte layers detected in figure 7 and figure 8. This is only attributed to the longer air-lift culture time performed in the two experiments, as figure 7 showed samples differentiated for 4 days and figure 8 for 14 days.

To verify the formation of a mature skin structure, histology and immunohistochemistry were performed on skin models generated with the neutralized bovine 10 mg/mL collagen solution. In comparison to human skin, *in vitro* models displayed a similar structure. H&E staining revealed the presence of a fibroblast-populated dermal compartment, and on top several layers of keratinocytes were detected (figure 9). The outer epidermal portion displayed several layers of flattened cells forming the stratum corneum, the terminal differentiation state of keratinocytes. IHC confirmed that keratinocytes below the stratum corneum displayed a late differentiation state, as they expressed loricrin similarly to human skin samples, while intermediate cells displayed the expression of cytokeratin 10, an intermediate differentiation marker (figure 9). Between dermis and epidermis, the basement membrane acts as an anchor for the epidermis, providing stability and integrity to the tissue. The positive expression of collagen IV in the area between dermis and epidermis showed that a basement membrane was also formed in the skin models, as it occurs in human skin. The detection of epithelial markers demonstrates that the *in vitro* generated tissue has all the characteristics of human mature skin as well as the desirable thickness for wound healing application.

The majority of collagen materials described in literature have a concentration below 4 mg/mL [73], even though their use involves gel contraction and low reproducibility. Collagen content in the range of 10 mg/mL is rarely employed, as evidenced in Antoine *et al.* [73], which is probably related to wider commercial availability and lower price of lower collagen concentrations. However, as here demonstrated, more concentrated collagen gels for skin model generation resulted in a reduced contraction of the gels over culture time, at the same time not interfering with cellular activity or medium supply to the upper layers, as a fully mature epidermal structure was confirmed with IHC.

6.1.2.   Limited reproducibility of *in vitro* skin wound models

6.1.2.1.   The choice of cells influences *in vitro* skin quality

In vitro skin models have mainly been generated with primary cells (i.e. [106,112,113,115,143–145]), which supported the formation of a mature skin structure. A limited number of studies has also employed immortalized keratinocytes, showing however both positive [75,146–148] and negative [149] results in terms of epidermalization. Indeed, in comparison to epidermis that employed primary keratinocytes, the use of immortalized cells showed inconsistent differentiation independently of the culture medium or scaffold employed [149]. The advantages of cell lines are usually correlated with lower costs and higher consistency of results, as well as carrying no ethical concerns [150]. However, such cells are a result of genetic manipulation, which means that their phenotype and functions may be altered during the process [151]. In addition, their ability to indeterminately proliferate might increase the genotypic and phenotypic variations [151], whose probability is amplified due to the long-term culture required for skin equivalents generation. Primary cells have characteristics that better mimic the *in vivo* situation compared to cell lines, providing a more relevant setting for evaluating human physiological responses. At the same time, the use of primary cells might also show variations in cell behavior due to intrinsic donor-to-donor variations, heterogeneous isolation procedures or variable culture conditions [150]. To balance advantages and drawbacks and limit the donor-to-donor variation, commercially available primary keratinocytes and fibroblasts were here employed for all experiments, each derived from a single donor. As a major factor influencing the quality of *in vitro* epidermalization is the proliferation state of keratinocytes [152], only sub-confluent cells were harvested prior to seeding into 3D skin models. As a matter of fact, when adjacent keratinocyte are in contact their proliferation is inhibited [152], and this could result in the lacking formation of a confluent layer in the 3D cultures.

6.1.2.2.   *In vitro* skin thickness and epidermal stratification are variable

As previously discussed, reproducibility is a crucial requirement of skin models for the investigation of drug effects on wound healing. More specifically, the comparison of wound healing in presence of different substances requires a comparable sample and wound size, to avoid the inclusion of confounding factors while evaluating healing. Skin models described in literature generally have an experimental heterogeneity with regard to cell source, scaffold used for dermal generation, culture medium, culture time and culture vessel [73,153]. Such fundamental differences between setups not only hamper data replication [153], but also hinder the advancement of skin models in substituting animal studies for preclinical investigation, as only robust and reliable models can potentially replace *in vivo*. The key event in the generation of a mature skin equivalent is the formation of a stratified, multilayered epidermis, which also represents the most challenging technical step. As here shown, differences in the number of epidermal layers could be detected between experiments, but also between different samples generated within the same experiment using common cells suspensions and concentrations (figure 10A). Generating a reproducible epidermal structure is a technically challenging process, despite the use of singe donor juvenile cells and standardized procedures. The differences observed after histological analysis derive in part from the sample processing itself, as dehydration and paraffin infiltration might lead to the alteration of the epidermal structure or to the loss of intermediate keratinocyte layers. However, as epidermalization occurs through a sequential differentiation of keratinocytes from the basement membrane to the outer part of skin, the detection of a stratum corneum was considered as successful differentiation despite the lack of intermediate layers. The heterogeneity of samples was also reflected in the variation of the sample thickness between experiments (figure 10B), likely originating from more or less pronounced remodeling of the matrix leading to vertical contraction. As previously discussed, the proliferation state of cells at the moment of harvest affects the amount of activity that will be observed in the 3D environment, therefore representing a source of variation. Clearly, also hydrogel fabrication parameters contribute to the generation of reproducible samples. Polymerization pH and temperature as well as ionic strength are known to influence collagen gel formation [73], and even though all procedure steps were standardized to limit variations, collagen batch-to-batch variability or human error might have influenced the quality of skin tissue. On a large scale, every small variation in the culture conditions might contribute to the heterogeneous sample structure observed after the long time required for skin maturation.

In regard to the existing literature on *in vitro* skin model culture, there is lack of consistency between collagen hydrogel fabrication procedures, which makes difficult to compare protocols used by different

research groups [73]. The described parameters have significant variations between experimental set-ups, which complicates the extrapolation of qualitatively useful data [73]. A better definition of the experimental conditions would benefit the advancement of more reproducible skin models, as well as providing more solid data that can be compared between groups. Furthermore, few reports describe a sufficient number of models to enable the estimation of reproducibility. For instance, Lange *et al.* [154] evaluated a total of 144 skin equivalents to investigate the influence of culture medium on skin tissue quality. However, such a large sample size represents an exception, and the described models normally include lower magnitudes, preventing the comparison of the findings illustrated here to the current literature.

6.1.2.3. Automated wounding optimization is required for reproducible wound formation

The challenge of reproducibility when using skin models is also reflected in the wounding process. Biopsy punch wounds had a shape ranging from circular to oval and elongated (figure 11A). While the wounds were generated with a circular biopsy punch, the samples required transfer and repositioning in new ThinCert™ inserts after wounding. Indeed, biopsy punch can only implement full thickness wounds, which also involve the excision of the ThinCert™ bottom membrane and thus required the transfer of the equivalent in another insert. This has been already described for other wounding processes, which also included the transfer of the wounded skin on top of a second collagen gel after wounding, to allow re-epithelialization on a natural matrix [79,81]. The extensive sample manipulation required during and after biopsy punch-inflicted wounds was not only reflected by the differently shaped wounds, but occasionally resulted in the delamination of the epidermal layer (figure 11B). Differently than *in vivo*, *in vitro* skin models lack the mechanical and tensile support from the surrounding tissue, resulting in an easy disruption of the basement membrane when stress is applied. Additionally, despite the detection of collagen IV in the skin models, the basement membrane might not possess the same composition as the *in vivo* structure. Biopsy punch-inflicted wounds are the most common type of excisional wounds described in literature [79–82], anyhow the process is highly dependent on the operator handling. The introduction of automated wounding represents an advancement for more reproducible wound formation [83], as it reduces sample manipulation and also the time required for wound implementation. At a macroscopic level ARTcut® wounds appeared to be homogeneous in terms of shape, with circular wounds detected in each sample (figure 11A). Histological analysis revealed that ARTcut®-implemented wounds had a variable penetration depth into the tissue, showing the formation of either full thickness or partial thickness wounds, even though the same wounding parameters were set in the software (figure 10C). The probable cause of the variability observed with

ARTcut® wound formation is the technical variability of the device itself, which has a precision of ±100 μm. On samples with an average thickness of 350 μm this represents a significant source of error. Additionally, the structure of skin tissue itself might influence laser surface detection. Despite the selection of a minimally contracting scaffold, the cells still remodel the collagen matrix, generating gels visibly at an angle and with a non-flat surface. Furthermore, the outer epidermal layer naturally displays a rippled surface that is characteristic of the stratum corneum morphology. The ARTcut® laser-based surface detection consists in the reflection of a laser beam on the sample surface then hitting a detector, which instructs the software in real-time on the distance of the sample surface. The presence of a non-flat surface on skin equivalents might scatter the laser beam differently, depending on which location of the sample is hit. As a consequence, the device may detect the surface in a more or less precise way, resulting in wound formation in proximity of the surface or in a higher position, obtaining wounds with a different penetration depth. Another detail revealed from the histological images is the incomplete removal of wounded tissue fragments. Despite thorough washing steps, additionally performed on a shaker, some samples could not be properly cleared of tissue debris. This might originate from the small area of the Transwell® available for liquid supplementation, leading to insufficient wash of the tissue surface.

Overall, both wounding methods present advantages and drawbacks. Biopsy punch-generated wounds showed comparable full-thickness wound formation between samples, as the entire tissue was cut out, however the extensive manipulation caused epidermis delamination and alteration of the wound shape. ARTcut®-generated wounds, conversely, displayed a reproducible wound shape and highly reduced the samples manipulation, however showing a non-reproducible penetration depth and incomplete tissue fragments removal after wounding. As ARTcut® is a recently designed device, there is scarcity of reports to compare our results. The only report describing the generation of wounds with ARTcut® showed a successful material removal from the wound channel after wounding [83]. However, the experimental setup employed skin models generated with a diverse scaffold, which most likely exhibits diverse resistance to wound formation.

Further optimization of the ARTcut® surface detection method might improve reproducibility, for instance by employing multiple lasers for the measurements to obtain a more accurate position of the surface. Anyhow, the precision range should be increased for application to 12-well cultured skin samples. Other wounding methods have shown improved reproducibility. Laser wounds, for instance, display a high degree of replicability, as laser power can be easily adjusted to generate partial-thickness or full-thickness wounds [82,85,86]. However, thermal wounds have a different etiology then excisional wounds, thus mimicking another physiological condition. Incisional wounds are more similar to excisional ones [76–78], but they generate wounds smaller in size. For healing assessment in presence

of drugs, excisional wounding currently represents the most relevant method, as its generated wounds can be easily filled with a target material or drug under investigation.

6.1.3. Fibrin is a suitable drug delivery system: comparison of different healing assessment methods

In vitro wound healing investigation after drug supplementation can be assessed through a large set of methods, including both end-point and real-time analyses. To evaluate the diverse methods in the described skin wound model, the effects of a fibrin hydrogel as wound-filling material were analyzed in comparison to non-supplemented wounds. Fibrin is a natural polymer participating in the initial phases of healing. Thus, it should not interfere with the healing process and represent a suitable delivery system for drug investigation. Thanks to its fast polymerization, the mixture of fibrinogen and thrombin could be precisely delivered into the wound area, where the components formed a hydrogel. The fibrin hydrogel could be detected through histological analysis until 4 days after wound formation (figure 12A). To assess wound closure, wound area was imaged over time with a stereomicroscope, showing that wound appearance changed over time, becoming from translucent to opaque as re-epithelialization occurred (figures 12B). The analysis of the images with ImageJ software demonstrated that supplementation of fibrin did not affect healing, as wound closure values were similar for both controls and fibrin-added samples (figures 12C). Quantification of wound closure through image analysis has been previously used to monitor healing of the same sample over time [79,155], providing a real-time and straight-forward method that does not require special equipment. However, supplementary analyses are required to confirm wound re-epithelialization. For this, histology and immunohistology represent the standard technique, allowing the observation of epidermal migration over the wound area and the quantification of proliferating cells at different time points [39,40,42,45]. Even though histology is the golden standard for *in vitro* healing evaluation, it requires skin sample fixation and processing, which could lead to alteration of the migrating epithelium structure.

Confocal microscopy, conversely, enables imaging of unprocessed, living wounded samples, as already reported in literature [52]. Confocal microscope 3D reconstructed images demonstrated cell migration into the wound area upon live/dead staining, confirming wound re-epithelialization (figure 13A). This method enables a more precise quantification of wound closure comparing to stereomicroscopy evaluation, however the use of CLSM also encompasses disadvantages. First, imaging living samples prevents the use of specific antibodies that require tissue fixation and permeabilization. Thus, the imaged cells migrating into the wound area could be epidermal or mesenchymal cells or a combination of both. The use of keratinocyte-specific antibodies for staining is challenging due to the thickness and optical

density of the skin samples, which represent a physical barrier to CLSM imaging. However, techniques as tissue clearing might offer a solution to the optical constraint of tissue imaging, as reviewed in Tainaka *et al.* [159]. Additionally, tissue transparency might extend the laser imaging depth, which without tissue treatment can only reach the papillary dermis, preventing the imaging of deeper tissue [157]. Other promising markers for wound healing imaging are endogenous autofluorescent metabolic markers, for instance nicotinamide adenine dinucleotide, which can be imaged via multiphoton imaging [160]. This technique has enabled to image keratinocytes at subcellular spatial resolution on *in vivo* skin, distinguishing the different epidermal layers by the diverse keratinocyte morphology [161]. Endogenous fluorophores are promising candidates for wound monitoring, as their expression increases in metabolically active cells. Anyhow, they would still require the identification of markers that are specific for keratinocytes. Similarly, epithelial migration could be tracked with the use of fluorescent cell trackers, as it has been shown for wounded *ex vivo* skin explants [162].

As here reported, *in vitro* skin models present variability and low reproducibility. For this reason, the ideal method to monitor wound healing includes real-time and non-invasive analyses, enabling to track wound closure of single samples over time. Real-time assessment of wound healing is not commonly employed in research, however promising techniques have been described. OCT enables to monitor wounded skin samples without the use of a contrast agent or tissue labeling prior imaging, and can penetrate for 2-3 mm depth in the sample depending on its composition [163]. This technique was used to obtain cross-sections and 3D reconstructions of the wounded tissue, allowing fast real-time and non-invasive image acquisition [164–167]. OCT has already been used to assess epithelial formation and differentiation in skin tissue equivalents [166,168], as well as for evaluating wound closure after laser irradiation in both *in vivo* [157,169] and *in vitro* experiments [155,158,163,167]. Thanks to Prof. Simon Pot, access to an OCT device was obtained, enabling to perform non-invasive analyses of wounded skin samples over 7 days. The here described skin model was suitable for OCT imaging, as dermis and epidermis could be clearly distinguished (figure 13B). Thanks to the image resolution, the wounded area was imaged over time, revealing the occurrence of re-epithelialization in the samples (figure 13B). Despite the fast imaging process, the amount of data generated from OCT are significant, making image analysis a complex process. Image evaluation might be performed either showing cross-section images of the wounded area to assess wound closure over time from a series of 2D images [167], or developing specific algorithms to reconstruct a 3D image of the wound area, providing a more precise quantification of the area over time [158,163]. As the ability to develop specific algorithms is elective, the easiest method for data analysis is the comparison of 2D images. However, appropriate evaluation of wound closure requires a strategy to compare sections taken at the same location over time. While in some cases it is not specified whether the shown images are representative of the same location over time, more relevant contributions demonstrate the comparison of images from the same

area thanks to the implementation of micro-beads at the sides of the wound [167]. As the experimental design for the described skin model had limited availability, the obtained cross sections of healing wounds were evaluated qualitatively, but no quantification was performed.

As a complementary and non-invasive method to assess tissue response to wound formation, inflammation is often evaluated by analyzing the cytokine content in cell culture supernatants. Diverse pro- and anti-inflammatory cytokines can currently be quantified by means of ELISA, indicating variations at a picogram scale. This allows to monitor the inflammatory response over time, a key information when novel drugs or materials are evaluated as potential novel therapeutic agents. Cytokine quantification is a commonly used method for healing assessment, providing information on the inflammatory response course [81,84]. IL-6 and IL-8 are pro-inflammatory cytokines, and their quantification in culture supernatants demonstrated that fibrin did not increase the inflammatory response of wounded samples comparing to wounds without fibrin supplementation (figure 14). Therefore, fibrin proved to be a suitable carrier system for introducing drugs into wound models, as it does not elicit inflammation on its own.

The quantification of inflammation can alternatively be performed by means of PCR, analyzing the genes involved in the response as MMPs, CXCL16, CXCL1, and IL1α [82]. Cytokine quantification in culture supernatants is a straightforward method, while the RNA isolation step prior PCR involves the lysis of the skin equivalents. This results in long incubation times required to dissolve the ECM, which could lead to eventual changes in gene expression. Additionally, the analysis is performed on all cell populations involved, not allowing the evaluation of single cell types activity.

6.2.   Key features of immunocompetent skin models

6.2.1.   The use of primary cells represents an advanced setup despite the donor-to-donor variation

Previously reported immunocompetent skin models have described the implementation of different immune cells into *in vitro* skin, including both cell lines [110,119] and primary cells [106,112,113,115,143–145]. With regard to macrophage inclusion, the co-culture of murine macrophage cell line RAW264.7 with skin equivalents has been described by Chung *et al.* [119]. Their model was used to demonstrate the protective effect of skin in regards of inflammation upon LPS stimulation. However, the setup included the combination of 2D macrophage cultures with 3D skin equivalents, not reflecting the *in vivo* setup. Furthermore, a murine cell line was combined with human primary cells, representing an obstacle to the translation of the results to human inflammation. In addition to this, despite murine cell lines and primary cells have shown responsiveness to inflammation, it was reported that mouse primary cells respond faster and more strongly to bacterial infection compared to cell lines [120]. Similarly, the use of human monocytic cell line-derived macrophages is contradictory. A comparative study between THP-1-derived macrophages and human monocyte-derived primary macrophages has shown that macrophage morphology, response to polarization and phagocytic ability are influenced by the THP-1 monocyte-to-macrophage differentiation conditions [170]. Therefore, diverse monocytic cell line differentiation conditions might provide results that are comparable to human primary cells or might generate cells with a different phenotype and behavior. To promote an *in vivo*-like setting and a more predictive cellular behavior, blood monocyte-derived macrophages were used for all experiments. A shortcoming of primary macrophages use is the limited number of cells obtained following isolation. This, together with the time-consuming isolation procedure, is probably the cause of a broader use of cell lines for inflammation assessment. However, the few models that described incorporation of macrophages into *in vitro* skin employed human primary cells [106,115], as also the majority of skin models described in literature are generated using primary fibroblasts and keratinocytes [82,109,112,114]. Despite primary cells present intrinsic donor-to-donor variation, they represent a more physiological mimic of the *in vivo* conditions. The here presented results only included human primary cells, for an improved translation to human biology and to allow the comparison with the existing literature.

6.2.2.   Design of a macrophage implementation strategy with reduced culture time

The choice of incorporating a specific immune cell type into *in vitro* skin reflects the process under investigation. Wound healing investigation requires the evaluation of the inflammatory response over time, as inflammation is a crucial phase determining normal wound closure or development of chronic nonhealing wounds. Furthermore, the preclinical investigation of novel drugs or biomaterials includes the analysis of whether the substance elicits inflammation. As previously explained, macrophages regulate the switch from inflammation to tissue repair, thus influencing the outcome of wound healing [40,51,118]. Despite macrophage implementation into skin equivalents would enhance their physiological relevance, few models including macrophages have been described [106,115], reflecting the challenges related to their incorporation. One of the key macrophage characteristics is their ability to switch between different phenotypes depending on the surrounding environment conditions, a process named plasticity [27,29,171]. As macrophages are extremely sensitive to the microenvironment, the implementation approach here described aimed at shortening cell culture time to its minimum. The two models reporting primary macrophage-fibroblast co-cultures into dermal compartment showed macrophage presence in the tissue after 1 [115] and 3 weeks [106]. Accordingly to the previously shown data, the *in vitro* wound healing evaluation is commonly performed for 7 days after wound formation [81,82,84]. Thus, the here presented macrophage implementation strategy was designed to have a duration of 7 days, an appropriate time frame for wound healing investigation as well as a suitable culture time for primary macrophages. As the combination of 2D and 3D cultures is not representative of the *in vivo* conditions, macrophages incorporation into 3D skin equivalents included the embedding of immune cells into collagen gels prior to implementation into skin models (figure 15A). By combining the macrophage-containing gel below skin equivalents, the *in vivo* immune cell recruitment was also mimicked. As a matter of fact, wound healing macrophages mainly derive from the extravasation of precursor cells from blood vessels. Blood monocyte-derived macrophage morphology appeared consistent over time comparing different isolations, with progressively adhering cells during the monocyte-to-macrophage differentiation and rounded, spread cells upon complete differentiation (figure 15B). The embedding in collagen gels was performed as for fibroblast encapsulation during dermis seeding, maintaining a 1:1 ratio between the two cells types. After embedding, macrophages showed a homogeneous distribution within the gel (figure 15C).

An analogue approach for combining immune cells into skin equivalents was employed by Kühbacher *et al.* [113] to study *Candida albicans* infection. T cells or peripheral blood mononuclear cells were first embedded into collagen-GAG gels and then placed below skin equivalents, demonstrating the protective role of dermal fibroblasts during infection. Similarly, Chau *et al.* [112] first embedded DCs into

agarose-fibronectin gels, which were then placed between dermis and dermis in a triple co-culture. Apart from the different immune cell types and materials used as scaffolds, these two setups have the closest resemblance to the here suggested incorporation method. Other models mainly describe the incorporation of immune cells as a direct co-culture with skin cells in the dermis [115] or epidermis [111], which translate in longer culture times that expose cells to an increased amount of stimuli. Immune cells implementation has also been described by seeding cells directly below the skin equivalent [109,172]. Although the cells showed the ability to migrate through the tissue after stimulation, it is questionable whether an *in vivo*-like environment was reproduced in the models.

6.2.3. Skin differentiation media vs RPMI control medium: negative effects on skin and immune cells in 2D cultures

The choice of a culture medium promoting the maturation of *in vitro* skin models displays a heterogeneous scenery. A plethora of media have been described, partially commercially available and in part formulated adding single supplements to a basal medium. The optimal conditions for obtaining a mature epithelium differ depending on the system used for culture [173], as different cell types and culture vessels are employed. Regardless, culture medium has a leading role in promoting epithelial stratification. Different supplements have shown to promote keratinocyte differentiation, while other are still under discussion, which results in medium formulations that differ between research groups. The role of serum is still controversial, as it has been demonstrated to both promote and inhibit differentiation of keratinocytes [174,175]. In spite of this, the skin culture media currently in use mostly include low serum concentrations [101,110,117,119] or serum-free formulations [113,176]. Furthermore, it has been shown that culturing keratinocytes in presence of serum prior to the incorporation into skin equivalents is required to obtain a mature epidermis [177]. A variety of supplements are added to culture media to promote epithelial differentiation. Supplementing calcium concentration above 1 mM has been shown to induce the formation of tight junctions between keratinocytes triggering differentiation [178,179]. Similarly, supplementation of vitamin C [77,176,180–182], fatty acids such as oleic, arachidonic, palmitic and linoleic acids [77,117], amino acids such as L-carnitine and L-serine [77,110,117,182] or transferrin [105,113,119] was shown to positively influence epidermalization. It was reported that different culture media formulations affect *in vitro* skin thickness, stability of dermo-epidermal junctions, number of epidermal layers [154] and collagen gel remodeling [183]. However, the effects of those media on primary immune cells remain largely unexplored. As previously discussed, macrophage polarization is affected by a wide range of cues from the surrounding environ-

ment. As a consequence, the composition of culture medium also influences cell phenotype and functions. Serum has been shown to have anti-inflammatory effects due to the presence of exosomes [184], as well as oleate, which enhances the M2-like polarization [185]. Conversely, palmitate has been shown to enhance M1-like polarization [185]. Isoproterenol and hydrocortisone are both immunosuppressive agents, inhibiting M1-like polarization [186,187] and phagocytic ability [188] of macrophages. However, the conditions where single supplements were investigated are highly heterogeneous, and both mouse cells [184,188] and human cell lines [185–187] have been used for the analysis.

As different components of skin differentiation media affect macrophage polarization state, and at the same time different media compositions affect skin structure, it is necessary to identify a suitable medium for the co-culture of macrophages and skin equivalents. At first, the effects of three selected media were evaluated on single 2D cultures of primary fibroblasts, keratinocytes and macrophage. Viability analysis showed that fibroblasts were not affected by culture in other media than fibroblasts proliferation medium, as the values increased in all conditions over time, while keratinocytes viability was negatively affected by culture in RPMI control medium (figure 16). Macrophages showed decreasing metabolic activity over time. As expected, culture in either skin differentiation media resulted in statistically significant lower viability when compared to RPMI control medium, for all time points analyzed (figure 16). The negative effects of RPMI control medium on keratinocyte viability are likely due to the lack of supplements such as KGF in the medium, as it promotes cell survival and proliferation [189,190]. Similarly, the low serum content of skin differentiation media 1 and 2, which is respectively 0% and 1.25%, is the probable cause of the detected lower macrophage viability. Proliferation quantification confirmed that skin differentiation medium 1 has a formulation designed to specifically increase fibroblast and keratinocyte performance, as both cell types showed increased values in presence of that medium when compared to the other conditions (figure 17). Likewise, metabolic activity, keratinocyte proliferation was negatively affected by RPMI control medium, showing lower values compared to the other media and a decrease over time.

Other than negatively affecting macrophage viability, skin differentiation media also showed to influence macrophage morphology. While in RPMI control medium cells displayed a round-shaped morphology, in skin media they appeared elongated and spindle-shaped, with this effect being more evident in presence of skin differentiation medium 1 (figure 18). An elongated cell morphology correlates with a shift toward an anti-inflammatory phenotype [191]. However, macrophages also displayed a brighter CD68 staining in skin differentiation media, which has been correlated with a skew to a pro-inflammatory phenotype as it was upregulated during inflammation [192,193]. To investigate the effects of culture medium on macrophage polarization, gene expression was measured before and after M1 and M2 stimulation, both in presence and absence of skin as a co-culture. Indeed, the presence of skin paracrine signaling might significantly influence the results, since it has been shown that dermal

fibroblasts have a protective role during infection [113]. Already before the application of stimuli, macrophages showed an increased expression of pro-inflammatory markers in presence of skin differentiation media. Conversely, the co-culture with skin equivalents displayed a significant upregulation of the anti-inflammatory markers (figure 19). After stimulation, the trends were similar (figure 20), confirming the effects observed by Kühbacher *et al.* [113] indicating that skin has a protective role against inflammation. Interestingly, in presence of skin macrophages showed a lower response to pro-inflammatory stimulation, with an upregulation of the anti-inflammatory markers. The results are in agreement with the M2-like polarization of macrophages in presence of skin reported from Limandjaja *et al.* [194]. The findings are particularly significant as skin differentiation medium 2 has a similar composition to the medium used in their experiments [194].

As immunocompetent skin wound models aim at detecting inflammation after drug supplementation, a suitable co-culture medium should allow cells to sense and respond to pro- and anti-inflammatory stimuli. The stimulation of macrophages to M1- or M2-like phenotypes did result in a higher expression of all genes compared to unstimulated cells, indicating successful polarization. However, both the analyzed media reduced the polarization span of cells, as they showed to inhibit the inflammatory response in presence of skin and a stronger response to anti-inflammatory stimuli. As previously mentioned, isoproterenol and hydrocortisone, both contained in skin differentiation medium 2, are probably responsible for the observed inhibition of inflammation in this medium. Hydrocortisone is also contained in skin differentiation medium 1, further supporting this hypothesis. However, the effects of the other supplements present in skin media have not been investigated on macrophages, therefore there might be other factors that affect the observed behavior.

To confirm that the effects on macrophage polarization are due to the culture in skin differentiation media, macrophage response to different monocyte-to-macrophage differentiation protocols was investigated. As a matter of fact, M-CSF has been shown to skew cells towards M2-like cells, while GM-CSF was indicated to steer cells towards a M1-like phenotype [123]. In the here presented data, monocytes were only supplemented with M-CSF to promote differentiation, which could have influenced cell fate and response to stimuli. The results of the different monocyte-to-macrophage differentiation did not confirm the findings reported by Fleetwood, *et al.* [123], as M2 markers were upregulated in presence of GM-CSF differentiation, while M1 markers showed contradictory results, with CD197 upregulated and CXCL10 downregulated in presence of GM-CSF (figure 21). Interestingly, the supplementation of a mixture of M- and GM-CSF showed a downregulation of the M1 markers and an upregulation of the M2 markers, with no difference between the 1:1 and 10:1 ratio. Despite the lack of statistical significance, the results did not indicate that the differences observed after polarization in skin differentiation media were due to the monocyte-to-macrophage differentiation conditions, indicating that the media themselves influence cell polarization.

Overall, the lack of statistical significance for stimulated cells in different media reflects one of the challenges related to primary immune cell culture. As expected, the donor-to-donor variation had a large influence on the distribution of the results. Variations were limited by only selecting healthy volunteers for blood donation, with no indication of eventual confounding factors as autoimmune disorders or anti-inflammatory drugs intake before donation, as these might alter immune cell response to stimuli. Furthermore, a standardized protocol for all isolations was implemented. Nevertheless, the natural human variation resulted in a highly heterogeneous response following stimulation, with some donors displaying a fast and intense response and others showing a weak response after stimulation. Data analysis was performed assuming a non-parametric distribution for all experiments employing human primary macrophages, and no values were labeled as outliers and discarded to preserve the diversity that is also detected *in vivo*.

6.2.4.   RPMI control medium does not support epidermal differentiation

Since skin differentiation media were previously shown to affect macrophage functionality in terms of morphology and polarization ability, the feasibility of culturing skin in RPMI control medium was investigated. The culture of skin equivalents in both skin differentiation media showed the formation of a mature epithelium. Conversely, RPMI control medium resulted in the lack of a stratified epidermis (figure 22). Few cells were detected on top of the dermal compartment, indicating a lack of cell attachment, spreading and proliferation. RPMI control medium already showed to negatively affect keratinocyte viability and proliferation in 2D (figures 16-17), and the same effects were observed in a 3D context. Differently from skin differentiation media, which contain specific elements that support skin cells culture, RPMI control medium is only supplemented with serum and antibiotics. Skin differentiation medium 1 has a proprietary composition, but skin differentiation medium 2 is known to contain KGF and $CaCl_2$, which promote keratinocyte survival and differentiation [190,195], and a number of further supplements designed to promote epidermal stratification. As we have observed that keratinocytes stratification does not occur in presence of RPMI control medium, the feasibility of switching medium once epithelial differentiation is accomplished was investigated. Skin equivalents were cultured in skin differentiation medium 1 or 2 until epidermal differentiation was achieved, then a part of the equivalents was supplemented with RPMI control medium for 7 days, the time frame selected for wound healing investigation. Loricrin staining showed that skin equivalents cultured in skin differentiation media positively expressed the late keratinocyte differentiation features. However, once the medium was changed to RPMI control the tissue underwent de-differentiation, indicated by the lack of loricrin

expression (figure 23). The findings underline the importance of providing a continuous source of supplements to *in vitro* skin equivalents, which are not only needed to promote differentiation but also to maintain a differentiated epidermis. As calcium has a key role in keratinocyte differentiation [195], its depletion from the culture medium might be the leading cause of the negative effects observed. However, the investigation on its role in the differentiation process mainly focus on the trigger of keratinocyte differentiation instead of its maintenance. Further investigation is required to assess whether calcium is the main element maintaining epidermal differentiation, or if other components are also involved in tissue de-differentiation.

6.2.5.   Skin differentiation media negatively affect the functionality of 3D-embedded macrophages

As the designed strategy for introducing macrophages into skin models includes the culture in a 3D environment, cell functionality was also assessed after embedding. Macrophage functionality in the different media was assessed through viability, polarization and migration ability. Live/dead staining of 3D-embedded macrophages showed a decrease in cell viability over time, similar to the behavior detected in 2D (figure 16). A higher number of dead cells was observed in skin differentiation medium 2 compared to the other conditions (figure 24A). Quantification of viability showed that skin differentiation medium 2 led to a significantly lower value compared to RPMI control and skin differentiation medium 1 after 7 days of culture (figure 24B). Surprisingly, skin differentiation medium 2 showed to negatively influence macrophage survival to a greater extent in 3D compared to 2D cultures, and the effects were evident at a later time point compared to the 2D setting. The highest cell mortality in 3D experiments is probably due to the presence of the gel around cells, preventing the removal of dead cells through medium change and leading to an increased dead cell fraction in the calculations. Also, the delayed decrease with respect to 2D culture is likely due to the presence of a 3D matrix, as the collagen seeding mixture contains concentrated medium that could have provided the cells with supplements that promoted survival in the initial culture time.

Even after embedding in collagen gels, macrophages retained the ability to sense pro-inflammatory cues and responded by eliciting inflammation, as demonstrated by the increased secretion of IL-6 and IL-8 in the supernatant compared to unstimulated gels (figure 25). While cytokine production was detected in all conditions, gels cultured in skin differentiation media secreted less IL-6 and IL-8 compared to samples in RPMI control medium. The findings confirm the inhibitory effects on inflammation of skin differentiation media also observed in 2D cultures. As previously discussed, the effects are probably due to the presence of hydrocortisone in the skin differentiation media, with the additional inhibitory effect of isoproterenol in skin differentiation medium 2.

The ability to migrate through a gel was investigated with a vertical invasion assay, seeding macrophages on empty collagen gels and culturing them in the different media for 48 hours. Sample imaging upon live/dead staining demonstrated that migration of cells was detected in all conditions (figure 26A). Migration quantification was performed on 3D reconstructed images and showed an increased migration depth in presence of skin differentiation medium 1 and decreased migration with skin differentiation 2, compared to RPMI control medium (figure 26B). However, the results were statistically not significant, and the migration distance observed was likely due to the different cell density detected after 48 hours of culture. Indeed, overview images of the gel surface showed a lower number of cells in skin differentiation medium 2 cultured samples compared to the other conditions (figure 26C). As previously discussed, macrophages are conventionally cultured in serum. Its depletion from the medium was shown to decrease cell viability [196], as also here demonstrated with the 2D viability assessment. The negative effects of serum deprivation can be balanced by supplementation of other factors, as described by Kreutz *et al.* [196]. Skin differentiation medium 1 has a serum-free composition but contains several micronutrients and supplements to enhance cell survival, even though the full composition has not been disclosed due to proprietary formulation. Skin differentiation medium 2 contains a low percentage of serum, and components that are specifically selected to enhance keratinocyte differentiation. Even though a direct comparison between the two media cannot be made, it could be speculated that the nutrients supplemented to skin differentiation medium 1 do compensate for the lack of serum, maintaining macrophage ability to survive, adhere to the collagen gel and migrate. Conversely, the nutrients contained in skin differentiation medium 2 might not counterbalance the negative effects of serum depletion, resulting in reduced cell attachment and proliferation.

6.3.   Immunocompetent skin wound models are responsive to stimuli but reflect the inhibitory effects of culture medium

The combination of macrophage-containing collagen gels with skin equivalents was performed after skin wound implementation, quantifying the inflammatory response and analyzing macrophage location after one week of co-culture in skin differentiation medium 2. Both 24 and 72 hours after wounding, cytokine secretion was higher for wounded samples compared to unwounded controls, except for IL-8 after 72 hours that was lower in wounded samples (figure 27). This is in agreement with the induction of an inflammatory response after wounding, as shown for other *in vitro* skin models [81,84]. For all conditions, cytokine concentrations detected in the culture medium were higher after 24 hours in comparison to 72 hours (figure 27), which is also in agreement with previous reports [81,84]. The findings are consistent with the *in vivo* pro-inflammatory response occurring after wounding, which is elicited 1 to 5 days after injury [7] and is then gradually resolved to promote the tissue repair phase, which occurs between 3 to 10 days after wound formation [33]. The supplementation of calcium pantothenate in the fibrin hydrogel filling the wound did not show to increase the inflammatory response, as the detected values were similar to samples that were supplemented with fibrin only. Calcium pantothenate is known to be essential for maintaining keratinocyte proliferation and differentiation [197] and has been shown to positively influence also migration and proliferation of fibroblasts [198]. Topical application of panthenol, the stable alcoholic analogue of calcium pantothenate, is commonly used in the clinics for wound regeneration and to treat a series of dermatological disorders [199]. By performing a scratch wound assay, a positive effect on cell migration for both fibroblasts and keratinocytes was confirmed (Appendix A), in agreement with literature [198]. For this reason, calcium pantothenate was selected as a positive reference for improved healing in the 3D skin wound model. While panthenol effects have been extensively investigated in both *in vitro* and *in vivo* skin [199], few reports on its interaction with immune cells have been reported. Recent findings showed that panthenol is involved in the regulation of macrophage maturity, promoting their phagocytic activity and boosting their pro-inflammatory effect during bacterial infection, as increased IL-6 secretion was detected after treatment with panthenol [200]. A pro-inflammatory effect of calcium pantothenate in the 3D skin wound models could not be confirmed, as the secretion levels of both IL-6 and IL-8 in immunocompetent wounded skin were lower than in wounded skin without macrophage co-culture (figure 27). These effects are probably due to the inhibitory effects that skin differentiation medium 2 has on macrophage inflammatory activity, as shown with both the 2D gene expression analysis (figures 19-20) and

the 3D quantification of macrophage cytokine secretion (figure 25). As previously discussed, isoproterenol and hydrocortisone are known to inhibit M1-like polarization [186,187], therefore the reduced IL-6 and IL-8 secretion is likely due to their presence in skin differentiation medium 2.

The IHC analysis of immunocompetent wounded skin samples showed that macrophages could be detected in culture until 7 days after wound formation (figure 28). CD68 marker was used to confirm immune cell phenotype, and IHC showed that macrophages were detected both in the immune compartment below skin equivalents and in the bottom part of dermis, which was in proximity of the macrophage-containing gels (figure 28A). This indicates that cells were slowly migrating towards the wounded tissue. However, the cells were not always positive for CD68 after embedding and culture, even the cells detected in the macrophage-containing gel placed below skin tissue (figure 28B). A similar scenario has been described by Leonard *et al.* [201], who introduced collagen-embedded macrophages in an *in vitro* intestine model. Despite they reported the successful implementation of both macrophages and DCs into the models, no specific immunofluorescent staining of immune cells could be achieved, which was attributed to the differentiation and loss of markers of the cells in culture [201]. Furthermore, literature reports controversial results on the use of CD68 as a macrophage marker. On one side, it has been shown that CD68 can be used both as a pan-macrophage marker and M1 marker [202], representing a useful tool to identify tumor-associated macrophages. If CD68 is only expressed by M1 macrophages, this could explain the observed different staining in the samples, as some cells might have polarized to a pro-inflammatory phenotype due to the stimuli in surrounding environment. Conversely, other evidence suggested that CD68 is expressed by both M1 and M2 macrophages [203]. Further investigation is needed to confirm whether CD68 can be reliably used to stain primary human macrophages. Additionally, it has been shown that CD68 can also be expressed by primary fibroblasts [204], suggesting the implementation of a second staining such as vimentin to distinguish fibroblasts from macrophages. Alternatively, other markers might be selected for macrophage staining. HLA-DR and DC-SIGN, for instance, have been successfully used by Bechetoille, *et al.* [115] to stain primary human macrophages.

Chapter 7:
Outlook and future perspectives

7.   Outlook and future perspectives

Taken together, all aspects for generating a reproducible *in vitro* skin wound model have been investigated and discussed in this thesis. The evaluation of diverse collagen scaffolds for *in vitro* skin culture integrates in the current skin tissue engineering trend to identify a scaffold supporting cell functionality and at the same time displaying stable mechanical properties. Despite collagen represents the most used material for *in vitro* tissue engineering [73], it is mainly obtained from animal sources, contradicting the perspective of implementing the 3R principles in research and introducing cross-species variables. A solution providing both the presence of biological native structures and animal-free origins is the use of human decellularized tissue. Decellularized scaffolds have been obtained from different organs and used for different applications, as reviewed in Hoshiba, *et al.* [205]. Diverse decellularization procedures have been described, and human decellularized dermal matrices are also commercially available [206], which underlines the feasibility of obtaining scaffolds applicable to *in vitro* tissue engineering. One drawback of human-derived materials is the scarce availability of donor tissue. Promoting a closer collaboration between research institutions and clinics would increase human source material availability, which would push forward the animal replacement.

Potentially, the combination of autologous cells with autologous decellularized dermis would mimic *in vitro* the patient-specific clinical picture, enabling to assess the efficacy of novel treatments directly on personalized skin models. Individual variations in the response to therapies are well known, as also underlined by the here presented findings following primary macrophage stimulation with pro- and anti-inflammatory cytokines. Consequently, fully allogeneic cultures represent the outmost setting for a significant preclinical drug evaluation. So far, fibroblasts and keratinocytes have been mainly isolated from healthy donors to generate skin equivalents. The use of patient-derived biopsies have recapitulated *in vitro* some features of chronic wounds [101], and more studies with a similar setup would offer the opportunity to study the effectiveness of novel treatments for specific healing disorders on *in vitro* diseased models.

A handful of synthetic materials has been developed for diverse tissue engineering applications [207][208], describing the use of many manufacturing processes for a controlled and reproducible production. Despite synthetic materials lack the biological presence of cell adhesion motifs, they have the potential to be engineered to improve cell adhesion and mimic the *in vivo* structures. Thanks to material engineering, there is a great potential for implementation of diverse appendices in skin models. For instance, the development of a modified polyvinyl alcohol hydrogel has demonstrated to precisely guide cell invasion through the matrix [209], representing a promising technique for introducing microvasculature in tissue models.

Another aspect that would benefit from a closer collaboration with the clinics is wound healing assessment. In order to monitor the healing of single wounds over time, more efforts towards the implementation of non-invasive methods is required. The potential of OCT for real-time monitoring of wound closure was here shown, however the access to the equipment is restricted to clinicians and requires training. Furthermore, image processing software should be available to avoid the use of custom-designed tools that are not reproducible, providing results that are more comparable between research groups. Decreasing the use of end-point analyses in favor of non-invasive methods for healing assessment will reduce experimental sample size, costs and increase the scientific validity of the data.

The macrophage incorporation strategy here described includes the combination of immune cells as an additional hydrogel compartment to shorten the culture time. This approach potentially translates in application to other *in vitro* organs, as it can be combined with any equivalent to achieve immune competency. Here macrophage functionality was only evaluated for the potential duration of an inflammatory response, as the target application is wound healing investigation. However, longer culture times might also result in preserved cellular viability and activity, further expanding the applications.

Before obtaining a fully functional immunocompetent skin model, culture medium requires optimization. As demonstrated in this thesis, the selection of media in use for skin and macrophage culture showed to affect either skin structure or macrophage functionality. So far, only few of the components present in skin differentiation media have been investigated for their effects on primary immune cells, as well as for the effects that their depletion from culture media has on epidermal differentiation. Deeper understanding of these interactions is the key to define novel media formulations that support immunocompetent skin culture. As a plethora of media has been described for skin and macrophage *in vitro* culture, a comprehensive literature study would contribute to identify the recurring components used for culture. Then, similarly as performed here, the effects of each component could be investigated on both single cultures and more complex 3D co-cultures, to identify which elements and in which concentration are key to successful skin maturation or macrophage polarization.

Bibliography

[1]   Som, P.M., Laitman, J.T., Mak, K., Embryology and anatomy of the skin, its appendages, and physiologic changes in the head and neck, *Neurographics*. 7 (2017) 390–415.

[2]   Kolarsick, P.A.J., Kolarsick, M.A., Goodwin, C., Anatomy and physiology of the skin, *J. Dermatol. Nurses. Assoc.* 3 (2011) 203–213.

[3]   McGrath, J.A., Eady, R.A.J., Pope, F.M., Anatomy and organization of human skin, *Rook's Textb. Dermatology*. (2004) 45–128.

[4]   Wikramanayake, T.C., Stojadinovic, O., Tomic-Canic, M., Epidermal differentiation in barrier maintenance and wound healing., *Adv. Wound Care*. 3 (2014) 272–280.

[5]   Baroni, A., Buommino, E., De Gregorio, V., Ruocco, E., et al., Structure and function of the epidermis related to barrier properties, *Clin. Dermatol.* 30 (2012) 257–262.

[6]   Webb, A., Li, A., Kaur, P., Location and phenotype of human adult keratinocyte stem cells of the skin, *Differentiation*. 72 (2004) 387–395.

[7]   Kirwan, H., Pignataro, R., The skin and wound healing, *Pathol. Interv. Musculoskelet. Rehabil.*, 2nd Ed., Elsevier Inc., 2016: pp. 25–62.

[8]   Carlson, B., Human Embryology and Developmental Biology, 6th Ed., Elsevier, 2018: p. 496.

[9]   Brenner, M., Hearing, J.V., The protective role of melanin against UV damage in human skin, *Photochem. Photobiol.* 84 (2008) 539–549.

[10]   Maricich, S.M., Lumpkin, E.A., Zoghbi, H.Y., Wellnitz, S.A., et al., Merkel cells are essential for light-touch responses, *Science (80-.).* 324 (2009) 1580–1582.

[11]   OpenStax, The integumentary system, *Anat. Physiol.* (https://opentextbc.ca/anatomyandphysiology).

[12]   Kalinin, A.E., Kajava, A. V., Steinert, P.M., Epithelial barrier function: Assembly and structural features of the cornified cell envelope, *BioEssays*. 24 (2002) 789–800.

[13]   van der Valk, P.G.M., Kucharekova, M., Tupker, R.A., Transepidermal water loss and its relation to barrier function and skin irritation, *Bioeng. Ski. Water Strat. Corneum*, 2nd Ed., Dermatology: Clinical & Basic Science, 2005: pp. 97–104.

[14]   Cui, C.Y., Schlessinger, D., Eccrine sweat gland development and sweat secretion, *Exp. Dermatol.* 24 (2015) 644–650.

[15]   Hu, Q.M., Yi, W.J., Su, M.Y., Jiang, S., et al., Induction of retinal-dependent calcium influx in human melanocytes by UVA or UVB radiation contributes to the stimulation of melanosome transfer, *Cell Prolif.* 50 (2017). DOI:10.1111/cpr.12372.

[16]   Yamaguchi, Y., Brenner, M., Hearing, V.J., The regulation of skin pigmentation, *J. Biol. Chem.* 282 (2007) 27557–27561.

[17]   Brandwein, M., Bentwich, Z., Steinberg, D., Endogenous antimicrobial peptide expression in response to bacterial epidermal colonization, *Front. Immunol.* 8 (2017) DOI:10.3389/fimmu.2017.01637.

[18]   Schauber, J., Gallo, R.L., Antimicrobal peptides and the skin imune defence system, *J. Allergy Clin. Immunol.* 122 (2008) 261–266.

[19]   Matejuk, A., Skin Immunity, *Arch. Immunol. Ther. Exp. (Warsz).* (2017) 45–54.

[20]   Seneschal, J., Clark, R.A., Gehad, A., Baecher-Allan, C.M., et al., Public Access NIH Public Access, *Immunity*. 36 (2012) 873–884.

[21]   Geissman, F., Manz, M.G., Jung, S., Sieweke, M.H., et al., Development of monocytes, macrophages and dendritic cells, *Science (80-.).* 327 (2010) 656–661.

[22]   Jakubzick, C., Gautier, E.L., Gibbings, S.L., Sojka, D.K., et al., Minimal differentiation of classical

monocytes as they survey steady state tissues and transport antigen to lymph nodes, *Immunity*. 39 (2013) 599–610.

[23]   Gregorio, J., Meller, S., Conrad, C., Di Nardo, A., et al., Plasmacytoid dendritic cells sense skin injury and promote wound healing through type I interferons, *J. Exp. Med.* 207 (2010) 2921–2930.

[24]   Guiducci, C., Tripodo, C., Gong, M., Sangaletti, S., et al., Autoimmune skin inflammation is dependent on plasmacytoid dendritic cell activation by nucleic acids via TLR7 and TLR9, *J. Exp. Med.* 207 (2010) 2931–2942.

[25]   Yona, S., Kim, K.W., Wolf, Y., Mildner, A., et al., Fate mapping reveals origins and dynamics of monocytes and tissue macrophages under homeostasis, *Immunity*. 38 (2013) 79–91.

[26]   Tamoutounour, S., Guilliams, M., MontananaSanchis, F., Liu, H., et al., Origins and functional specialization of macrophages and of conventional and monocyte-derived dendritic cells in mouse skin, *Immunity*. 39 (2013) 925–938.

[27]   Mosser, D.M., Edwards, J.P., Exploring the full spectrum of macrophage activation., *Nat. Rev. Immunol.* 8 (2008) 958–69.

[28]   Delavary, B.M., van der Veer, W.M., van Egmond, M., Niessen, F.B., et al., Macrophages in skin injury and repair, *Immunobiology*. 216 (2011) 753–762.

[29]   Biswas, S.K., Mantovani, A., Orchestration of metabolism by macrophages, *Cell Metab.* 15 (2012) 432–437.

[30]   Amin, K., The role of mast cells in allergic inflammation, *Respir. Med.* 106 (2012) 9–14.

[31]   Pupovac, A., Senturk, B., Griffoni, C., Maniura-Weber, K., et al., Toward immunocompetent 3D skin models, *Adv. Healthc. Mater.* 7 (2018). DOI:10.1002/adhm.201701405.

[32]   Clark, R.A., Skin resident T cells: the ups and downs of on site immunity, *J. Invest. Dermatol.* 130 (2010) 362–370.

[33]   Reinke, J.M., Sorg, H., Wound repair and regeneration, *Eur. Surg. Res.* 49 (2012) 35–43.

[34]   Mescher, A.L., Macrophages and fibroblasts during inflammation and tissue repair in models of organ regeneration, *Regeneration*. 4 (2017) 39–53.

[35]   Frykberg, R.G., Banks, J., Challenges in the Treatment of Chronic Wounds, *Adv. Wound Care*. 4 (2015) 560–582.

[36]   Werner, S., Grose, R., Regulation of wound healing by growth factors and cytokines, *Physiol. Rev.* 83 (2003) 835–870.

[37]   Wynn, T.A., Vannella, K.M., Macrophages in tissue repair, regeneration, and fibrosis Thomas, *Immunity*. 44 (2016) 450–462.

[38]   Nestle, F.O., Di Meglio, P., Qin, J.-Z., Nickoloff, B.J., Skin immune sentinels in health and disease, *Nat. Rev. Immunol.* 9 (2009) 679–691.

[39]   Willenborg, S., Eming, S.A., Macrophages – sensors and effectors coordinating skin damage and repair, *J. Ger. Soc. Dermatology*. 12 (2014) 214–223.

[40]   Murray, P., Wynn, T.A., Protective and pathogenic functions of macrophage subsets, *Nat. Rev. Immunol.* 11 (2011) 723–737.

[41]   Tejiram, S., Kavalukas, S.L., Shupp, J.W., Barbul, A., Wound healing, *Wound Heal. Biomater.*, Elsevier Ltd, 2016: pp. 3–39.

[42]   Clark, R.A.F., Lanigan, J.M., DellaPelle, P., Manseau, E., et al., Fibronectin and fibrin provide a provisional matrix for epidermal cell migration during wound reepithelialization, *J. Invest. Dermatol.* 79 (1982) 264–269.

[43]   Clark, R.A.F., Fibronectin in the skin, *J. Invest. Dermatol.* 81 (1983) 475–479.

[44]   Jacinto, A., Martinez-Arias, A., Martin, P., Mechanisms of epithelial fusion and repair, *Nat. Cell Biol.* 3 (2001) 117–123.

[45]   Madden, J.W., Peacock, E.E., Studies on the biology of collagen during wound healing, *Ann.*

Surg. 174 (1971) 511–518.

[46] Brown, L.F., Yeo, K.-T., Berse, B., Yeo, T.-K., et al., Expression of vascular permeability factor (vascular endothelial growth factor) by epidermal keratinocytes during wound healing, *J. Exp. Med.* 176 (1992) 1375–1379.

[47] Frank, S., Hübner, G., Breier, G., Longaker, M.T., et al., Regulation of vascular endothelial growth factor expression in cultured keratinocytes, *J. Biol. Chem.* 270 (1995) 12607–12613.

[48] Hinz, B., Formation and function of the myofibroblast during tissue repair, *J. Invest. Dermatol.* 127 (2007) 526–537.

[49] Martinez-Ferrer, M., Afshar-Sherif, A.R., Uwamariya, C., De Crombrugghe, B., et al., Dermal transforming growth factor-β responsiveness mediates wound contraction and epithelial closure, *Am. J. Pathol.* 176 (2010) 98–107.

[50] Greenhalgh, D.G., The role of apoptosis in wound healing, *Te Int. J. Biochem. Cell Biol.* 30 (1998) 1019–1030.

[51] Gould, L., Abadir, P., Brem, H., Carter, M., et al., Chronic wound repair and healing in older adults: current status and future research, *Wound Repair Regen.* 23 (2015) DOI:10.1111/wrr.12245.

[52] Van de Kerkhof, P.C.M., Van Bergen, B., Spruijt, K., Kuiper, J.P., Age-related changes in wound healing, *Clin. Exp. Dermatol.* 19 (1994) 369–374.

[53] Gosain, A., DiPietro, L.A., Aging and wound healing, *World J. Surg.* 28 (2004) 321–326.

[54] Martin, L.G., Demography and aging, *Handb. Aging Soc. Sci.*, 7th Ed., 2011: pp. 33–45.

[55] Sen, C.K., Gordillo, G.M., Roy, S., Kirsner, R., et al., Human skin wounds: a major and snowballing threat to public health and the economy, *Wound Repair Regen.* 17 (2009) 763–771.

[56] Eming, S.A., Martin, P., Tomic-Canic, M., Wound repair and regeneration: mechanisms, signaling, and translation., *Sci. Transl. Med.* 6 (2014). DOI:10.1126/scitranslmed.3009337.

[57] Ågren, M.S., Steenfos, H.H., Dabelsteen, S., Hansen, J.B., et al., Proliferation and mitogenic response to PDGF-BB of fibroblasts isolated from chronic venous leg ulcers is ulcer-age dependent, *J. Invest. Dermatol.* 112 (1999) 463–469.

[58] Kim, B.C., Kim, H.T., Park, S.H., Cha, J.S., et al., Fibroblasts from chronic wounds show altered TGF-β-signaling and decreased TGF-β type II receptor expression, *J. Cell. Physiol.* 195 (2003) 331–336.

[59] Khanna, S., Biswas, S., Shang, Y., Collard, E., et al., Macrophage dysfunction impairs resolution of inflammation in the wounds of diabetic mice, *PLoS One*. 5 (2010). DOI:10.1371/journal.pone.0009539.

[60] Bell, E., Ehrlich, H.P., Buttle, D.J., Nakatsuji, T., et al., Living tissue formed in vitro and accepted as skin-equivalent tissue of full thickness, *Science (80-.).* 211 (1981) 1052–1054.

[61] Groeber, F., Holeiter, M., Hampel, M., Hinderer, S., et al., Skin tissue engineering - In vivo and in vitro applications, *Adv. Drug Deliv. Rev.* 63 (2011) 352–366.

[62] Seaton, M., Hocking, A., Gibran, N.S., Porcine models of cutaneous wound healing, *ILAR J.* 56 (2015) 127–138.

[63] Dunn, L., Prosser, H.C.G., Tan, J.T.M., Vanags, L.Z., et al., Murine model of wound healing, *J. Vis. Exp.* (2013) DOI:10.3791/50265.

[64] Pasparakis, M., Haase, I., Nestle, F.O., Mechanisms regulating skin immunity and inflammation, *Nat. Rev. Immunol.* 14 (2014) 289–301.

[65] Seok, J., Warren, S.H., Cuenca, A.G., Mindrinos, M.N., et al., Genomic responses in mouse models poorly mimic human inflammatory diseases, *PNAS.* 110 (2013) 3507–3512.

[66] Stamm, A., Reimers, K., Strauss, S., Vogt, P., et al., In vitro wound healing assays - State of the art, *BioNanoMaterials*. 17 (2016) 79–87.

[67]   Hulkower, K.I., Herber, R.L., Cell migration and invasion assays as tools for drug discovery, *Pharmaceutics*. 3 (2011) 107–124.

[68]   Jonkman, J.E.N., Cathcart, J.A., Xu, F., Bartolini, M.E., et al., An introduction to the wound healing assay using live-cell microscopy, *Cell Adh. Migr.* 8 (2014) 440–451.

[69]   Liang, C.C., Park, A.Y., Guan, J.L., In vitro scratch assay: a convenient and inexpensive method for analysis of cell migration in vitro, *Nat. Protoc.* 2 (2007) 329–333.

[70]   Keese, C.R., Wegener, J., Walker, S.R., Giaever, I., Electrical wound-healing assay for cells in vitro, *Proc. Natl. Acad. Sci. U. S. A.* 101 (2004) 1554–1559.

[71]   Szulcek, R., Bogaard, H.J., van Nieuw Amerongen, G.P., Electric cell-substrate impedance sensing for the quantification of endothelial proliferation, barrier function, and motility, *J. Vis. Exp.* (2014) 1–12.

[72]   Ulrich, M.M.W., Vlig, M., Boekema, B.K.H.L., Biomaterials for dermal substitutes, *Wound Heal. Biomater.*, Elsevier Ltd, 2016: pp. 227–252.

[73]   Antoine, E.E., Vlachos, P.P., Rylander, M.N., Review of collagen I hydrogels for bioengineered tissue microenvironments: characterization of mechanics, structure, and transport, *Tissue Eng. Part B, Rev.* 20 (2014) 683–696.

[74]   Allen-Hoffmann, B.L., Schlosser, S.J., Ivarie, C.A.R., Sattler, C.A., et al., Normal growth and differentiation in a spontaneously immortalized near- diploid human keratinocyte cell line, NIKS, *J. Invest. Dermatol.* 114 (2000) 444–455.

[75]   Reijnders, C.M.A., van Lier, A., Roffel, S., Kramer, D., et al., Development of a Full-Thickness Human Skin Equivalent In Vitro Model Derived from TERT-Immortalized Keratinocytes and Fibroblasts, *Tissue Eng. Part A*. 21 (2015) 2448–59.

[76]   Falanga, V., Isaacs, C., Paquette, D., Downing, G., et al., Wounding of bioengineered skin: Cellular and molecular aspects after injury, *J. Invest. Dermatol.* 119 (2002) 653–660.

[77]   Geer, D.J., Swartz, D.D., Andreadis, S.T., Fibrin promotes migration in a three-dimensional in vitro model of wound regeneration., *Tissue Eng.* 8 (2002) 787–798.

[78]   El Ghalbzouri, A., Hensbergen, P., Gibbs, S., Kempenaar, J., et al., Fibroblasts facilitate re-epithelialization in wounded human skin equivalents, *Lab. Investig.* 84 (2004) 102–112.

[79]   Laplante, A.F., Germain, L., Auger, F.A., Moulin, V., Mechanisms of wound reepithelialization: hints from a tissue-engineered reconstructed skin to long-standing questions., *FASEB J.* 15 (2001) 2377–2389.

[80]   Xie, Y., Rizzi, S.C., Dawson, R., Lynam, E., et al., Development of a three-dimensional human skin equivalent wound model for investigating novel wound healing therapies, *Tissue Eng. Part C, Methods*. 16 (2010) 1111–1123.

[81]   Safferling, K., Sütterlin, T., Westphal, K., Ernst, C., et al., Wound healing revised: a novel reepithelialization mechanism revealed by in vitro and in silico models, *J. Cell Biol.* 203 (2013) 691–709.

[82]   Marquardt, Y., Amann, P.M., Heise, R., Czaja, K., et al., Characterization of a novel standardized human three-dimensional skin wound healing model using non-sequential fractional ultrapulsed CO2 laser treatments, *Lasers Surg. Med.* 47 (2015) 257–265.

[83]   Rossi, A., Appelt-Menzel, A., Kurdyn, S., Walles, H., et al., Generation of a three-dimensional full thickness skin equivalent and automated wounding., *J. Vis. Exp.* (2015) DOI:doi:10.3791/52576.

[84]   Breetveld, M., Richters, C.D., Rustemeyer, T., Scheper, R.J., et al., Comparison of wound closure after burn and cold injury in human skin equivalents., *J. Invest. Dermatol.* 126 (2006) 1918–1921.

[85]   Amann, P.M., Marquardt, Y., Steiner, T., Hölzle, F., et al., Effects of non-ablative fractional erbium glass laser treatment on gene regulation in human three-dimensional skin models, *Lasers Med. Sci.* 31 (2016) 397–404.

[86]   Vaughan, M.B., Ramirez, R.D., Brown, S. a, Yang, J.C., et al., A reproducible laser-wounded skin equivalent model to study the effects of aging in vitro., *Rejuvenation Res.* 7 (2004) 99–110.

[87]   Xu, W., Jong Hong, S., Jia, S., Zhao, Y., et al., Application of a partial-thickness human ex vivo skin culture model in cutaneous wound healing study, *Lab. Investig.* 92 (2012) 584–599.

[88]   Pastar, I., Liang, L., Sawaya, A.P., Wikramanayake, T.C., et al., Preclinical models for wound-healing studies, *Ski. Tissue Model.*, Elsevier, 2018: pp. 223–251.

[89]   Yosouf, Y., Amini-Nik, S., Jeschke, M.G., Overall perspective on the clinical importance of skin models, *Ski. Tissue Model.*, Elsevier, 2018. DOI:doi.org/10.1016/B978-0-12-810545-0.00002-4.

[90]   S, R.W.M., L, B.R., The principles of humane experimental techniques, (1959).

[91]   Parliament, E., Regulation No 1223/2009, EU, 2009.

[92]   Parliament, E., Directive 2010/63/EU, EU, 2010.

[93]   National Centre for the Replacement Refinement & Reduction of Animals in Research. The 3Rs (https://www.nc3rs.org.uk/).

[94]   Edmondson, R., Broglie, J.J., Adcock, A.F., Yang, L., Three-dimensional cell culture systems and their applications in drug discovery and cell-based biosensors, *Assay Drug Dev. Technol.* 12 (2014) 207–218.

[95]   Coulomb, B., Lebreton, C., Dubertret, L., Influence of human dermal fibroblasts on epidermalization, *J. Invest. Dermatol.* 92 (1989) 122–125.

[96]   Wojtowicz, A.M., Oliveira, S., Carlson, M.W., Zawadzka, A., et al., The importance of both fibroblasts and keratinocytes in a bilayered living cellular construct used in wound healing, *Wound Repair Regen.* 22 (2014) 246–255.

[97]   Bernerd, F., Asselineau, D., An organotypic model of skin to study photodamage and photoprotection in vitro, *J. Am. Acad. Dermatol.* 58 (2008) S155–S159.

[98]   Lerebour, G., Cupferman, S., Bellon-Fontaine, M.N., Adhesion of Staphylococcus aureus and Staphylococcus epidermidis to the Episkin® reconstructed epidermis model and to an inert 304 stainless steel substrate, *J. Appl. Microbiol.* 97 (2004) 7–16.

[99]   Hayden, P.J., Bachelor, M., Ayehunie, S., Letasiova, S., et al., Application of MatTek in vitro reconstructed human skin models for safety, efficacy screening, and basic preclinical research, *Appl. Vitr. Toxicol.* 1 (2015) 226–233.

[100]   Li, L., Fukunaga-Kalabis, M., Herlyn, M., The three-dimensional human skin reconstruct model: a tool to study normal skin and melanoma progression, *J. Vis. Exp.* (2011) DOI:10.3791/2937.

[101]   Maione, A.G., Brudno, Y., Stojadinovic, O., Park, L.K., et al., Three-dimensional human tissue models that incorporate diabetic foot ulcer-derived fibroblasts mimic in vivo features of chronic wounds, *Tissue Eng. Part C, Methods*. 21 (2015) 499–508.

[102]   van den Broek, L.J., Niessen, F.B., Scheper, R.J., Gibbs, S., Development, validation and testing of a human tissue engineered hypertrophic scar model, *ALTEX*. 29 (2012) 389–402.

[103]   Caley, M., Wall, I.B., Peake, M., Kipling, D., et al., Development and characterisation of a human chronic skin wound cell line—towards an alternative for animal experimentation, *Int. J. Mol. Sci.* 19 (2018) DOI: 10.3390/ijms19041001.

[104]   Margulis, A., Zhang, W., Alt-Holland, A., Crawford, H.C., et al., E-cadherin suppression accelerates squamous cell carcinoma progression in three-dimensional, human tissue constructs, *Cancer Res.* 65 (2005) 1783–1791.

[105]   Carlson, M.W., Alt-Holland, A., Egles, C., Garlick, J.A., Three-dimensional tissue models of normal and diseased skin, *Curr. Protoc. Cell Biol.* chap 19 (2008). DOI:10.1002/0471143030.cb1909s41.

[106]   Linde, N., Gutschalk, C.M., Hoffmann, C., Yilmaz, D., et al., Integrating macrophages into organotypic co-cultures: A 3D in vitro model to study tumor-associated macrophages, *PLoS One*. 7 (2012). DOI:10.1371/journal.pone.0040058.

[107] Todd, C., Hewitt, S.D., Kempenaar, J., Noz, K., et al., Co-culture of human melanocytes and keratinocytes in a skin equivalent model: effect of ultraviolet radiation, *Arch. Dermatol. Res.* 285 (1993) 455–459.

[108] Laubach, V., Zöller, N., Rossberg, M., Görg, K., et al., Integration of Langerhans-like cells into a human skin equivalent, *Arch. Dermatol. Res.* 303 (2011) 135–139.

[109] Ouwehand, K., Spiekstra, S.W., Waaijman, T., Breetveld, M., et al., CCL5 and CCL20 mediate immigration of Langerhans cells into the epidermis of full thickness human skin equivalents, *Eur. J. Cell Biol.* 91 (2012) 765–773.

[110] Ouwehand, K., Spiekstra, S.W., Waaijman, T., Scheper, R.J., et al., Technical advance: Langerhans cells derived from a human cell line in a full-thickness skin equivalent undergo allergen-induced maturation and migration, *J. Leukoc. Biol.* 90 (2011) 1027–1033.

[111] Bechetoille, N., Dezutter-Dambuyant, C., Damour, O., André, V., et al., Effects of solar ultraviolet radiation on engineered human skin equivalent containing both Langerhans cells and dermal Dendritic cells, *Tissue Eng.* 13 (2007) 2667–2679.

[112] Chau, D.Y.S., Johnson, C., Macneil, S., Haycock, J.W., et al., The development of a 3D immunocompetent model of human skin, *Biofabrication*. 5 (2013). DOI:10.1088/1758-5082/5/3/035011.

[113] Kühbacher, A., Henkel, H., Stevens, P., Grumaz, C., et al., Central role for dermal fibroblasts in skin model protection against candida albicans, *J. Infect. Dis.* 215 (2017) 1742–1752.

[114] Groeber, F., Engelhardt, L., Lange, J., Kurdyn, S., et al., A first vascularized skin equivalent as an alternative to animal experimentation, *ALTEX*. 33 (2016) 415–422.

[115] Bechetoille, N., Vachon, H., Gaydon, A., Boher, A., et al., A new organotypic model containing dermal-type macrophages, *Exp. Dermatol.* 20 (2011) 1035–1037.

[116] Boehnke, K., Mirancea, N., Pavesio, A., Fusenig, N.E., et al., Effects of fibroblasts and microenvironment on epidermal regeneration and tissue function in long-term skin equivalents, *Eur. J. Cell Biol.* 86 (2007) 731–746.

[117] Spiekstra, S.W., Breetveld, M., Rustemeyer, T., Scheper, R.J., et al., Wound-healing factors secreted by epidermal keratinocytes and dermal fibroblasts in skin substitutes, *Wound Repair Regen.* 15 (2007) 708–717.

[118] Lucas, T., Waisman, A., Ranjan, R., Roes, J., et al., Differential roles of macrophages in diverse phases of skin repair., *J. Immunol.* 184 (2010) 3964–3977.

[119] Chung, E., Choi, H., Lim, J.E., Son, Y., Development of skin inflammation test model by co-culture of reconstituted 3D skin and RAW264.7 cells, *Tissue Eng. Regen. Med.* 11 (2014) 87–92.

[120] Andreu, N., Phelan, J., De Sessions, P.F., Cliff, J.M., et al., Primary macrophages and J774 cells respond differently to infection with Mycobacterium tuberculosis, *Sci. Rep.* 7 (2017). DOI:10.1038/srep42225.

[121] Bell, E., Ivarsson, B., Merrill, C., Production of a tissue-like structure by contraction of collagen lattices by human fibroblasts of different proliferative potential in vitro, *Proc. Natl. Acad. Sci. U. S. A.* 76 (1979) 1274–1278.

[122] Souren, J.E., Ponec, M., van Wijk, A., Contraction of collagen by human fibroblasts and keratinocytes, *Vitr. Cell. Dev. Biol.* 25 (1989) 1039–1045.

[123] Fleetwood, A.J., Dinh, H., Cook, A.D., Hertzog, P.J., et al., GM-CSF- and M-CSF-dependent macrophage phenotypes display differential dependence on Type I interferon signaling, *J. Leukoc. Biol.* 86 (2009) 411–421.

[124] Akagawa, K.S., Functional heterogeneity of colony-stimulating factor-induced human monocyte-derived macrophages, *Int. J. Hematol.* 76 (2002) 27–34.

[125] Cross, V.L., Zheng, Y., Choi, N.W., Verbridge, S.S., et al., Dense type I collagen matrices that support cellular remodeling and microfabrication for studies of tumor angiogenesis and

vasculogenesis in vitro, *Biomaterials*. 31 (2010) 8596–8607.

[126]   Randall, M.J., Jüngel, A., Rimann, M., Wuertz-Kozak, K., Advances in the biofabrication of 3D skin in vitro: healthy and pathological models, *Front. Bioeng. Biotechnol.* 6 (2018). DOI:10.3389/fbioe.2018.00154.

[127]   Leitinger, B., Hohenester, E., Mammalian collagen receptors, *Matrix Biol.* 26 (2007) 146–155.

[128]   Davison-Kotler, E., Marshall, W.S., García-Gareta, E., Sources of collagen for biomaterials in skin wound healing, *Bioengineering*. 6 (2019). DOI:10.3390/bioengineering6030056.

[129]   Vidal, S.E.L., Tamamoto, K.A., Nguyen, H., Abbott, R.D., et al., 3D biomaterial matrix to support long term, full thickness, immuno-competent human skin equivalents with nervous system components, *Biomaterials*. 198 (2019) 194–203.

[130]   Braziulis, E., Diezi, M., Biedermann, T., Pontiggia, L., et al., Modified plastic compression of collagen hydrogels provides an ideal matrix for clinically applicable skin substitutes, *Tissue Eng. Part C, Methods*. 18 (2012) 464–474.

[131]   Witherel, C.E., Graney, P.L., Freytes, D.O., Weingarten, M.S., et al., Response of human macrophages to wound matrices in vitro, *Wound Repair Regen.* 24 (2016) 514–524.

[132]   Ahn, S., Yoon, H., Kim, G., Kim, Y., et al., Designed three-dimensional collagen scaffolds for skin tissue regeneration, *Tissue Eng. Part C, Methods*. 16 (2010) 813–820.

[133]   Schoof, H., Apel, J., Heschel, I., Rau, G., Control of pore structure and size in freeze-dried collagen sponges, *J. Biomed. Mater. Res.* 58 (2001) 352–357.

[134]   O'Brien, F.J., Harley, B.A., Yannas, I. V., Gibson, L., Influence of freezing rate on pore structure in freeze-dried collagen-GAG scaffolds, *Biomaterials*. 25 (2004) 1077–1086.

[135]   Powell, H.M., Boyce, S.T., EDC cross-linking improves skin substitute strength and stability, *Biomaterials*. 27 (2006) 5821–5827.

[136]   Haugh, M.G., Murphy, C.M., O'Brien, F.J., Novel freeze-drying methods to produce a range of collagen-glycosaminoglycan scaffolds with tailored mean pore sizes, *Tissue Eng. Part C, Methods*. 16 (2010) 887–894.

[137]   Yannas, I. V., Burke, J.F., Design of an artificial skin. I. Basic design principles, *J. Biomed. Mater. Res.* 14 (1980) 65–81.

[138]   Brougham, C.M. properties and enhanced capacity to resist cell-mediated contraction., Levingstone, T.J., Jockenhoevel, S., Flanagan, T.C., et al., Incorporation of fibrin into a collagen-glycosaminoglycan matrix results in a scaffold with improved mechanical, *Acta Biomater.* 26 (2015) 205–214.

[139]   Olde Damink, L.H.H., Dijkstra, P.J., Van Luyn, M.J.A., Van Wachem, P.B., et al., Cross-linking of dermal sheep collagen using a water-soluble carbodiimide, *Biomaterials*. 17 (1996) 765–773.

[140]   Hafemann, B., Ghofrani, K., Gattner, H.G., Stieve, H., et al., Cross-linking by 1-ethyl-3-(3-dimethylaminopropyl)-carbodiimide (EDC) of a collagen/elastin membrane meant to be used as a dermal substitute: Effects on physical, biochemical and biological features in vitro, *J. Mater. Sci. Mater. Med.* 12 (2001) 437–446.

[141]   Haugh, M.G., Murphy, C.M., McKiernan, R.C., Altenbuchner, C., et al., Crosslinking and mechanical properties significantly influence cell attachment, proliferation, and migration within collagen glycosaminoglycan scaffolds, *Tissue Eng. Part A*. 17 (2011) 1201–1208.

[142]   Li, J., Ren, N., Qiu, J., Jiang, H., et al., Carbodiimide crosslinked collagen from porcine dermal matrix for high-strength tissue engineering scaffold, *Int. J. Biol. Macromol.* 61 (2013) 69–74.

[143]   Guironnet, G., Dezutter-Dambuyant, C., Gaudillère, A., Maréchal, S., et al., Phenotypic and functional outcome of human monocytes or monocyte-derived dendritic cells in a dermal equivalent., *J. Invest. Dermatol.* 116 (2001) 933–939.

[144]   Régnier, M., Staquet, M.J., Schmitt, D., Schmidt, R., Integration of Langerhans cells into a pigmented reconstructed human epidermis, *J. Invest. Dermatol.* 102 (1997) 510–512.

[145] Ramsamooj, R., Strande, L., Kain, M.H., Doolin, E.J., et al., A novel in vitro model for xenorejection and immune mechanisms using bioengineered living skin equivalents, *Transplant. Proc.* 30 (1998) 1087–1088.

[146] Van Drongelen, V., Danso, M.O., Mulder, A., Mieremet, A., et al., Barrier properties of an N/TERT-based human skin equivalent, *Tissue Eng. Part A*. 20 (2014) 3041–3049.

[147] Dickson, M.A., Hahn, W.C., Ino, Y., Ronfard, V., et al., Human keratinocytes that express hTERT and also bypass a p16INK4a-enforced mechanism that limits life span become immortal yet retain normal growth and differentiation characteristics, *Mol. Cell. Biol.* 20 (2000) 1436–1447.

[148] Man, Y.K.S., Trolove, C., Tattersall, D., Thomas, A.C., et al., A deafness associated mutant human connexin 26 improves the epithelial barrier in vitro, *J. Membr. Biol.* 218 (2007) 29–37.

[149] Boelsma, E., Verhoeven, M.C.H., Ponec, M., Reconstruction of a human skin equivalent using a spontaneously transformed keratinocyte cell line (HaCaT), *J. Invest. Dermatol.* 112 (1999) 489–498.

[150] Stacey, G., Primary cell cultures and immortal cell lines, *Encycl. Life Sci.* (2005) DOI:10.1038/npg.els.0003960.

[151] Kaur, G., Dufour, J.M., Cell lines - Valuable tools or useless artifacts, *Spermatogenesis*. 2 (2012) DOI:10.4161/spmg.2.1.19885.

[152] Hirata, H., Samsonov, M., Sokabe, M., Actomyosin contractility provokes contact inhibition in E-cadherin-ligated keratinocytes, *Sci. Rep.* 7 (2017) DOI: 10.1038/srep46326.

[153] Niehues, H., Bouwstra, J.A., El Ghalbzouri, A., Brandner, J.M., et al., 3D skin models for 3R research: the potential of 3D reconstructed skin models to study skin barrier function, *Exp. Dermatol.* 27 (2018) 501–511.

[154] Lange, J., Weil, F., Riegler, C., Groeber, F., et al., Interactions of donor sources and media influence the histo-morphological quality of full-thickness skin models, *Biotechnol. J.* 11 (2016) 1352–1361.

[155] Ferraq, Y., Black, D.R., Theunis, J., Mordon, S., Superficial wounding model for epidermal barrier repair studies: Comparison of erbium:YAG laser and the suction blister method, *Lasers Surg. Med.* 44 (2012) 525–532.

[156] Ferraq, Y., Black, D., Lagarde, J.M., Schmitt, a M., et al., Use of a 3-D imaging technique for non-invasive monitoring of the depth of experimentally induced wounds, *Ski. Res. Technol.* 13 (2007) 399–405.

[157] Sattler, E.C.E., Poloczek, K., Kästle, R., Welzel, J., Confocal laser scanning microscopy and optical coherence tomography for the evaluation of the kinetics and quantification of wound healing after fractional laser therapy, *J. Am. Acad. Dermatol.* 69 (2013) 165–173.

[158] Tsai, M.-T., Yang, C.-H., Shen, S.-C., Lee, Y.-J., et al., Monitoring of wound healing process of human skin after fractional laser treatments with optical coherence tomography, *Biomed. Opt. Express*. 4 (2013). DOI:10.1364/boe.4.002362.

[159] Tainaka, K., Kuno, A., Kubota, S.I., Murakami, T., et al., Chemical principles in tissue clearing and staining protocols for whole-body cell profiling, *Annu. Rev. Cell Dev. Biol.* 32 (2016) 713–741.

[160] Deka, G., Chu, S.-W., Kao, F.-J., Skin wound healing revealed by multimodal optical microscopies, 2016. DOI:10.5772/64088.

[161] Cicchi, R., Kapsokalyvas, D., Pavone, F.S., Clinical nonlinear laser imaging of human skin: A review, *Biomed Res. Int.* (2014). DOI:10.1155/2014/903589.

[162] Nasir, N.A.M., Paus, R., Ansell, D.M., Fluorescent cell tracer dye permits real-time assessment of re-epithelialization in a serum-free ex vivo human skin wound assay, *Wound Repair Regen.* 27 (2019) 126–133.

[163] Ahn, Y., Lee, C.-Y., Baek, S., Kim, T., et al., Quantitative monitoring of laser-treated engineered skin using optical coherence tomography, *Biomed. Opt. Express*. 7 (2016)

DOI:10.1364/BOE.7.0001030.

[164]   Huang, D., Swanson, E.A., Lin, C.P., Schuman, J.S., et al., Optical coherence tomography, *Science (80-.).* 254 (1991) 1178–1181.

[165]   Welzel, J., Lankenau, E., Birngruber, R., Engelhardt, R., Optical coherence tomography of the human skin, *J. Am. Acad. Dermatol.* 37 (1997) 958–963.

[166]   Spöler, F., Först, M., Marquardt, Y., Hoeller, D., et al., High-resolution optical coherence tomography as a non-destructive monitoring tool for the engineering of skin equivalents, *Ski. Res. Technol.* 12 (2006) 261–267.

[167]   Jung, W., Kao, B., Kelly, K.M., Liaw, L.H.L., et al., Optical coherence tomography for in vitro monitoring of wound healing after laser irradiation, *IEEE J. Sel. Top. Quantum Electron.* 9 (2003) 222–226.

[168]   Smith, L.E., Bonesi, M., Smallwood, R., Matcher, S.J., et al., Using swept-source optical coherence tomography to monitor the formation of neo-epidermis in tissue-engineered skin, *J. Tissue Eng. Regen. Med.* 4 (2010) 652–658.

[169]   Cobb, M.J., Chen, Y., Underwood, R.A., Thariani, R.A., et al., Assessment of cutaneous wound healing using ultrahigh-resolution optical coherence tomography, *J. Biomed. Opt.* 11 (2006) DOI:10.1117/1.2388152.

[170]   Daigneault, M., Preston, J.A., Marriott, H.M., Whyte, M.K.B., et al., The identification of markers of macrophage differentiation in PMA-stimulated THP-1 cells and monocyte-derived macrophages, *PLoS One.* 5 (2010). DOI:10.1371/journal.pone.0008668.

[171]   Khallou-Laschet, J., Varthaman, A., Fornasa, G., Compain, C., et al., Macrophage plasticity in experimental atherosclerosis, *PLoS One.* 5 (2010). DOI:doi:10.1371/journal.pone.0008852.

[172]   Van Den Bogaard, E.H., Tjabringa, G.S., Joosten, I., Vonk-Bergers, M., et al., Crosstalk between keratinocytes and T cells in a 3D microenvironment: A model to study inflammatory skin diseases, *J. Invest. Dermatol.* 134 (2014) 719–727.

[173]   Borowiec, A.S., Delcourt, P., Dewailly, E., Bidaux, G., Optimal differentiation of in vitro keratinocytes requires multifactorial external control, *PLoS One.* 8 (2013) DOI:10.1371/journal.pone.0077507.

[174]   Berghard, A., Gradin, K., Toftgard, R., Serum and extracellular calcium modulate induction of cytochrome P-450IA1 in human keratinocytes, *J. Biol. Chem.* 265 (1990) 21086–21090.

[175]   Bertolero, F., Kaighn, M.E., Camalier, R.F., Saffiotti, U., Effects of serum and serum-derived factors on growth and differentiation of mouse keratinocytes, *Vitr. Cell. Dev. Biol.* 22 (1986) 423–428.

[176]   Jannasch, M., Groeber, F., Brattig, N.W., Unger, C., et al., Development and application of three-dimensional skin equivalents for the investigation of percutaneous worm invasion, *Exp. Parasitol.* 150 (2015) 22–30.

[177]   Lamb, R., Ambler, C.A., Keratinocytes propagated in serum-free, feeder-free culture conditions fail to form stratified epidermis in a reconstituted skin model, *PLoS One.* 8 (2013) DOI:10.1371/journal.pone.0052494.

[178]   Hennings, H., Holbrook, K., Steinert, P., Yuspa, S., Growth and differentiation of mouse epidermal cells in culture: effects of extracellular calcium., *Curr. Probl. Dermatol.* 10 (1980) 3–25.

[179]   Boyce, S.T., Ham, R.G., Calcium-regulated differentiation of normal human epidermal keratinocytes in chemically defined clonal culture and serum-free serial culture, *J. Invest. Dermatol.* 81 (1983) 33–40.

[180]   Ponec, M., Weerheim, A., Kempenaar, J., Mulder, A., et al., The formation of competent barrier lipids in reconstructed human epidermis requires the presence of vitamin C, *J. Invest. Dermatol.* 109 (1997) 348–355.

[181]   Black, A.F., Bouez, C., Perrier, E., Schlotmann, K., et al., Optimization and characterization of an engineered human skin equivalent, *Tissue Eng.* 11 (2005) 723–733.

[182]   Kosten, I.J., Buskermolen, J.K., Spiekstra, S.W., De Gruijl, T.D., et al., Gingiva equivalents secrete negligible amounts of key chemokines involved in Langerhans cell migration compared to skin equivalents, *J. Immunol. Res.* 2015 (2015) 13–17.

[183]   Pensalfini, M., Ehret, A.E., Stüdeli, S., Marino, D., et al., Factors affecting the mechanical behavior of collagen hydrogels for skin tissue engineering, *J. Mech. Behav. Biomed. Mater.* 69 (2017) 85–97.

[184]   Beninson, L.A., Fleshner, M., Exosomes in fetal bovine serum dampen primary macrophage IL-1β response to lipopolysaccharide (LPS) challenge, *Immunol. Lett.* 163 (2015) 187–192.

[185]   Pardo, V., González-Rodríguez, Á., Guijas, C., Balsinde, J., et al., Opposite cross-talk by oleate and palmitate on insulin signaling in hepatocytes through macrophage activation, *J. Biol. Chem.* 290 (2015) 11663–11677.

[186]   Haskó, G., Németh, Z.H., Szabó, C., Zsilla, G., et al., Isoproterenol inhibits IL-10, TNF-α, and nitric oxide production in RAW 264.7 macrophages, *Brain Res. Bull.* 45 (1998) 183–187.

[187]   Dong, J., Li, J., Cui, L., Wang, Y., et al., Cortisol modulates inflammatory responses in LPS-stimulated RAW264.7 cells via the NF-ΚB and MAPK pathways, *BMC Vet. Res.* 14 (2018) DOI:10.1186/s12917-018-1360-0.

[188]   Koncz, S., Horváth, E.J., Different action of IBMX, isoproterenol and rutin on orthovanadate-induced nitric oxide release in mouse macrophage cells, *Acta Vet. Hung.* 50 (2002) 323–341.

[189]   Yen, T.T.H., Thao, D.T.P., Thuoc, T.L., An overview on Keratinocyte Growth Factor: From the molecular properties to clinical applications, *Protein Pept. Lett.* 21 (2014) 306–317.

[190]   Rubin, J.S., Bottaro, D.P., Chedid, M., Miki, T., et al., Keratinocytes growth factor, *Cell Biol. Int.* 19 (1995) 399–441.

[191]   McWhorter, F.Y., Wang, T., Nguyen, P., Chung, T., et al., Modulation of macrophage phenotype by cell shape, *Proc. Natl. Acad. Sci. U. S. A.* 110 (2013) 17253–17258.

[192]   O'Reilly, D., Quinn, C.M., El-Shanawany, T., Gordon, S., et al., Multiple Ets factors and interferon regulatory factor-4 modulate CD68 expression in a cell type-specific manner, *J. Biol. Chem.* 278 (2003) 21909–21919.

[193]   O'Reilly, D., Greaves, D.R., Cell-type-specific expression of the human CD68 gene is associated with changes in Pol II phosphorylation and short-range intrachromosomal gene looping, *Genomics*. 90 (2007) 407–415.

[194]   Limandjaja, G.C., Waaijman, T., Roffel, S., Niessen, F.B., et al., Monocytes co-cultured with reconstructed keloid and normal skin models skew towards M2 macrophage phenotype, *Arch. Dermatol. Res.* (2019). DOI:10.1007/s00403-019-01942-9.

[195]   Bikle, D.D., Yie, Z., Tu, C.-L., Calcium regulation of keratinocyte differentiation, *Expert Rev. Endocrinol. Metab.* 7 (2012) 461–472.

[196]   Kreutz, M., Krause, S.W., Hennemann, B., Rehm, A., et al., Macrophage heterogeneity and differentiation: defined serum-free culture conditions induce different types of macrophages in vitro, *Res. Immunol.* 143 (1992) 107–115.

[197]   Kobayashi, D., Kusama, M., Onda, M., Nakahata, N., The effect of pantothenic acid deficiency on keratinocyte proliferation and the synthesis of keratinocyte growth factor and collagen in fibroblasts, *J. Pharmacol. Sci.* 115 (2011) 230–234.

[198]   Wiederholt, T., Heise, R., Skazik, C., Marquardt, Y., et al., Calcium pantothenate modulates gene expression in proliferating human dermal fibroblasts, *Exp. Dermatol.* 18 (2009) 969–978.

[199]   Ebner, F., Heller, A., Rippke, F., Tausch, I., Topical use of dexpanthenol in skin disorders, *Am. J. Clin. Dermatol.* 3 (2002) 427–433.

[200]   He, W., Hu, S., Du, X., Wen, Q., et al., Vitamin B5 reduces bacterial growth via regulating

innate immunity and adaptive immunity in mice infected with Mycobacterium tuberculosis, *Front. Immunol.* 9 (2018). DOI:10.3389/fimmu.2018.00365.

[201] Leonard, F., Collnot, E.M., Lehr, C.M., A three-dimensional coculture of enterocytes, monocytes and dendritic cells to model inflamed intestinal mucosa in vitro, *Mol. Pharm.* 7 (2010) 2103–2119.

[202] Minami, K., Hiwatashi, K., Ueno, S., Sakoda, M., et al., Prognostic significance of CD68, CD163 and Folate receptor-β positive macrophages in hepatocellular carcinoma, *Exp. Ther. Med.* 15 (2018) 4465–4476.

[203] Heusinkveld, M., van der Burg, S.H., Identification and manipulation of tumor associated macrophages in human cancers, *J. Transl. Med.* 9 (2011). DOI:10.1186/1479-5876-9-216.

[204] Gottfried, E., Kunz-Schughart, L.A., Weber, A., Rehli, M., et al., Expression of CD68 in non-myeloid cell types, *Scand. J. Immunol.* 67 (2008) 453–463.

[205] Hoshiba, T., Lu, H., Kawayoe, N., Chen, G., Decellularized matrices for tissue engineering, *Expert Opin. Biol. Ther.* 10 (2010) 1717–1728.

[206] Badylak, S.F., Decellularized allogeneic and xenogeneic tissue as a bioscaffold for regenerative medicine: Factors that influence the host response, *Ann. Biomed. Eng.* 42 (2014) 1517–1527.

[207] BS, K., DJ, M., Development of biocompatible synthetic extracellular matrices for tissue engineering, *Trends Biotechnol.* 16 (1998) 224–230.

[208] Shin, H., Jo, S., Mikos, A.G., Biomimetic materials for tissue engineering, *Biomaterials*. 24 (2003) 4353–4364.

[209] Qin, X.-H., Wang, X., Rottmar, M., Nelson, B.J., et al., Near-infrared light-sensitive polyvinyl alcohol hydrogel photoresist for spatiotemporal control of cell-instructive 3D microenvironments, *Adv. Mater.* 30 (2018). DOI:10.1002/adma.201705564.

Appendix A

This chapter contains the supplemental data of the experimental work.

A.1. Scratch wound assay

Different compounds were analyzed with scratch wound assay to identify a substance enhancing cell migration, in order to establish a positive reference for improved healing. The measured wound closure rates after 5 hours were higher when calcium pantothenate was supplemented to the medium comparing to the controls, both for HDF and HEK (figure A.1.), showing that calcium pantothenate has a positive effect on cell migration. Between all the concentrations tested, the supplementation of 60 µg/mL calcium pantothenate to HDF culture medium resulted in 38% scratch closure comparing to 25% in control wells (figure A.1.). For HEK, the same concentration of 60 µg/mL calcium pantothenate increased wound closure to 70% compared to 37% in the controls (figure 16). Despite the differences in wound closure, no statistical significance was observed.
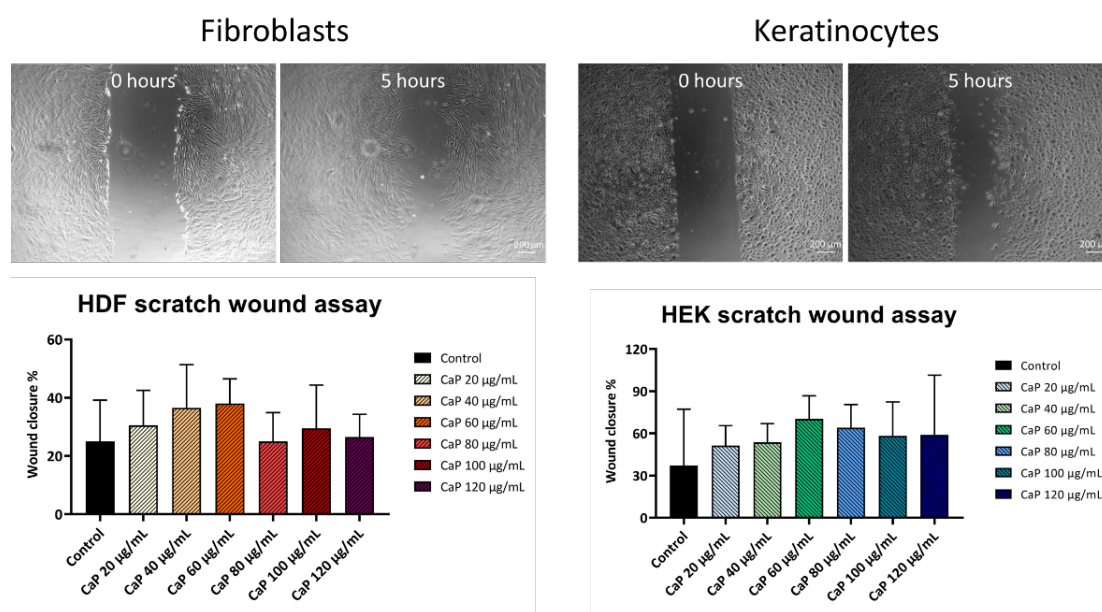

Figure A.1. Scratch wound assay performed on primary fibroblasts (HDF) and keratinocytes (HEK) in presence of different concentrations of calcium pantothenate. Representative images show scratches in the confluent cell layers right after wound formation (0 hours) and at time of quantification, 5 hours later (5 hours). Scratch closure quantification was performed by measuring scratch areas with ImageJ software, and results are shown as wound % closure at 5 hours compared to 0 hours. CaP: calcium pantothenate. Scale bars: 200 µm. N=3, error bars represent standard deviation (one-way ANOVA).

Appendix B

Curriculum vitae

Chiara Griffoni

Stampfenbrunnenstrasse, 3
8048 Zürich
CH
ch.griffoni@gmail.com | +41 76 325 21 65
07.11.1988 | Italian | Female

Working Experience

PhD Student

Empa - Swiss Federal Laboratories for Materials Science and Technology   *02.2016 - 07.2019*

Lerchenfeldstrasse 5, 9014 St Gallen, CH

Biointerfaces / Cells at Surfaces

- Development of an immunocompetent *in vitro* skin model for detection of inflammatory responses in injured skin

Education

MSc in Tissue Engineering and Regenerative Medicine

University of Applied Sciences Technikum Wien, Austria   *08.2014 - 09.2015*

Tissue Engineering, Biomaterials, Immunology, Stem cells, Corporate Management

- Thesis: *Monitoring Stem Cell Differentiation under Combined Physiological Stimulation Using Lab-on-a-chip Technology*
- Lab: Prof. Cornelia Kasper, Department of Biotechnology, University of Natural Resources and Life Sciences, Vienna (BOKU)

MSc in Experimental and Medical Biosciences

Linköping University, Sweden   *08.2013 - 06.2014*

Laboratory and Analytical Techniques, Tumor Biology, Advanced Immunology

- Thesis: *In vitro and in vivo Evaluation of Materials Designed for Cardiac Patches*
- Lab: Prof. May Griffith, Sweden Integrative Regenerative Medicine (IGEN) Center, Linköping University

BSc in Biology

Università degli Studi di Parma, Italy   *09.2008 - 07.2012*

Biology, Genetics, Molecular Biology, Biochemistry, Botanic, Statistics

- Thesis: *Genetic Cloning and Construction of Mutant Strains in Saccharomyces cerevisiae*
- Lab: Prof. Claudia Donnini, Faculty of Biology, Università degli Studi di Parma
- Grade: 97/110

Appendix C

List of publications and conference participation

Publications

- <u>Griffoni C</u>, Senturk B, Yang K, Groeber-Becker F, Maniura-Weber K, Dandekar T, Walles H, Rottmar M. Culture media for immunocompetent skin models down-regulate the primary macrophage inflammatory response. Submitted for publication to *Biotechnology Journal*

- Pupovac A, Senturk B, <u>Griffoni C</u>, Maniura-Weber K, Rottmar M, McArthur SL. Toward Immunocompetent 3D Skin Models. *Adv. Healthcare Mater.* 2018;(7),1701405. https://doi.org/10.1002/adhm.201701405

Conferences

- SSBRM 2016, Zürich, Switzerland (Poster)

  "Advanced 3D skin wound healing model for the study and development of materials"

- TEDD Annual Meeting, 2016, ZHAW, Wädenswil, Switzerland (Poster)

  "3D skin wound healing model for the study and development of materials"

- Empa PhD Symposium 2016, Zürich, Switzerland (Poster)

  "3D skin wound healing model for the study and development of materials"

- SSBRM 2017, St Gallen, Switzerland (Poster)

  "An *in vitro* model for evaluating novel skin wound healing therapies"

- TERMIS-EU, 2017, Davos, Switzerland, (Poster)

  "An advanced 3D model to study and develop materials for skin wound healing"

  Co-chair of session: "Gene2Skin Twinning H2020 Project- Roadmap for advanced genetic engineering-based skin therapies"

- Biointerfaces International 2018, Zürich, Switzerland (Poster)

  "Towards immunocompetent skin models: relevance of co-culture medium"

- Empa PhD Symposium 2018 Zürich, Switzerland (Talk)

  "Towards immunocompetent skin models for preclinical evaluation of novel therapies"

  2nd place Oral Presentation Award

Appendix D

Eidesstattliche Erklärung/Affidavit

Eidesstattliche Erklärung

Hiermit erkläre ich an Eides statt, die Dissertation: „**Auf dem Weg zu fortschrittlichen immunkompetenten Hautwundmodellen für die *in vitro* Medikamentenbewertung**", eigenständig, d. h. insbesondere selbständig und ohne Hilfe eines kommerziellen Promotionsberaters, angefertigt und keine anderen, als die von mir angegebenen Quellen und Hilfsmittel verwendet zu haben.

Ich erkläre außerdem, dass die Dissertation weder in gleicher noch in ähnlicher Form bereits in einem anderen Prüfungsverfahren vorgelegen hat.

Weiterhin erkläre ich, dass bei allen Abbildungen und Texten bei denen die Verwertungsrechte (Copyright) nicht bei mir liegen, diese von den Rechtsinhabern eingeholt wurden und die Textstellen bzw. Abbildungen entsprechend den rechtlichen Vorgaben gekennzeichnet sind sowie bei Abbbildungen, die dem Internet entnommen wurden, der entsprechende Hypertextlink angegeben wurde.

Affidavit

I hereby declare that my thesis entitled: „**Towards advanced immunocompetent skin wound models for *in vitro* drug evaluation**" is the result of my own work. I did not receive any help or support from commercial consultants. All sources and / or materials applied are listed and specified in the thesis.

Furthermore I verify that the thesis has not been submitted as part of another examination process neither in identical nor in similar form.

Besides I declare that if I do not hold the copyright for figures and paragraphs, I obtained it from the rights holder and that paragraphs and figures have been marked according to law or for figures taken from the internet the hyperlink has been added accordingly.

Würzburg, den 13.09.2019

Signature PhD-student

Appendix E

Überprüfung der Dissertation durch eine Plagiatssoftware

Sehr geehrte Damen und Herren,

hiermit erkläre ich mein Einverständnis damit, dass meine Dissertation durch eine Plagiatssoftware überprüft werden darf.

Der Titel meiner Dissertation lautet:
„Auf dem Weg zu fortschrittlichen immunkompetenten Hautwundmodellen für die *in vitro* Medikamentenbewertung"

Würzburg, den 13.09.2019

Unterschrift Promovend

Review of the PhD-thesis by a plagiarism software

Dear Sir and Madam,

I hereby declare my consent that my PhD-thesis could be reviewed by a plagiarism software.

My dissertation is entitled:
„Towards advanced immunocompetent skin wound models for *in vitro* drug evaluation"

Würzburg, den 13.09.2019

Signature PhD-student

Appendix F

Acknowledgements

First of all, I would like to thank Prof. Katharina Maniura-Weber and Dr. Markus Rottmar for giving me the opportunity to join the Biointerfaces team at Empa and for their support and mentoring during my PhD.

I would like to thank my committee in Würzburg, Prof. Heike Walles and Prof. Thomas Dandekar, for their continuous support despite the physical distance. I am grateful for your help, scientific input and valuable advice during my work.

A special thanks also goes to Dr. Florian Groeber-Becker, who has given me great scientific input and technical advice, implementing my knowledge with several tips and tricks.

Working at Empa has been an experience of exponential personal and scientific growth, which wouldn't have happened without great co-workers.

Thanks to my office mates, who have filled my days, both good and bad ones, with creative talks, chocolate, coffee and, most importantly, a lot of laughter. I will really miss our daily chats.

Thanks to all the Biointerfaces team, for providing an efficient network and a great working environment. In particular, thanks to all the Cells at Surfaces group, for all the scientific and non-scientific exchange and activities. You have been a great support for my personal and professional growth.

I would like to specially thank Yvonne for being my "lab mum". Not only have you given me an enormous technical help, in particular after my wrist surgery. With your smile and your kindness, you have always supported me also personally, and I will miss working with you. The cell lab has been my second home for the past years, and you definitely made it welcoming despite my ups and downs.

A thank goes to my other fellow PhD students at Empa. Sharing with you ideas and feelings, from both private and work life, has always been comforting and supportive. In particular, I would like to thank Anne-Sophie, Claudia and Sarah. You have always been there, particularly in the bad days, providing me with exceptional advice and fundamental scientific and personal support. Sharing this bumpy ride with you has been my safety net.

Last but not least, the biggest thank goes to whom made all this possible: my family, who supported me through all my studies and also during the PhD time. Travelling back home and spending time with you, even if always for a short weekend, has always been and will always be my certain way to remember that I can do anything I want.

Last to be mentioned, but not for importance, a special thank you to my partner in crime: Massimo. Most than anyone you have lived this journey with me, being there every day and experiencing with me every positive and negative event of the last years. Your support has given me the strength and tenacity to always look ahead. Thank you for supporting me and believing in me no matter what.